PolyPublie
Polytechnique Montréal

POLYTECHNIQUE MONTRÉAL
UNIVERSITÉ D'INGÉNIERIE

Titre: Title:	Implementation of the analytic nodal method in the ndf code and applications to candu reactors
Auteur: Author:	Jinchao Mao
Date:	2000
Type:	Mémoire ou thèse / Dissertation or Thesis
Référence: Citation:	Mao, J. (2000). Implementation of the analytic nodal method in the ndf code and applications to candu reactors [Master's thesis, École Polytechnique de Montréal]. PolyPublie. https://publications.polymtl.ca/8798/

Document en libre accès dans PolyPublie
Open Access document in PolyPublie

URL de PolyPublie: PolyPublie URL:	https://publications.polymtl.ca/8798/
Directeurs de recherche: Advisors:	
Programme: Program:	Unspecified

Ce fichier a été téléchargé à partir de PolyPublie, le dépôt institutionnel de Polytechnique Montréal
This file has been downloaded from PolyPublie, the institutional repository of Polytechnique Montréal

https://publications.polymtl.ca

UNIVERSITÉ DE MONTRÉAL

IMPLEMENTATION OF THE ANALYTIC NODAL METHOD IN THE NDF CODE AND APPLICATIONS TO CANDU REACTORS

JINCHAO MAO
DÉPARTEMENT DE GÉNIE MÉCANIQUE
ÉCOLE POLYTECHNIQUE DE MONTRÉAL

MÉMOIRE PRÉSENTÉ EN VUE DE L'OBTENTION
DU DIPLÔME DE MAÎTRISE ÈS SCIENCES APPLIQUÉES
(GÉNIE ÉNERGÉTIQUE)
AVRIL 2000

© Jinchao Mao, 2000.

National Library of Canada
Acquisitions and Bibliographic Services
395 Wellington Street
Ottawa ON K1A 0N4
Canada

Bibliothèque nationale du Canada
Acquisitions et services bibliographiques
395, rue Wellington
Ottawa ON K1A 0N4
Canada

Your file Votre référence

Our file Notre référence

The author has granted a non-exclusive licence allowing the National Library of Canada to reproduce, loan, distribute or sell copies of this thesis in microform, paper or electronic formats.

L'auteur a accordé une licence non exclusive permettant à la Bibliothèque nationale du Canada de reproduire, prêter, distribuer ou vendre des copies de cette thèse sous la forme de microfiche/film, de reproduction sur papier ou sur format électronique.

The author retains ownership of the copyright in this thesis. Neither the thesis nor substantial extracts from it may be printed or otherwise reproduced without the author's permission.

L'auteur conserve la propriété du droit d'auteur qui protège cette thèse. Ni la thèse ni des extraits substantiels de celle-ci ne doivent être imprimés ou autrement reproduits sans son autorisation.

0-612-57418-0

Canada

UNIVERSITÉ DE MONTRÉAL

ÉCOLE POLYTECHNIQUE DE MONTRÉAL

Ce mémoire intitulé :

IMPLEMENTATION OF THE ANALYTIC NODAL METHOD IN THE NDF CODE AND APPLICATIONS TO CANDU REACTORS

présenté par : MAO Jinchao

en vue de l'obtention du diplôme de : Maîtrise ès sciences appliquées

a été dûment accepté par le jury d'examen constitué :

M. ROZON Daniel, Ph.D., président

M. KOCLAS Jean, Ph.D., membre et directeur de recherche

M. ROY Robert, Ph.D., membre

To my husband and daughter,

Whom I love the most.

ACKNOWLEDGMENTS

I would like to thank my thesis director Dr. Jean Koclas for the invaluable help and guidance he has given to me throughout the course of this work. I am sure he knows how much I appreciate the help he has given during the last 2 years.

I would like to extend my special thanks to Dr. Daniel Rozon for his invaluable help during the admission process. Without his help, I would not have been able to begin my studies at IGN.

This work would not have been possible without the help of my husband Dr. Wei Shen. Also, I wish to thank my daughter and my parents who have given me a lot of encouragement.

Finally, my special gratitude goes to S. Kaveh-Khorie (Ph. D. candidate) for his assistance in the preparation of the NDF code.

RÉSUMÉ

Dans ce document, la méthode nodale analytique est formulée avec une approximation de fuites transversales constantes, ce qui constitue la seule approximation utilisée. Le couplage spatial est obtenu à partir de la solution analytique des équations de diffusions unidimensionnelles résultantes. Les équations qui découlent sont exprimées en terme des flux moyens et des fuites nettes de surface. Ces équations ont la forme d'un problème aux valeurs propres classique, qui est résolu par la méthode des itérations sur les sources.

Les modules nécessaires aux calculs statiques et dynamiques en 3-D ont été développés et intégrés dans le code NDF, qui ne disposent que des différences finies centrées. Deux problèmes ont été analysés avec ces modules : premièrement, le problème du CANDU benchmark et un modèle de CANDU-6 typique, avec les mécanismes de réactivité (19 barres liquides et 21 barres compensatrices) présents dans le cœur. Les propriétés du combustible et des mécanismes de réactivité proviennent de DRAGON / DONJON.

Les calculs démontrent que la méthode nodale analytique avec fuites constantes est plus précise que la méthode des différences finies centrées pour l'étude des réacteurs CANDU, spécialement pour la prédiction des puissances de canal dans les régimes à haute puissance. Les calculs cinétiques espace-temps en 3–D démontrent aussi la supériorité de la méthode pour les analyses des transitoires.

ABSTRACT

In this thesis, the formulation of the Analytic Nodal Method (ANM) is derived with the flat transverse leakage approximation, which is the only approximation introduced during derivation. The spatial coupling is determined by the analytic solutions of the one-dimensional diffusion equations. The resulting super-matrix equations can be written in terms of nodal-averaged fluxes and face-averaged net leakages, the form of classical eigenvalue problem which can be solved by a standard source iteration procedure.

Based on the proposed method, the modules used for 3-D static and kinetic calculations were developed and programmed into the NDF code, which was a finite-difference code specially designed for 3-D CANDU kinetics calculation. Two problems were tested for these modules: one is a standard CANDU benchmark problem, another is a typical CANDU-6 core with in-core reactivity devices (21 adjuster rods and 14 liquid zone controllers) present. The fuel and reactivity device properties used in the calculations were generated by the DRAGON/DONJON chain code.

The calculations demonstrate that the ANM with flat leakage approximation is more accurate than the Coarse Mesh Finite Difference (CMFD) method for CANDU analysis, especially for the channel-power prediction in the central high-power region. The application of the ANM with flat leakage approximation to 3-D CANDU kinetics calculation shows that the ANM with flat leakage approximation is more accurate than the CMFD for 3-D CANDU transient analysis.

CONDENSÉ EN FRANCAIS

I Introduction

Des méthodes nodales ont été utilisées pour l'analyse du cœur des réacteurs à eau légère (LWR) et pour les analyses de sûreté pendant plus de vint années. Dans les deux dernières décennies, les méthodes nodales modernes, par exemple la méthode d'expansion nodale (Finnemann et autres, 1977), la méthode nodale analytique (ANM) (Smith, 1979) et la méthode nodale de fonction de Green (NGFM) (Laurent et autres, 1980), ont été développées avec succès pour résoudre le problème spatial du LWR. Cependant, à cause de la grande zone de migration des neutrons dans l'eau lourde la méthode des différences finies centrées (CMFD) s'est généralement avérée adéquate et a été intensivement utilisée pour l'analyse de CANDU pendant les trente dernières années. Pour répondre à la demande d'une plus grande exactitude des analyses actuelles et futures, nous avons étudié l'utilisation de la méthode nodale comme outil alternatif pour l'analyse du CANDU.

Parmi les nombreuses méthodes nodales avancées, ANM est considérée comme méthode numérique précise et efficace pour résoudre l'équation de diffusion dynamique, multidimensionnelle, à deux groupes d'énergie pour LWR (Smith, 1979). Cependant, le code d'ANM -QUANDRY (Smith, 1979) ne peut pas être utilisé directement pour l'analyse du CANDU parce qu'il a été spécifiquement conçu pour LWR. Un grand nombre de difficultés ont été rencontrées dans QUANDRY en effectuant des analyses de transitoires de CANDU avec les mécanismes de contrôle de le réactivité insérés perpendiculairement par rapport au combustible. Une voie alternative est de réétudier le formalisme d'ANM et de développer des modules

indépendants pour un code de diffusion actuel de CANDU. Le code NDF a été utilisé dans cette étude. Le premier objectif de l'auteure est de mettre en application l'ANM dans l'environnement de DRAGON/DONJON puis, d'appliquer cette méthode à l'analyse des réacteurs CANDU.

Les objectifs du travail actuel sont divisés en trois parties. D'abord, réétudier la procédure de dérivation de la méthode nodale analytique avec l'approximation de fuite transversale plate, qui est la seule approximation présentée pendant la dérivation. Ensuite, résoudre les équations statiques et cinétiques en utilisant la procédure itérative appropriée. Le deuxième objectif consiste à développer les modules utilisés par la méthode nodale analytique et mettre en application ces modules dans le code NDF. Le troisième objectif est d'appliquer la méthode nodale analytique au problème de référence de CANDU et au problème CANDU-6 typique. La solution de la méthode nodale analytique sera comparée à la solution de la méthode des différences finies centrées.

II. Synthèse du problème

Dans la plupart des situations rencontrées dans l'analyse des réacteurs, il est suffisant de modéliser le comportement neutronique du réacteur par une approximation dans l'équation de transport des neutrons formellement exacte. L'approximation la plus répandue est la théorie de diffusion multigroupe. L'équation de diffusion peut être écrite comme 1.1. Si la distribution des propriétés matérielles dans l'espace et dans le temps, la distribution initiale de flux de neutrons dans l'espace et dans l'énergie et les conditions aux limites appropriées sont indiquées, une unique solution à l'équation existe. Les trois conditions aux limites les plus généralement utilisées à la surface externe du réacteur sont: le flux nul, le courant réentrant nul et le courant net nul.

Normalement, le cœur du réacteur est divisé en un certain nombre de parallélépipèdes rectangulaires contigus (ou nœuds). Nous supposons également que les propriétés nucléaires, les sections efficaces macroscopiques et les coefficients de diffusion sont constants en espace dans chaque nœud, bien qu'elles puissent changer par rapport au temps. Par conséquent, le calcul du cœur complet est réduit à celui de la détermination de la distribution spatiale du flux dans un réacteur contenant plusieurs milliers de nœuds.

III Descriptions des méthodes

Méthode des Différences Finis de Maille Grossière

Plusieurs méthodes pour résoudre les équations de diffusion multigroupe dépendantes du temps sont actuellement à la disposition de la communauté nucléaire. La méthode la plus répandue pour le réacteur CANDU est la méthode des différences finies centrées grossière. Cette méthode possède plusieurs avantages par rapport à la plupart des autres méthodes pour le réacteur CANDU. Par exemple, cette méthode est conceptuellement simple et les équations algébriques résultantes pour les flux sont telles que seulement des nœuds adjacents sont couplés. Une propriété très importante de la méthode des différences finies est la suivante : il est prouvé que cette méthode converge à la solution exacte des équations de diffusion multigroupes dans la limite de maille infiniment fine. En outre, par suite de la grande utilisation de cette méthode, les méthodes numériques associées ont également atteint des niveaux élevés de sophistication. Le seul véritable inconvénient de CMFD est que des mailles spatiales fines sont exigées pour atteindre une précision acceptable.

Des travaux récents (Koclas, 1998) ont montré qu'à partir de la méthode nodale analytique, en forçant à zéro les fuites transversales et en tronquant l'expansion des

exponentielles de matrice qui surgissent, CMFD pourrait être obtenu. Ceci indique aussi que CMFD est la méthode nodale d'ordre le plus bas. La méthode nodale devrait nous permettre d'obtenir des résultats plus précis lors de l'analyse des réacteurs de type CANDU.

Méthode nodale analytique

Une autre classe de techniques employées pour résoudre les équations de diffusion multigroupes est la méthode nodale. Pendant les vint dernières années, la méthode nodale a été utilisée avec succès pour la physique des réacteurs à eau légère (LWR) et les analyses de sûreté. Mais elle est rarement utilisée pour le réacteur de type CANDU parce que le CMFD s'est généralement avéré adéquat.

La plupart des méthodes nodales utilisent les flux moyens associés avec de larges régions spatiales (définies par des nœuds) et les courants moyens à des sourfaces définies par les nœuds. Aucune approximation n'est nécessaire par rapport à l'équation de diffusion des neutrons dans la dérivation des équations nodales de bilan. La difficulté avec les méthodes nodales est que le rapport entre les flux moyens dans les nœuds et les courants moyens sur les surfaces doit être connu. Une fois que les rapports entre les flux moyens dans les nœuds et les courants moyens sur les surfaces sont spécifiés, des équations de couplage peuvent être construites. Plusicurs approches différentes ont été proposées pour déterminer le couplage flux-courant. Comparé à d'autres méthodes nodales, la méthode nodale analytique utilise seulement une approximation pour les termes de couplage, soit la forme des fuites transversales.

L'approximation de fuite transversale plate et l'approximation de fuite transversale quadratique sont les deux approximations généralement utilisées. Dans cette thèse, nous utilisons l'approximation de fuite transversale plate, pour les raisons suivantes :

a) Dans un réacteur CANDU, le courant est très petit par rapport au flux et les fuites transversales ont une petite valeur.
b) Dans un réacteur CANDU, habituellement la CMFD est adéquat. La CMFD est la méthode nodale d'ordre le plus bas et utilise l'approximation des fuites transversales nulles. Ainsi, il est raisonnable d'utiliser l'approximation des fuites transversales plates dans l'analyse du réacteur CANDU.

La méthode nodale analytique utilise la solution analytique de l'équation unidimensionnelle de diffusion à deux groupes pour déterminer le couplage spatial. Les équations finales résultantes peuvent être écrites en terme des flux moyens et des fuites nettes de surface. Pour les calcules statiques, elles sont données par l'équation 1.40; pour la cinétique, elles sont données par l'équation 5.12.

IV Techniques numériques

Calcul statique

L'équation statique pour laquelle une solution est recherchée dans la méthode nodale analytique est donnée par 1.40. L'équation sous terme super de matrice est un ensemble d'équations linéaires de quatre vecteurs d'inconnus: flux moyen pour le premier vecteur et les fuites nettes de surface pour chaque direction pour les trois autres vecteurs. L'équation se présente sous la forme d'un problème classique de valeur propre, sauf que les éléments de la matrice de coefficient [H] dépendent de la valeur propre. Afin d'éviter des caractéristiques indésirables, les trois derniers blocs sont substitués dans le premier bloc d'équation pour obtenir l'équation 3.1. Le schéma itératif général pour résoudre cette équation est comme suit:

1. Une valeur initiale pour γ (habituellement γ=1.5) est employée pour évaluer les composants de la matrice de coefficient [H].

2. Une itération accélérée de source de fission (externe) est utilisée pour déterminer itérativement la valeur propre maximale et le vecteur propre correspondant (γ et [φ]).
3. Après quelques itérations externes (habituellement 5-10), la dernière évaluation de γ est employée pour mettre à jour les composants de la matrice de coefficient [H].
4. Utilisez une méthode "modifiée" de Gauss-Seidel par bloc pour effectuer les itérations internes.
5. La méthode d'itération semi-cyclique de Chebyshev (CCSI), ou la méthode d'itération de Gauss-Seidel est utilisée pour l'itération de flux.

Le fait que la matrice de coefficients [H] dépende de la valeur propre du problème statique global donne aux itérations externes un caractère non linéaire. La pratique de mettre à jour les matrices chaque 5 à 10 itérations externes semble appropriée. En utilisant la technique de décalage de valeur propre (Wielandt shift) pendant les itérations externes, le taux de convergence des itérations externes peut être sensiblement augmenté. Les itération internes sont faibles en étapes. D'abord, les flux sont déterminés à partir de l'ancienne source de fission et des anciennes fuites. Ensuite, les nouvelles fuites nettes sont déterminées par les nouveaux flux et les anciennes fuites. Normalement, seulement une itération interne par itération externe est disponible parce que les fuites sont très petites comparées au flux moyen. L'itération pour le flux peut être accélérée en utilisant la méthode de Cyclic Chebyshev Semi-Iteration (CCSI) ou la méthode d'itération de Gauss-Seidel. L'itération continue jusqu'à ce que la convergence soit atteinte.

Calcul cinétique

Les équations dépendant du temps d'ANM sont données par les équations 5.12 et 5.1b. Seul le premier bloc de l'équation 5.12 fait participer un opérateur temporel. Les

derniers trois blocs sont simplement des expressions pour les fuites transversales, au temps t, et ne font pas participer des opérateurs temporels. Par conséquent, tout schéma d'intégration qui rapproche les dérivées temporelles peut être utilisé pour résoudre les équations dépendantes du temps. Nous utilisons la méthode implicite comme méthode d'itération temporelle. Les grandes lignes d'algorithme de solution de cinétique sont tracées ci-dessous:

1. Choisir les temps (0, T_1, T_2, T_3...T_i) qui divisent le problème cinétique en domaines. Pour chaque domaine de temps, le critère de convergence de flux ε est une constante.
2. Supposer que les valeurs initiales sont connues au temps t.
3. Si $t_n = T_i$, changer Δt et ε afin de correspondre à ceux du domaine de temps i+1. Calculer les nouveaux paramètres d'optimisation de CCSI.
4. Modifier les sections efficaces pour correspondre à la configuration du cœur au temps t_{n+1}.
5. Calculer des éléments de matrice.
6. Obtenir les approximations pour $\left[\overline{\phi}\right]^{n+1} et \left[\overline{L}_u\right]^{n+1}$ par une procédure d'extrapolation.
7. Effectuer l'itération de flux pour obtenir $\left[\overline{\phi}\right]^{n+1} et \left[\overline{L}_u\right]^{n+1}$.
8. Résoudre l'équation pour obtenir $\left[\overline{C}_d\right]^{n+1}$.
9. Calculer les nouvelles fréquences d'extrapolation pour le prochain intervalle de temps. Répéter les étapes 3 à 9 pour chaque intervalle de temps jusqu'à la fin de la dernière étape de temps.

La mise à jour complète de matrices peut être effectuée toutes les 3 à 10 étapes de temps. La matricielle CCSI ou la méthode SOR peuvent être utilisées. Comme les fuites et les flux sont estimés par une procédure d'extrapolation, l'effort de calcul exigé pour résoudre les équations nodales de diffusion cinétique est sensiblement réduit.

V Résultats

Les modules employés par la méthode d'ANM pour des cas statiques et cinétiques ont été écrits et se mettent en application dans le code NDF. Deux problèmes CANDU et un problème PWR ont été testés. Les résultats sont comparés à des solutions avec maille fine CMFD et avec maille grossière CMFD.

Résultats statiques

a) Le problème de référence CANDU

Le problème de référence CANDU (ANL, 1985) est un problème de référence tridimensionnel simplifié, à deux groupes d'énergie, cinétique, comme décrit dans la section A1.2 de l'annexe 1. Il est considéré comme une norme très importante par laquelle le progrès dans des méthodes de calcul de CANDU est mesuré. Nous utilisons les résultats d'un calcul à maille fine de CMFD (72 x 72 x 40) comme référence. Les résultats détaillés se trouvent montrés dans le chapitre 4.

Les résultats indiquent que les erreurs maximales pour les densités de puissance de grappe pour ANM et CMFD sont d'environ 4.3% et 5.9% respectivement et situées dans le nœud (5,5,2), près de la frontière axiale ou Z. Les erreurs maximales des densités de puissance de canal pour ANM et CMFD sont d'environ 4.3% et 5.9% respectivement, pour un canal situé près du réflecteur. Ces résultats montrent que les nœuds avec les plus grandes erreurs de densités de puissance sont dans des régions de puissance faible, près du réflecteur. La comparaison des solutions de la méthode de CMFD et de la méthode d'ANM montre qu'avec la même maille, l'ANM obtient une solution plus précise.

b) Le problème du CANDU-6 typique

Le problème typique du CANDU-6 (Koclas, 1998 et Navarro Arias, 1996) est un plein cœur 3D complet simplifié, avec deux groupes d'énergie, avec les mécanismes principaux de réactivité, tels que les contrôleurs liquides de zone et barres de compensation présents dans le cœur. Ce problème est similaire à un véritable réacteur CANDU-6, contrairement au problème de référence CANDU. Ce problème est introduit pour la simulation dynamique. Le problème est en quelque sorte simplifié, car l'entaille axiale dans le réflecteur n'est pas présente dans ce modèle. Les sections efficaces macroscopiques du combustible et des mécanismes de réactivité sont calculées en utilisant la chaîne de calcul DRAGON/DONJON (Marleau et al., 1993.1994; Roy et al., 1993). La section A1.3 de l'annexe 1 donne la description détaillée de ce problème. Nous utilisons les résultats d'un calcul à maille fine (104 x 104 x 48) de CMFD comme référence. Les résultats détaillés sont donnés dans le chapitre 4.

Les résultats obtenus avec CMFD et ANM tels que la puissance maximale du canal et la puissance maximale de grappe sont tous conformes aux valeurs de référence. Comparé aux valeurs de référence, les erreurs moyennes et maximales, prévues par ANM, dans le canal et les densités de puissance de grappe sont toutes plus petites que celles prévues par CMFD. Les erreurs maximales des densités de puissance de grappe pour ANM et CMFD sont environ 2.8% et 6.0% respectivement; les erreurs maximales des densités de puissance de canal pour ANM et CMFD sont environ 1.6% et 2.2% respectivement. Pour des calculs d'ANM, le pourcentage maximum de l'erreur des densités de puissance de canal et de grappe est localisé à W13 et (W14, 4) respectivement, qui est dans la région périphérique du cœur à côté du réflecteur. De

façon générale, la comparaison entre CMFD et ANM prouve que les résultats d'ANM sont plus précis comme prévu.

L'effet xénon aéré calculé avec le ANM et CMFD pour ce même réacteur. Les résultats détaillés peuvent être trouvés dans le chapitre 4, la charge de xénon est de 0.028mk dans les deux cas.

Résultats de la cinétique

a) Le problème de référence de CANDU

Un problème tridimensionnel simplifié de référence CANDU (ANL, 1985) avec la mise en place asymétrique de mécanismes de réactivité est utilisé afin de contrôler notre mise en œuvre de l'ANM dans le code NDF. Une description détaillée peut être trouvée dans la section A1.2 de l'annexe 1.

Afin d'évaluer l'exactitude des différentes méthodes, il est nécessaire d'avoir une solution de référence. Malheureusement, toutes les solutions publiées pour ce problème proviennent de la CMFD avec une maille grossière (18 x 18 x 10), qui n'est pas considérée comme une référence appropriée. Par conséquent, des résultats d'un calcul CMFD avec 54 x 54 x 30 mailles spatiales sont utilisés comme référence dans cette étude. Les calculs de référence utilisent un pas de temps de 12.5 ms. Le critère de convergence utilisée par ces calculs est de 10^{-6} pour les flux. Les résultats détaillés sont donnés en chapitre 6.

La comparaison des erreurs en pourcentage de la puissance totale obtenues par ANM et CMFD avec les mêmes intervalles de temps et la même maille indique que la

puissance dépendante du temps obtenue par la méthode nodale analytique est en excellent accord avec les valeurs de référence. L'erreur maximale de la puissance totale est de 3 %, et il n'y a aucune perte de précision significative pour la méthode nodale analytique durant la transitoire. La différence entre les résultats CMFD et les valeurs de référence s'accorde bien (légèrement plus grands que les résultats d'ANM) au début de la transitoire et augmente rapidement pendant 1.2 secondes et atteint approximativement 13% après 1.8 secondes. Des conclusions semblables sont observées pour les prédictions de puissance de canal et de puissance de grappe, comme il est représenté sur les figures 7.5 à 7.10, séparément. Cette diminution significative de précision indique que CMFD n'est pas aussi fiable que l'ANM pour le scénario de transitoire rapide avec distribution de fuite significative dans le cœur. Pour augmenter la précision de calcul dans CMFD, une maille très fine doit être appliquée.

b) Le problème de CANDU-6 typique

Dans cette thèse, nous utilisons pour la simulation une éjection de barres. Le transit est initialisé par le retrait instantané du premier banc de 5 barres de compensation qui sont initialement dans le cœur. La transitoire résultante est suivie pendant 900 secondes. La description détaillée de ce problème peut être trouvée dans la section A1.3.

Le système de régulation de réacteur est utilisé dans ce problème. Au début, tous les mécanismes sont placés en position de référence (Marleau et al., 1996; Varin et al., 1996). Chaque mécanisme est alors déplacé et placé à une nouvelle position basée sur les résultats des algorithmes de régulation de système de réacteur. Aucune solution de référence n'est disponible pour ce problème; par conséquent, il est difficile de mesurer, dans le sens absolu, les erreurs dans la solution de la méthode nodale analytique.

Les calculs ANM ont utilisé la maille 26 x 26 x 12 et un pas de temps de 25 ms. Le critère de convergence utilisé par ANM était 10^{-6}. Les calculs CMFD ont utilisé la même maille, le même pas de temps et le même critère de convergence. Les résultats détaillés sont donnés dans le chapitre 6. Tous les résultats montrent que la réponse avec ANM est très semblable à la réponse obtenue avec CMFD. ANM constitue donc une bonne méthode pour la simulation du réacteur de type CANDU.

VI Conclusion

CMFD s'avère la méthode nodale d'ordre le plus bas. Les calculs prouvent que CMFD est généralement adéquate pour l'analyse statique de CANDU. La différence entre CMFD et ANM s'avère négligeable. Cependant, pour les scénarios de transitoire, avec fuites significatives, la différence entre CMFD et ANM n'est pas considérée négligeable. Avec les demandes de précisions augmentant pour les analyses actuelles et futures, CMFD maille fine ou une méthode nodale d'ordre supérieur devront être appliquées pour l'analyse de CANDU.

Les résultats de calculs pour la réacteurs CANDU et pour le modèle CANDU-6 typique montrent que des solutions précises de cinétique pourraient être obtenues avec les mailles spatiales de taille de grappe. Les comparaisons avec la CMFD ont indiqué que les erreurs de ANM étaient faibles.

L'ANM avec l'approximation de fuite plate s'est avéré une méthode supérieure à CMFD pour résoudre l'équation de diffusion cinétique ou statique, multidimensionnelle à deux groupes d'énergie pour le réacteur CANDU. La méthode nodale analytique avec la fuite plate constitue une méthode très précise pour l'analyse et la conception de réacteur CANDU.

TABLE OF CONTENTS

LIST OF FIGURES

LIST OF TABLES

NOMENCLATURE

[A]	Coefficient matrix	[-]
[B]	Coefficient matrix	[-]
C_d	Density of delayed neutron precursors in family d	[cm^{-3}]
D	Total number of delayed neutron precursor families	[-]
D_g	Diffusion coefficient for group g	[cm]
D_{gu}	Diffusion coefficient of x direction for group g (u = x, y, z)	[cm]
$[D_u]$	Diffusion coefficient matrix of u direction for group g (u = x, y, z)	[-]
[F], $[F_u]$	Coefficient matrix (u = x, y ,z)	[-]
G	Total number of neutron energy groups	[-]
$[G_u]$	Coefficient matrix (u = x, y, z)	[-]
h_u^l	Node widths (u = x, y, z; l = i, j, k)	[cm]
[H]	Coefficient matrix	[-]
i, j, k	Node indices	[-]
$\bar{J}(\bar{r}, t)$	Net current	[-]
J_{gu}	U direction transverse integrated current (u = x, y, z)	[-]
$[J_u]$	U direction transverse integrated current vector (u = x, y, z)	[-]
$[L_u]$	Net leakage vector (u = x, y, z)	[-]
[M]	Coefficient matrix	[-]
[N]	Coefficient matrix	[-]
P	Power density	[w/cm^3]
[P]	Coefficient matrix	[-]

S_u	U direction transverse leakage (u = x, y, z)	[-]
$[S_u]$	U direction transverse leakage vector (u = x, y, z)	[-]
t	time	[ms]
v	Average neutron speed	[cm·s^{-1}]
V	Volume	[cm^3]
â	Total fractional yield of delayed neutron precursors per fission	[-]
$â_d$	Fractional yield of delayed neutron precursors in family d per fission	[-]
ã	Eigenvalue	[-]
å	Convergence criterion	[-]
$\bar{\varepsilon}$	Average error of bundle (or channel) power density	[-]
ε_{max}	Maximum error of bundle (or channel) power density	[-]
ë$_d$	Decay constant for delayed neutron precursor family d	[sec^{-1}]
ñ	Reactivity	[mk]
υ	Mean number of neutrons emitted per fission	[-]
χ_{g_p}	Prompt fission neutron spectrum to group g	[-]
χ_{g_d}	Delayed neutron spectrum for family d in group g	[-]
Σ_{tg}	Macroscopic total cross section for group g	[cm^{-1}]
$\Sigma_{g\leftarrow g'}$	Macroscopic transfer cross section from group g' to group g	[cm^{-1}]
Σ_{fg}	Macroscopic fission cross section for group g	[cm^{-1}]
$[\Sigma]$	Macroscopic fission cross section coefficient matrix	[-]
ϕ_g	Scalar neutron flux in group g	[cm^{-2} sec^{-1}]
$\bar{\phi}_{g,i,j,k}$	Average neutron flux of group g in node (i, j, k)	[cm^{-2} sec^{-1}]
$[\bar{\phi}]$	Average neutron flux vector	[-]

INTRODUCTION

0.1 Nature of the Problem

Nodal methods have been used for Light Water Reactors (LWR) core-physics and safety analysis for more than 20 years. In the past two decades, the modern nodal methods, for example, the Nodal Expansion Method (NEM) (Finnemann et al., 1977), the Analytic Nodal Method (ANM) (Smith, 1979), and the Nodal Green's Function method (NGFM) (Lawrence et al., 1980), have successfully been developed to solve the spatial problem of the LWR. However, because of the large migration area of heavy-water system, the Coarse Mesh Finite Difference method (CMFD) has generally been found to be adequate and has been extensively used for CANDU analysis in the past 30 years. To address the increased accuracy requirements of current and future analysis, we investigated the use of nodal method as an alternative tool for CANDU analysis.

Among numerous advanced nodal methods, ANM is noted as an accurate and efficient numerical method for solving the time-dependent, multidimensional, 2-group neutron diffusion equation for LWR. However, the ANM-based QUANDRY code (Smith, 1979) cannot be used directly for CANDU analysis because it was specifically designed for LWR. A large number of difficulties would be encountered for QUANDRY to perform 3-D CANDU transient analysis with the reactivity devices inserted perpendicular to the fuel. An alternate way is to review the ANM formalism and develop independent modules to a current CANDU diffusion code. The NDF code was used in this study. The primary objective of the author is to implement the ANM in the DRAGON/DONJON environment then apply this method to analysis of CANDU reactors.

0.2 Purpose of Present Work and Organization of Thesis

The objectives of the present work are divided into three parts. First to review the derivation procedure of Analytic Nodal Method with flat transverse leakage approximation, which is the only approximation introduced during the derivation. The suitable iterative scheme employed for solving the static and kinetic equations will also be investigated. The second objective consists of developing the modules used for Analytic Nodal Method and implementing these modules into the NDF code. The third objective is to apply the Analytic Nodal Method to the CANDU benchmark problem and a typical CANDU-6 problem. The solution from Analytic Nodal Method will be compared with the solution from Coarse Mesh Finite Difference method. These objectives are discussed in the following chapters of this thesis:

In Chapter 1, the neutron diffusion equations of Analytic Nodal Method for 2 energy groups, with the only approximation that the transverse leakages are constants, are derived. These equations are written in terms of node-averaged fluxes and face-averaged net leakages. The Coarse Mesh Finite Difference equation are then obtained from the nodal equations.

The Coarse Mesh Finite Difference Method, which is the lowest order nodal method, is used to analyze a typical CANDU-6 model in Chapter 2. Accuracy as a function of the coarse mesh size is investigated.

The properties of the static nodal diffusion equations are examined in Chapter 3. Iterative solution technique used for the solution of nodal diffusions is also presented.

The results of three-dimensional static CANDU problems are exhibited in Chapter 4. The Analytic Nodal Method with flat leakage approximation is shown to be an accurate method for solving the multidimensional two-group static diffusion equation for the CANDU reactor. It is found that for typical CANDU-6 problem, with the standard coarse mesh size, the Analytic Nodal Method yields channel-averaged powers accurate to within about 2% and static reactor eigenvalue accurate to within about 0.02% comparing to a very fine mesh reference solution.

In Chapter 5, the time-dependent Analytic Nodal diffusion equations are derived. The fully implicit time iteration method is employed to solve these equations. An algorithm, which makes use of many of the steady-state iterative procedures, is detailed for solving the three-dimension two-group diffusion equations of space-time kinetics.

Results from CANDU benchmark and typical CANDU-6 model are presented in Chapter 6. These results demonstrate that accurate kinetics solutions are obtained with bundle size spatial meshes. Comparisons with Coarse Mesh Finite Difference Method indicate that the errors Analytic Nodal Method are lower. Thus, the Analytic Nodal Method with flat leakage is a very accurate method for CANDU reactor analysis and design.

Finally, a summary of the conclusions about Analytic Nodal Method, and recommendations for future research are given in Chapter 7.

CHAPTER 1
REVIEW OF THE ANALYTIC NODAL METHOD FOR 3-D STATIC NEUTRON DIFFUSION EQUATION

1.1 Introduction

In this chapter, the derivation of the Analytic Nodal Method for solving the static multigroup diffusion equations is reviewed. Approximations such as flat transverse leakage and the truncation of the matrix exponential will also be presented in this chapter. Throughout the derivation of the Analytic Nodal Method, it is assumed that equivalent homogenized diffusion theory parameters, which are spatially constants over the nodes are available. Therefore, only regions that have constant material properties will be considered. All derivations will be done in three-dimensional Cartesian geometry.

1.2 Neutron Diffusion Theory

In most situations encountered in the analysis of power reactors, it is sufficient to model the neutronic behavior of the reactor by a low order approximation to the formally exact neutron transport equation. The most widely used of these approximations is multigroup neutron diffusion theory. For this model, the set of time- and space- dependent coupled partial differential equations (Henry, 1975) for which approximate solutions are sought can be written as

$$-\nabla\cdot\bar{J}_g(\bar{r},t)-\Sigma_{tg}(\bar{r},t)\phi_g(\bar{r},t)+\sum_{g'=1}^{G}(\Sigma_{g\leftarrow g'}(\bar{r},t)+(1-\beta)\chi_{g_p}\frac{1}{\gamma}\upsilon\Sigma_{fg'}(\bar{r},t))\phi_{g'}(\bar{r},t)$$

$$+\sum_{d=1}^{D}\chi_{g_d}\lambda_d C_d(\bar{r},t)=\frac{1}{v_g}\frac{\partial}{\partial t}\phi_g(\bar{r},t)$$

$$\bar{J}_g(\bar{r},t)=-D_g(\bar{r},t)\bar{\nabla}\phi_g(\bar{r},t)$$

g=1,2,3,...G

$$\beta_d\sum_{g=1}^{G}\frac{\upsilon}{\gamma}\Sigma_{fg}(\bar{r},t)\phi_g(\bar{r},t)-\lambda_d C_d(\bar{r},t)=\frac{\partial}{\partial t}C_d(\bar{r},t) \qquad 1.1$$

d=1,2,3,...D

where

G = total number of neutron energy groups

D = total number of delayed neutron precursor families

C_d = density of delayed neutron precursors in family d (cm^{-3})

D_g = diffusion coefficient for group g (cm)

Σ_{tg} ≡ macroscopic total cross section for group g (cm^{-1})

$\Sigma_{g\leftarrow g'}$ ≡ macroscopic transfer cross section from group g' to group g (cm^{-1})

Σ_{fg} ≡ macroscopic fission cross section for group g (cm^{-1})

ϕ_g = scalar neutron flux in group g (cm^{-2} sec^{-1})

χ_{g_p} ≡ prompt fission neutron spectrum to group g

χ_{g_d} ≡ delayed neutron spectrum for family d in group g

υ = mean number of neutrons emitted per fission

γ = eigenvalue which makes all of the time derivatives identically zero for the initial conditions in the core

λ_d = decay constant for delayed neutron precursor family d (sec^{-1})

β_d = fractional yield of delayed neutron precursors in family d per fission, $(\beta=\sum_{d=1}^{D}\beta_d)$

v_g = neutron velocity for group g (cm sec^{-1})

The fission neutron spectrum is assumed to be that of the predominant fissioning isotope. If the distribution of material properties in space and time, the initial neutron flux distribution in space and energy, and the appropriate boundary conditions are specified, a unique solution to equations 1.1 exists.

The solution to equations 1.1 is usually obtained by first assuming that the reactor is in an initial critical configuration; all of the properties of the reactor are independent of time. Hence all of the time derivatives in equations 1.1 are identically zero. The static solution of the equations 1.1 is obtained by varying the parameter γ (the critical eigenvalue) such that a nontrivial solution positive everywhere to the static multigroup equations exists. The static multigroup equations can be written as

$$-\nabla \cdot \bar{J}_g(\bar{r}) - \Sigma_{tg}(\bar{r})\phi_g(\bar{r}) + \sum_{g'=1}^{G}(\Sigma_{g\leftarrow g'}(\bar{r}) + \chi_{g_p}\frac{1}{\gamma}\upsilon\Sigma_{fg'}(\bar{r}))\phi_{g'}(\bar{r}) = 0 \qquad 1.2$$

$$\bar{J}_g(\bar{r}) = -D_g(\bar{r})\bar{\nabla}\phi_g(\bar{r})$$

g=1,2,3,...G

In principle, the spatial power distribution in a reactor can be determined by applying equations 1.2 and explicitly representing all of the geometrical detail that is present. The geometrical complexity of reactors is such that direct representation of full geometrical heterogeneity is precluded for reasons of practicality. The approach that is generally taken to alleviate this difficulty is to treat large spatial regions, the lattice cell, as homogenized. The actual spatial detail within each of the homogenized regions is treated in an auxiliary calculation, to obtain "equivalent homogenized diffusion theory parameters" which are spatially constant within each region. This homogenization is commonly performed for regions that usually contain one fuel bundle. The full core reactor calculation is thus reduced to that of determining the spatial power distribution within a domain containing several thousand homogenized regions.

1.3 Nodal Balance Equation

The global reactor problem is treated in three-dimensional Cartesian geometry, where x, y, and z represent the three coordinate directions. The reactor core is divided into a number of contiguous rectangular parallelepiped (or nodes), and the nodes are then individually specified by their positions on the coordinate axis. As shown in Fig.1.1, the node widths are easily obtained by taking the appropriate differences along each coordinate axis. We also assume that the nuclear properties (macroscopic cross sections and diffusion coefficients) are spatially constant over each such node.

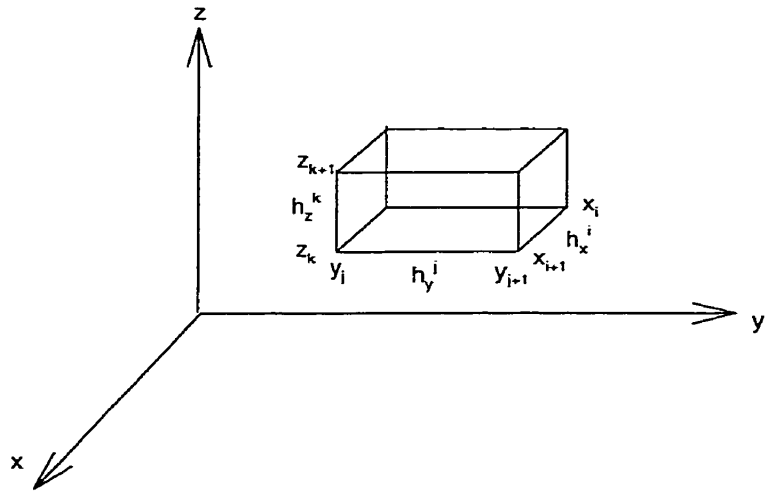

Figure 1.1: Coordinate system

We integrate equations 1.2 over the volume of an arbitrary node (i, j, k). The average flux in the node (i, j, k) is simply

$$\bar{\phi}_{i,j,k} = \frac{1}{h_z^k}\frac{1}{h_y^j}\frac{1}{h_x^i}\int_{z_k}^{z_{k+1}} dz \int_{y_j}^{y_{j+1}} dy \int_{x_i}^{x_{i+1}} dx \; \phi_g(x, y, z) \qquad 1.3$$

We then apply theorem of Gauss to replace the volume integral of the divergence of the neutron current by a surface integral. We get the flux equation,

$$-(\bar{J}_{gx,j,k}(x_{i+1})-\bar{J}_{gx,j,k}(x_i))h_y^j h_z^k-(\bar{J}_{gy,i,k}(y_{j+1})-\bar{J}_{gy,i,k}(y_j))h_x^i h_z^k$$
$$-(\bar{J}_{gz,i,j}(z_{k+1})-\bar{J}_{gz,i,j}(z_k))h_x^i h_y^j-\Sigma_{tg,i,j,k}\bar{\phi}_{g,i,j,k}V_{i,j,k}+\sum_{g'=1}^{G}\Sigma_{g\leftarrow g',i,j,k}\bar{\phi}_{g',i,j,k}V_{i,j,k}$$
$$+\frac{1}{\gamma}\chi^p\sum_{g'=1}^{G}\upsilon\Sigma_{fg',i,j,k}\bar{\phi}_{g',i,j,k}V_{i,j,k}=0 \qquad 1.4$$

in this equation the surface average current over the nodal surface at $x=x_i$ is given by

$$\bar{J}_{gx,j,k}(x_i)=\frac{1}{h_y^j}\frac{1}{h_z^k}\int_{y_j}^{y_{j+1}}dy\int_{z_k}^{z_{k+1}}dzJ_{gx}(x_i,y,z) \qquad 1.5$$

The expressions for the other five surface currents are similar. Equation 1.4 involves nodal average fluxes, and average nuclear properties within node (i,j,k).

The situation is quite different with equation 1.2, which represents the exact neutron balance equation within node (i,j,k). In equation 1.4, relationship between the surface average currents and the volume average fluxes is not known. Modern nodal methods are used to provide these relationships.

1.4 Transverse Integration Procedure

The approach generally taken to obtain the relationships between the surface average currents and volume average fluxes is the transverse integration technique which consists in the integration of the diffusion equation over any two directions simultaneously. This gives rise to a linear system in one dimension, which can be solved to obtain surface average currents in terms of the average fluxes of neighboring nodes. Repeating this process in all three directions in turn will provide expressions for each of the six surface average currents appearing in the nodal balance equation. We illustrate the process for the x direction.

1.4.1 Equation for the Fluxes

Let us integrate equations 1.2 over the direction y and direction z, within the node (i,j,k). In other words, we apply the operator $\frac{1}{h_y^j}\frac{1}{h_z^k}\int_{y_j}^{y_{j+1}}dy\int_{z_k}^{z_{k+1}}dz$ to the equation.

We obtain,

$$
\begin{aligned}
&-\frac{1}{h_y^j}\frac{1}{h_z^k}\int_{y_j}^{y_{j+1}}dy\int_{z_k}^{z_{k+1}}dz\frac{\partial}{\partial x}J_{gx}(x,y,z)-\frac{1}{h_y^j}\frac{1}{h_z^k}\int_{y_j}^{y_{j+1}}dy\int_{z_k}^{z_{k+1}}dz\frac{\partial}{\partial y}J_{gy}(x,y,z)\\
&-\frac{1}{h_y^j}\frac{1}{h_z^k}\int_{y_j}^{y_{j+1}}dy\int_{z_k}^{z_{k+1}}dz\frac{\partial}{\partial z}J_{gz}(x,y,z)-\frac{1}{h_y^j}\frac{1}{h_z^k}\Sigma_{tg,i,j,k}\int_{y_j}^{y_{j+1}}dy\int_{z_k}^{z_{k+1}}dz\phi_g(x,y,z)\\
&+\frac{1}{h_y^j}\frac{1}{h_z^k}\sum_{g'=1}^{G}\Sigma_{g\leftarrow g',i,j,k}\int_{y_j}^{y_{j+1}}dy\int_{z_k}^{z_{k+1}}dz\ \phi_{g'}(x,y,z)\\
&+\frac{1}{\gamma}\frac{1}{h_y^j}\frac{1}{h_z^k}\chi^p\sum_{g'=1}^{G}\upsilon\Sigma_{fg',i,j,k}\int_{y_j}^{y_{j+1}}dy\int_{z_k}^{z_{k+1}}dz\ \phi_{g'}(x,y,z)=0
\end{aligned}
\qquad 1.6
$$

To simplify the equation, we define the following quantities:

- The transverse integrated flux,

$$\phi_{g,i,j,k}(x)\equiv\frac{1}{h_y^j}\frac{1}{h_z^k}\int_{y_j}^{y_{j+1}}dy\int_{z_k}^{z_{k+1}}dz\phi_{g,i,j,k}(x,y,z) \qquad 1.7$$

- The x direction transverse integrated current,

$$J_{gx,i,j,k}(x)\equiv\frac{1}{h_y^j}\frac{1}{h_z^k}\int_{y_j}^{y_{j+1}}dy\int_{z_k}^{z_{k+1}}dzJ_{gx}(x,y,z) \qquad 1.8$$

- The x directed transverse leakage along Y,

$$S_{gy,i,j,k}(x)\equiv\frac{1}{h_y^j}\frac{1}{h_z^k}\int_{z_k}^{z_{k+1}}dz(J_{gy}(x,y_{j+1},z)-J_{gy}(x,y_j,z)) \qquad 1.9$$

- The x directed transverse leakage along Z,

$$S_{gz,i,j,k}(x)\equiv\frac{1}{h_y^j}\frac{1}{h_z^k}\int_{y_j}^{y_{j+1}}dy(J_{gz}(x,y,z_{k+1})-J_{gz}(x,y,z_k)) \qquad 1.10$$

- The net x directed transverse leakage

$$s_{gx,i,j,k}(x) \equiv s_{gy,i,j,k}(x) + s_{gz,i,j,k}(x) \tag{1.11}$$

It is also worthwhile to point out that:

$$\frac{1}{h_x^i}\int_{x_i}^{x_{i+1}} dx\phi_{g,i,j,k}(x) = \bar{\phi}_{g,i,j,k}$$
$$J_{gx,i,j,k}(x_i) = \bar{J}_{gx,i,j,k}(x_i)$$
$$J_{gx,i,j,k}(x_{i+1}) = \bar{J}_{gx,i,j,k}(x_{i+1})$$

With all these definitions, equation 2-6 for node (i, j, k) can be simply written:

$$-\frac{\partial}{\partial x}J_{gx,i,j,k}(x) - S_{gx,i,j,k}(x) - \Sigma_{tg,i,j,k}\,\phi_{g,i,j,k}(x) + \sum_{g'=1}^{G}\Sigma_{g\leftarrow g'}\phi_{g',i,j,k}(x)$$
$$+\frac{1}{\gamma}\chi^p\sum_{g'=1}^{G}\upsilon\Sigma_{fg',i,j,k}\,\phi_{g',i,j,k}(x) = 0 \tag{1.12}$$

By introducing matrix notation, this equation can be written as

$$\frac{\partial}{\partial x}[J_x(x)]_{i,j,k} = -[S_x(x)]_{i,j,k} + [\Sigma]_{i,j,k}[\phi(x)]_{i,j,k} + \frac{1}{\gamma}[\chi^p]\,[\upsilon\Sigma_f]^T_{i,j,k}[\phi(x)]_{i,j,k} \tag{1.13}$$

We define a new matrix $[\Sigma']$

$$[\Sigma'] \equiv [\Sigma] - \frac{1}{\gamma}[\chi^p]\,[\upsilon\Sigma_f]^T \tag{1.14}$$

Finally we get the flux equation

$$\frac{\partial}{\partial x}[J_x(x)]_{i,j,k} + [\Sigma']_{i,j,k}[\phi(x)]_{i,j,k} = -[S_x(x)]_{i,j,k} \tag{1.15}$$

1.4.2 Equation for the Currents

An extra relationship is furnished between these variables by Fick's law, $\vec{J}_g = -D_g\vec{\nabla}\cdot\phi_g$, which we also transverse integrate over directions Y and Z within node (i, j, k),

$$\frac{1}{h_y^j}\frac{1}{h_z^k}\int_{y_j}^{y_{j+1}} dy \int_{z_k}^{z_{k+1}} dz J_{gx}(x,y,z) = -D_{gx}\ \frac{1}{h_y^j}\frac{1}{h_z^k}\int_{y_j}^{y_{j+1}} dy \int_{z_k}^{z_{k+1}} dz \frac{\partial}{\partial x}\phi_g(x,y,z) \qquad 1.16$$

which gives

$$J_{gx,i,j,k}(x) = -D_{gx}\frac{\partial}{\partial x}\phi_{g,i,j,k}(x) \qquad 1.17$$

By introducing matrix notation, we get the current equation,

$$[J_x(x)]_{i,j,k} = -[D_x]_{i,j,k}\frac{\partial}{\partial x}[\phi(x)]_{i,j,k} \qquad 1.18$$

1.4.3 Final Form of the One-dimensional System

We group flux equation and current equation and define the following vectors and matrix,

$$[\psi(x)]_{i,j,k} = \begin{bmatrix} [\phi(x)]_{i,j,k} \\ [J_x(x)]_{i,j,k} \end{bmatrix} \qquad 1.19$$

$$[S'_x(x)]_{i,j,k} = \begin{bmatrix} [0] \\ -[S_x(x)]_{i,j,k} \end{bmatrix} \qquad 1.20$$

$$[N]_{i,j,k} = \begin{bmatrix} [0] & [D_x]^{-1}_{i,j,k} \\ [\Sigma']_{i,j,k} & [0] \end{bmatrix} \qquad 1.21$$

We now have the following simultaneous equation system for the flux and current

$$\frac{\partial}{\partial x}[\psi(x)]_{i,j,k} + [N]_{i,j,k}[\psi(x)]_{i,j,k} = [S_x'(x)]_{i,j,k} \qquad 1.22$$

To obtain relationships between the transverse integrated fluxes and the directed transverse integrated currents, one need only solve the equation 1.22 for $[\psi(x)]_{i,j,k}$. Unfortunately, the x-dependence of the transverse leakage source term on the right hand side of equation 1.22 must be known or approximated if the solution of the equation is to be found. This circumstance makes necessary the first, and the only, approximation of the Analytic Nodal Method.

1.5 Transverse Leakage Approximation

The possibilities for the approximation of the transverse leakage shape in equation 1.22 appear to be unlimited. It seems reasonable to expect that the more complicated the assumed shape, the more difficult it will be to solve equation 1.22. The "flat" approximation and the "quadratic" (Smith, 1979) approximation are the two most commonly used approximations. We illustrate the approximation process for the x direction.

The "flat" approximation assumes the transverse leakage shape as spatially flat across each node, that is,

$$[S_x(x)]_{i,j,k} = [\bar{S}_x]_{i,j,k} \tag{1.23}$$

where $[\bar{S}_x]_{i,j,k}$ is the nodal-averaged, x directed, net transverse leakage. With the definition of x directed net transverse leakage 1.11, we obtain

$$\begin{aligned}\bar{S}_{gx,i,j,k} = &\frac{1}{h_x^i}\frac{1}{h_y^j}\frac{1}{h_z^k}\int_{x_i}^{x_{i+1}} dx \int_{z_k}^{z_{k+1}} dz (J_{gy}(x, y_{j+1}, z) - J_{gy}(x, y_j, z)) \\ &+ \frac{1}{h_x^i}\frac{1}{h_y^j}\frac{1}{h_z^k}\int_{x_i}^{x_{i+1}} dx \int_{y_j}^{y_{j+1}} dy (J_{gz}(x, y, z_{k+1}) - J_{gz}(x, y, z_k))\end{aligned} \tag{1.24}$$

To simplify this equation we define the following quantities:

Nodal face-averaged, x directed, net leakage,

$$[\bar{L}_x]_{i,j,k} = [J_x(x_{i+1})]_{i+1,j,k} - [J_x(x_i)]_{i,j,k} \tag{1.25}$$

Nodal face-averaged, y directed, net leakage,

$$[\bar{L}_y]_{i,j,k} = [J_y(y_{j+1})]_{i,j+1,k} - [J_y(y_j)]_{i,j,k} \tag{1.26}$$

Nodal face-averaged, z directed, net leakage,

$$[\bar{L}_z]_{i,j,k} = [J_z(z_{k+1})]_{i,j,k+1} - [J_z(z_k)]_{i,j,k} \tag{1.27}$$

with all these definitions, equation 1.24 can be written as

$$[\bar{S}_x]_{i,j,k} = \frac{1}{h_y^j}[\bar{L}_y]_{i,j,k} + \frac{1}{h_z^k}[\bar{L}_z]_{i,j,k} \quad 1.28$$

"Quadratic" approximation assumes the spatial shape of the transverse leakage can be fit by quadratic polynomials in each node, that is,

$$[S_x(x)]_{i,j,k} \equiv [\bar{S}_x]_{i-1,j,k}\rho_{x_i}^{i-1}(x) + [\bar{S}_x]_{i,j,k}\rho_{x_i}^{i}(x) + [\bar{S}_x]_{i+1,j,k}\rho_{x_i}^{i+1}(x) \quad 1.29$$

where each of the ρ is a quadratic polynomial in x, $[\bar{S}_x]_{i-1,j,k}, [\bar{S}_x]_{i,j,k}, [\bar{S}_x]_{i+1,j,k}$ are the average net x directed transverse leakages in three adjacent nodes.

In earlier work (Smith, 1979), it was found that the Analytic Nodal Method with "quadratic" approximation could obtain more accurate results for LWR analysis. However our current approach is that, for CANDU analysis the flat leakage approximation should be sufficiently accurate.

1.6 Method for Solving the Spatial Coupling Equations with Flat Transverse Leakage Approximation

In Analytic Nodal Method, the spatial coupling equation 1.22 is solved analytically. The flat approximation version of 1.22 is

$$\frac{\partial}{\partial x}[\psi(x)]_{i,j,k} + [N]_{i,j,k}[\psi(x)]_{i,j,k} = [\bar{S}'_x]_{i,j,k} \quad 1.30$$

and the solution of this equation can be written formally as

$$[\psi(x)]_{i,j,k} = \exp(-[N]_{i,j,k}x)[A] + [N]_{i,j,k}^{-1}[\bar{S}'_x]_{i,j,k} \quad 1.31$$

where the solution of the vector [A] is arbitrary, but can be determined by the choice of initial conditions chosen for [ø]. If we chose as initial condition the value of φ at $x = x_i$, we will have

$$[\psi(x_i)]_{i,j,k} = \exp(-[N]_{i,j,k}x_i)[A] + [N]_{i,j,k}^{-1}[\bar{S}'_x]_{i,j,k} \quad 1.32$$

and then

$$[A]=\exp([N]_{i,j,k}x_i)\Big\langle\ [\psi(x_i)]_{i,j,k}-[N]^{-1}_{i,j,k}[\bar{S}'_x]_{i,j,k}\ \Big\rangle \tag{1.33}$$

and it follows that

$$\begin{aligned}[\psi(x)]_{i,j,k} &= \exp(-[N]_{i,j,k}(x-x_i))[\psi(x_i)]_{i,j,k}\\ &+[N]^{-1}_{i,j,k}\Big\langle\ [I]-\exp(-[N]_{i,j,k}(x-x_i)\ \Big\rangle[\bar{S}'_x]_{i,j,k}\end{aligned} \tag{1.34}$$

on the other hand, if we chose as initial condition the value of ø at $x=x_{i+1}$,we will have

$$\begin{aligned}[\psi(x)]_{i,j,k} &= \exp([N]_{i,j,k}(x_{i+1}-x))[\psi(x_{i+1})]_{i,j,k}\\ &+[N]^{-1}_{i,j,k}\Big\langle\ [I]-\exp([N]_{i,j,k}(x_{i+1}-x)\ \Big\rangle[\bar{S}'_x]_{i,j,k}\end{aligned} \tag{1.35}$$

In order to close the nodal balance equations, we have to find a relationship between the surface average fluxes and currents of each node. To get it we integrate equation 1.34 and 1.35 over x and divide by the width h^i_x of node (i,j,k). We find after integration,

$$\begin{aligned}[\bar{\psi}]_{i,j,k} &= \frac{1}{h^i_x}[N]^{-1}_{i,j,k}\Big\langle\ [I]-\exp(-[N]_{i,j,k}h^i_x)\ \Big\rangle[\psi(x_i)]_{i,j,k}\\ &+\frac{1}{h^i_x}[N]^{-1}_{i,j,k}\Big\langle\ h^i_x[I]-[N]^{-1}_{i,j,k}([I]-\exp(-[N]_{i,j,k}h^i_x)\ \Big\rangle[\bar{S}'_x]_{i,j,k}\end{aligned} \tag{1.36}$$

and

$$\begin{aligned}[\bar{\psi}]_{i,j,k} &= \frac{1}{h^i_x}[N]^{-1}_{i,j,k}\Big\langle\ -[I]+\exp([N]_{i,j,k}h^i_x)\ \Big\rangle[\psi(x_{i+1})]_{i,j,k}\\ &+\frac{1}{h^i_x}[N]^{-1}_{i,j,k}\Big\langle\ h^i_x[I]-[N]^{-1}_{i,j,k}(-[I]+\exp([N]_{i,j,k}h^i_x)\ \Big\rangle[\bar{S}'_x]_{i,j,k}\end{aligned} \tag{1.37}$$

We rewrite the equation 1.37 for the node $(i-1,j,k)$

$$[\overline{\psi}]_{i-1,j,k} = \frac{1}{h_x^{i-1}}[N]^{-1}_{i-1,j,k}\left\langle\ -[I]+\exp([N]_{i-1,j,k}h_x^{i-1})\ \right\rangle[\psi(x_i)]_{i-1,j,k}$$
$$+\frac{1}{h_x^{i-1}}[N]^{-1}_{i-1,j,k}\left\langle\ h_x^{i-1}[I]-[N]^{-1}_{i-1,j,k}(-[I]+\exp([N]_{i-1,j,k}h_x^{i-1})\ \right\rangle[\overline{S}_x]_{i-1,j,k} \quad 1.38$$

Since equation 1.36 and equation 1.38 are expressed in terms of $[\psi(x_i)]_{i,j,k}$ and $[\psi(x_i)]_{i-1,j,k}$, and these two terms are identical. Thus, it is possible to find a relationship between node-averaged fluxes, face-averaged net leakages, and $[J_x(x_i)]_{i,j,k}$.

The procedure can be repeated to derive a relationship between node-averaged fluxes, face-averaged net leakages, and $[J_x(x_{i+1})]_{i+1,j,k}$. Taking the difference of these last two relationships into equation 1.25 finally allows us to obtain an equation relating node-averaged fluxes and face- averaged net leakages.

The final equation relating node-averaged fluxes and face-averaged net leakages for x direction can be expressed in the form

$$[\overline{L}_x]_{i,j,k} = [F_x^{i-1}]_{i,j,k}[\overline{\phi}]_{i-1,j,k} + [F_x^{i}]_{i,j,k}[\overline{\phi}]_{i,j,k} + [F_x^{i+1}]_{i,j,k}[\overline{\phi}]_{i+1,j,k}$$
$$+[G_x^{i-1}]_{i,j,k}[\overline{S}_x]_{i-1,j,k} + [G_x^{i}]_{i,j,k}[\overline{S}_x]_{i,j,k} + [G_x^{i+1}]_{i,j,k}[\overline{S}_x]_{i+1,j,k} \quad 1.39$$

This equation reveals that x directed net leakage is coupled to node-averaged fluxes in three adjacent nodes in the x direction, as well as to the transverse leakage in three adjacent nodes.

A similar approach can be followed for the other two directions. Finally we obtain three equations of net leakages. With the neutron balance equation, the resulting super-matrix equation (Smith, 1979) can be written as

$$\begin{bmatrix} [\Sigma_T] & h_y^j h_z^k [I] & h_x^i h_z^k [I] & h_x^i h_y^j [I] \\ [F_x] & -[I] & \frac{1}{h_y^j}[G_x] & \frac{1}{h_z^k}[G_x] \\ [F_y] & \frac{1}{h_x^i}[G_y] & -[I] & \frac{1}{h_z^k}[G_y] \\ [F_z] & \frac{1}{h_x^i}[G_z] & \frac{1}{h_y^j}[G_z] & -[I] \end{bmatrix} \begin{bmatrix} [\bar{\phi}] \\ [\bar{L}_x] \\ [\bar{L}_y] \\ [\bar{L}_z] \end{bmatrix} = \frac{1}{\gamma} \begin{bmatrix} [M] & [0] & [0] & [0] \\ [0] & [0] & [0] & [0] \\ [0] & [0] & [0] & [0] \\ [0] & [0] & [0] & [0] \end{bmatrix} \begin{bmatrix} [\bar{\phi}] \\ [\bar{L}_x] \\ [\bar{L}_y] \\ [\bar{L}_z] \end{bmatrix} \qquad 1.40$$

where

$[\bar{\phi}] \equiv$ a column vector of length G x I x J x K (= N) containing the node-averaged fluxes (ordered first by group, then X direction, then Y direction, and finally Z direction).

$[\bar{L}_u] \equiv$ a column vector of length N containing the u-direction net leakage, $u = x, y, z$.

$[F_u] \equiv$ a block tridiagonal matrix of order N x N containing the elements of $[F_u^{l'}]_{i,j,k}$, $u = x, y, z$, $l' = i-1, i, i+1, j-1, j, j+1, k-1, k, k+1$.

$[G_u] \equiv$ a block tridiagonal matrix of order N x N containing the elements of $[G_u^{l'}]_{i,j,k}$, $u = x, y, z$, $l' = i-1, i, i+1, j-1, j, j+1, k-1, k, k+1$.

$[\Sigma_T] \equiv$ a block diagonal matrix of order N x N containing the elements of $V_{i,j,k}[\Sigma]_{i,j,k}$.

$[M] \equiv$ a block diagonal matrix of order N x N containing the elements of $V_{i,j,k}[\upsilon \Sigma_f]_{i,j,k}$.

The global reactor equation as expressed in equation 1.40 can be cast the form of a classical eigenvalue problem,

$$[A]^{-1}[B]\,[X] = \gamma[X]$$

except for the fact that the elements of [A] depend on the eigenvalue γ.

Equation 1.40 forms the basis of the Analytic Nodal Method with flat transverse leakage approximation. These equations, along with the appropriate boundary conditions applied to the reactor surface, fully specify the global system of static nodal diffusion equations.

1.7 Evaluation of Spatial Coupling Matrix

The actual application of the Analytic Nodal Method requires evaluation of the matrices defined in equation 1.39. Each of these matrices is a G x G matrix whose elements depend on the properties of a single node. The essential difficulty in evaluating these matrices stems from the fact that the exponential of $[N_{i,j,k}]$, as defined in equation 1.36, must be evaluated. $[N_{i,j,k}]$ is a block antidiagonal with its lower block being partially comprised of the G x G group-to group scattering matrix. In the general multigroup case, it is not apparent how to obtain this exponential.

If the number of neutron energy groups is restricted to a small number, direct evaluation of the matrices becomes feasible. Since two-group diffusion theory is commonly used for normal reactor analysis, we evaluate these matrices directly.

The Analytic Nodal Method uses the analytic solution of one-dimensional, source-free, two-group, diffusion equation for a homogeneous region to evaluate the exponential. The procedure is detailed in (Smith, 1979). The final results show that all the matrices depend on the eigenvalue of the global static reactor problem.

1.8 The Coarse Mesh Finite Difference Approximation

The first approximation leading to the Coarse Mesh Finite Difference is to neglect the transverse leakage terms of $[\bar{S}_x]_{i,j,k}$ *and* $[\bar{S}_x]_{i-1,j,k}$ on expressions 1.36 and 1.38. This hypothesis may be questionable, but detailed calculations using nodal methods show that these transverse leakages are comparatively small in comparison to the fluxes (Koclas, 1998).

The other approximation leading to the Coarse Mesh Finite Difference consists in blocking the series expansion of the matrix exponentials of expression 1.36 and of 1.38 to linear terms in x. Therefore

$$[\bar{\psi}]_{i,j,k} \approx \left\langle [I] - \frac{h_x^i}{2}[N]_{i,j,k} \right\rangle [\psi(x_i)]_{i,j,k} \qquad 1.41$$

$$[\bar{\psi}]_{i-1,j,k} \approx \left\langle [I] + \frac{h_x^{i-1}}{2}[N]_{i-1,j,k} \right\rangle [\psi(x_i)]_{i-1,j,k} \qquad 1.42$$

The flux parts of 1.41 and of 1.42 are

$$[\bar{\phi}]_{i,j,k} = [\phi(x_i)]_{i,j,k} - \frac{h_x^i}{2}[D_x]^{-1}_{i,j,k}[J_x(x_i)]_{i,j,k} \qquad 1.43$$

$$[\bar{\phi}]_{i-1,j,k} = [\phi(x_i)]_{i-1,j,k} + \frac{h_x^{i-1}}{2}[D_x]^{-1}_{i-1,j,k}[J_x(x_i)]_{i-1,j,k} \qquad 1.44$$

We take the difference between 1.43 and 1.44, and use flux and current continuity to find

$$[J_x(x_i)]_{i,j,k} = -(\frac{h_x^i}{2}[D_x]^{-1}_{i,j,k} + \frac{h_x^{i-1}}{2}[D_x]^{-1}_{i-1,j,k})^{-1}([\bar{\phi}]_{i,j,k} - [\bar{\phi}]_{i-1,j,k}) \qquad 1.45$$

which gives the relationship between a surface average current and the average fluxes of the two nodes delimited by the surface. An identical calculation for the node $(i+1, j, k)$ gives the result

$$[J_x(x_{i+1})]_{i,j,k} = -(\frac{h_x^{i+1}}{2}[D_x]^{-1}_{i+1,j,k} + \frac{h_x^i}{2}[D_x]^{-1}_{i,j,k})^{-1}([\bar{\phi}]_{i+1,j,k} - [\bar{\phi}]_{i,j,k}) \quad 1.46$$

A similar approach can be done for the other two directions. We substitute all these results to the neutron balance equation 1.4, to obtain

$$\begin{aligned}
&h_y^j h_z^k (\frac{h_x^{i+1}}{2} D^{-1}_{gx,i+1,j,k} + \frac{h_x^i}{2} D^{-1}_{gx,i,j,k})^{-1} \bar{\phi}_{g,i+1,j,k} + h_y^j h_z^k (\frac{h_x^i}{2} D^{-1}_{gx,i,j,k} + \frac{h_x^{i-1}}{2} D^{-1}_{gx,i-1,j,k})^{-1} \bar{\phi}_{g,i-1,j,k} \\
&+ h_x^i h_z^k (\frac{h_y^{j+1}}{2} D^{-1}_{gy,i,j+1,k} + \frac{h_y^j}{2} D^{-1}_{gy,i,j,k})^{-1} \bar{\phi}_{g,i,j+1,k} + h_x^i h_z^k (\frac{h_y^j}{2} D^{-1}_{gy,i,j,k} + \frac{h_y^{j-1}}{2} D^{-1}_{gy,i,j-1,k})^{-1} \bar{\phi}_{g,i,j-1,k} \\
&+ h_x^i h_y^j (\frac{h_z^{k+1}}{2} D^{-1}_{gz,i,j,k+1} + \frac{h_z^k}{2} D^{-1}_{gz,i,j,k})^{-1} \bar{\phi}_{g,i,j,k+1} + h_x^i h_y^j (\frac{h_z^k}{2} D^{-1}_{gz,i,j,k} + \frac{h_z^{k-1}}{2} D^{-1}_{gz,i,j,k-1})^{-1} \bar{\phi}_{g,i,j,k-1} \\
&+ \begin{pmatrix}
-h_y^j h_z^k (\frac{h_x^{i+1}}{2} D^{-1}_{gx,i+1,j,k} + \frac{h_x^i}{2} D^{-1}_{gx,i,j,k})^{-1} \\
-h_y^j h_z^k (\frac{h_x^i}{2} D^{-1}_{gx,i,j,k} + \frac{h_x^{i-1}}{2} D^{-1}_{gx,i-1,j,k})^{-1} \\
-h_x^i h_z^k (\frac{h_y^{j+1}}{2} D^{-1}_{gy,i,j+1,k} + \frac{h_y^j}{2} D^{-1}_{gy,i,j,k})^{-1} \\
-h_x^i h_z^k (\frac{h_y^j}{2} D^{-1}_{gy,i,j,k} + \frac{h_y^{j-1}}{2} D^{-1}_{gy,i,j-1,k})^{-1} \\
-h_x^i h_y^j (\frac{h_z^{k+1}}{2} D^{-1}_{gz,i,j,k+1} + \frac{h_z^k}{2} D^{-1}_{gz,i,j,k})^{-1} \\
-h_x^i h_y^j (\frac{h_z^k}{2} D^{-1}_{gz,i,j,k} + \frac{h_z^{k-1}}{2} D^{-1}_{gz,i,j,k-1})^{-1}
\end{pmatrix} \bar{\phi}_{g,i,j,k} - \Sigma_{tg} \bar{\phi}_{g,i,j,k} V_{i,j,k} + \sum_{g'=1}^{G} \Sigma_{g \leftarrow g',i,j,k} \bar{\phi}_{g'} V_{i,j,k} \\
&+ \frac{1}{\gamma} \chi_g^p \sum_{g'=1}^{G} \upsilon \Sigma_{fg'} \bar{\phi}_{g'} V_{i,j,k} = 0
\end{aligned} \quad 1.47$$

We write equation 1.47 in matrix form,

$$[F]\,[\phi] = \frac{1}{\gamma}[M]\,[\phi] \quad 1.48$$

which is the form of a generalized eigenvalue problem, and the elements [F] and [M] depend on the size of the mesh and the properties of the material. The kinetic distortion term does not appear.

Equation 1.47 is the standard Coarse Mesh Finite Difference equation. The derivation illustrates that the Coarse Mesh Finite Difference approximation is the lowest order of all nodal methods (Koclas, 1998).

1.9 Boundary Conditions

The application of boundary conditions on the surface of the reactor slightly alters form of equation 1.39. Application of a zero current boundary condition on the $x_i = 0$ surface node (i, j, k) implies that the analogue equation to 1.25 is

$$[\bar{L}_x]_{i.j.k} = [J_x(x_{i+1})]_{i+1.j.k} \qquad 1.49$$

Albedo boundary conditions are also permitted. The particular form of the albedo is

$$[\phi(x_i)]_{i.j.k} = [\alpha]\ [J_x(x_i)]_{i.j.k} \qquad 1.50$$

where [α] is a G x G matrix.. The zero flux boundary condition is applied by setting [α] equal to the null matrix. An extrapolated flux (logarithmic derivative) approximation to a zero incoming current boundary condition for the two-group problem is achieved by setting

$$[\alpha] = \begin{bmatrix} 3d\,\Sigma_{tr1} & 0 \\ 0 & 3d\,\Sigma_{tr2} \end{bmatrix} \qquad 1.51$$

where d is the extrapolation distance and $\Sigma_{tr\ g}$ is the macroscopic transport cross section of each group g.

1.10 Summary

In this chapter, the complete derivation of nodal diffusion equations from multigroup diffusion theory has been reviewed. The only approximation that is necessary for the Analytic Nodal Method is the spatial shape of the transverse leakage within a node. The resulting equations were written in terms of node-averaged fluxes and face-

averaged net leakages. The final super matrix equation is of the form of a classical eigenvalue problem. If we introduce linear expansions for all terms, we can get the Coarse Mesh Finite Difference equation from the nodal method. It shows that the Coarse Mesh Finite Difference method is a lowest nodal method.

In Appendix 2, we will introduce the Coarse Mesh Finite Difference Method with flat transverse leakage approximation, the results of this kind of approximation will also be presented. In Chapter 2, we will discuss the numerical methods of Coarse Mesh Finite Difference Method used in the code NDF. The applications of this method to the CANDU benchmark problems and to typical CANDU-6 problems will be presented in Chapter 2 too. In Chapter 3, we will discuss the numerical considerations of Analytic Nodal Method.

CHAPTER 2
DESCRIPTION OF THE COARSE MESH FINITE DIFFERENCE METHOD IN THE CODE NDF AND STATIC APPLICATIONS

2.1 Introduction

In Chapter 1, the spatially-discretized static nodal diffusion equations for Analytic Nodal Method were derived from the solution of multigroup diffusion equations. Based on some approximations, the Coarse Mesh Finite Difference equation can be obtained. Because of the large migration area in a heavy-water system, Coarse Mesh Finite Difference method (CMFD) is generally considered sufficient and has been used extensively for CANDU analysis in the past 30 years. In this chapter, results from application of Coarse Finite Difference Method to two-group three-dimensional typical CANDU-6 problem are presented. Throughout this chapter, the effect of mesh size is indicated.

2.2 Coarse Mesh Finite Difference Method in the NDF Code

The NDF computer code has been developed to perform complicated static and dynamic calculations related to control and safety simulations of CANDU-6 reactor. (Kaveh et al. 1999). The computer code NDF can handle static and dynamic calculations using the Coarse Mesh Finite Difference method and now also with Analytic Nodal Method.

NDF is written in FORTRAN 77 language. The code was compiled under the Visual Fortran 5.0 compiler with full optimization and in single precision. The macroscopic

cross-section used by NDF can be provided by the input file or by the DRAGON/DONJON (Marleau et al.,1993, 1994; Roy et al., 1994) code.

The Coarse Mesh Finite Difference equation 1.48 can be solved by using the general iterative scheme in the NDF code

1. The components of matrix [F] are evaluated by the coupling coefficient calculation module.
2. An accelerated fission source (outer) iteration is employed to determine iteratively the maximum eigenvalue and the corresponding eigenvector.
3. The modified block Gauss-Seidel or successive over-relaxation iteration method is used for flux iteration.
4. The iteration continues until both the convergence criterions on node-averaged fluxes and on eigenvalue are attained.
5. The fluxes are normalized and collapsed into coarse mesh arrangement.

2.3 Mesh Size Effect for the Typical CANDU-6 Problem

One disadvantage of the Coarse Mesh Finite Difference Method is that obtaining an acceptable degree of accuracy in the flux calculations requires small mesh size. Within a typical CANDU-6 reactor, the natural choice for the numerical mesh spacing is the channel lattice pitch and the bundle length, i.e., 28.575 x 28.575 x 49.53 cm in x, y and z directions respectively . At present, the number of meshes used for the CANDU-6 problem is 26 x 26 x 12. The details of this problem are shown in Section A1.3 of Appendix 1. We use finer mesh (number of mesh points double or triple or more those in the original coarse mesh in x, y and z directions) to study the sensitivity of typical CANDU-6 problem on mesh spacing.

The following mesh-spacing were selected for x, y and z directions

1. Normal lattices in x, y and z direction, the number of meshes is 26 x 26 x 12.

2. Normal lattices in x and y directions, spacing uniformly refined by a factor of 2 in z direction, the number of meshes is 26 x 26 x 24.
3. All mesh spacing uniformly refined by a factor of 2 in x, y and z direction, the number of meshes is 52 x 52 x 24.
4. All mesh spacing uniformly refined by a factor of 3 in x, y and z direction, the number of meshes is 78 x 78 x 36.
5. All mesh spacing uniformly refined by a factor of 4 in x, y and z direction, the number of meshes is 104 x 104 x 48.

To evaluate the influence of mesh spacing, calculations for the above 5 different mesh spacing were carried out by the NDF code. The convergence criterion of flux is 10^{-5}. The results are summarized in Table 2.1. These results indicate that more iterations and CPU time are required for fine-mesh calculation than for coarse-mesh calculation. A comparison of the coarse-mesh results (26 x 26 x 12) with the fine-mesh results indicates that small differences appear in absolute eigenvalues and in maximum channel (1-2%) and bundle powers (1-2%).

Figures 2.1 to 2.4 show the percent changes introduced in channel power densities by mesh size effect. It should be noted that the high channel powers in the core center obtained by the coarse mesh size (26 x 26 x 12) are not conservative, because the differences of some meshes are positive but are negative of the other meshes.

2.4 Summary

In this chapter, the Coarse Finite Difference Method used in NDF code and the results of typical CANDU-6 model from this code were presented. The Coarse Mesh Finite Difference Method was shown to be a significant method for solving the

multidimensional, two-group static diffusion equation. It was also demonstrated this method could achieve high accuracy by fine mesh size.

In Chapter 1, the Coarse Mesh Finite Difference equation could be obtained from the Analytic Nodal equations based on some approximations. Without these approximations, the results are expected to be more accurate. Hence, in Chapter 3 and Chapter 4 the Analytic Nodal Method and the applications will be presented.

Table 2.1: Summary of results from different mesh size for CMFD method

Case	Meshes			Eigenvalue	Max. channel power	Max. bundle power	Oute iterations
	X	Y	Z				
1	104	104	48	1.03057	1.2495(F,15)	1.8461(E12,7)	229
2	78	78	36	1.03053	1.2493(F,15)	1.8376(E12,7)	191
3	52	52	24	1.03071	1.2503(F,15)	1.8398(E12,7)	155
4	26	26	24	1.03055	1.2542(E,14)	1.8566(E12,6)	120
5	26	26	12	1.03067	1.2549(E,14)	1.8528(E12,6)	91

	1	2	3	4	5	6	7	8	9	10	11	12	13	14	15	16	17	18	19	20	21	22
A									-0.06	-0.02	-0.06	-0.08	-0.06	-0.13								
B						-0.02	0.04	0.06	0.16	0.16	0.14	0.12	0.12	0.09	-0.04	-0.08	-0.16					
C					0.07	0.24	0.23	0.21	0.18	0.15	0.13	0.12	0.10	0.11	0.11	0.10	0.09	-0.11				
D				0.06	0.26	0.26	0.22	0.20	0.17	0.13	0.12	0.10	0.08	0.08	0.09	0.09	0.10	0.08	-0.14			
E			-0.01	0.24	0.26	0.23	0.20	0.17	0.14	0.10	0.08	0.06	0.05	0.06	0.06	0.06	0.06	0.07	0.04	-0.23		
F			0.10	0.24	0.23	0.19	0.15	0.10	0.04	-0.01	-0.04	-0.06	-0.07	-0.05	-0.02	0.00	0.02	0.03	0.03	-0.13		
G		-0.05	0.20	0.21	0.20	0.15	0.09	0.05	0.01	-0.03	-0.05	-0.07	-0.09	-0.09	-0.08	-0.06	-0.03	-0.01	-0.01	-0.04	**-0.30**	
H		0.09	0.22	0.19	0.18	0.12	0.06	0.02	-0.03	-0.07	-0.10	-0.12	-0.13	-0.13	-0.11	-0.10	-0.06	-0.03	-0.04	-0.03	-0.17	
J	-0.02	0.19	0.21	0.17	0.16	0.07	0.01	-0.04	-0.07	-0.11	-0.14	-0.16	-0.17	-0.17	-0.17	-0.16	-0.12	-0.06	-0.06	-0.04	-0.07	-0.30
K	0.03	0.21	0.20	0.15	0.13	0.04	-0.01	-0.05	-0.10	-0.14	-0.17	-0.19	-0.21	-0.20	-0.19	-0.18	-0.16	-0.09	-0.08	-0.06	-0.05	-0.25
L	0.00	0.20	0.19	0.16	0.15	0.07	0.00	-0.06	-0.12	-0.16	-0.18	-0.21	-0.23	-0.22	-0.20	-0.17	-0.13	-0.06	-0.07	-0.06	-0.06	-0.28
M	0.00	0.20	0.20	0.17	0.15	0.07	0.00	-0.06	-0.12	-0.17	-0.20	-0.22	-0.23	-0.22	-0.20	-0.17	-0.13	-0.07	-0.07	-0.05	-0.06	-0.28
N	0.02	0.21	0.20	0.17	0.15	0.06	0.00	-0.05	-0.11	-0.16	-0.19	-0.21	-0.22	-0.21	-0.19	-0.16	-0.13	-0.07	-0.06	-0.05	-0.05	-0.25
O	-0.04	0.18	0.20	0.18	0.17	0.08	0.01	-0.04	-0.09	-0.13	-0.14	-0.16	-0.18	-0.18	-0.17	-0.15	-0.10	-0.04	-0.05	-0.04	-0.07	-0.30
P		0.06	0.19	0.16	0.14	0.08	0.03	-0.01	-0.06	-0.10	-0.12	-0.14	-0.15	-0.15	-0.14	-0.12	-0.09	-0.06	-0.05	-0.04	-0.18	
Q		-0.10	0.15	0.15	0.14	0.09	0.03	-0.01	-0.04	-0.07	-0.10	-0.12	-0.12	-0.12	-0.12	-0.11	-0.08	-0.04	-0.05	-0.08	-0.33	
R			0.02	0.16	0.16	0.10	0.07	0.04	-0.02	-0.05	-0.07	-0.08	-0.10	-0.09	-0.07	-0.07	-0.06	-0.02	-0.04	-0.19		
S			-0.10	0.14	0.17	0.12	0.11	0.10	0.09	0.05	0.04	0.03	0.01	0.01	0.00	-0.01	-0.02	0.00	-0.04	-0.30		
T				-0.03	0.18	0.18	0.14	0.12	0.10	0.07	0.06	0.05	0.03	0.03	0.03	0.03	0.04	0.03	-0.20			
U					-0.03	0.16	0.16	0.14	0.11	0.08	0.06	0.05	0.04	0.05	0.05	0.05	0.03	-0.18				
V						-0.11	-0.04	-0.02	0.09	0.10	0.09	0.07	0.06	0.03	-0.09	-0.14	-0.23					
W									-0.14	-0.09	-0.14	-0.15	-0.13	-0.19								

The maximum percent change is shown in bold character

Figure 2.1: Relative percent change of channel power introduced by mesh spacing (104 x104 x 48 vs 78 x 78 x 36)

	1	2	3	4	5	6	7	8	9	10	11	12	13	14	15	16	17	18	19	20	21	22
A									-0.68	-0.55	-0.74	-0.76	-0.62	-0.80								
B						-0.68	-0.41	-0.29	0.07	0.11	-0.02	-0.05	0.03	-0.06	-0.47	-0.63	-0.94					
C					-0.46	0.17	0.25	0.23	0.23	0.21	0.07	0.04	0.12	0.09	0.05	0.02	-0.10	-0.77				
D				-0.38	0.22	0.28	0.30	0.29	0.28	0.29	0.13	0.09	0.20	0.13	0.09	0.05	-0.01	-0.11	-0.74			
E			-0.58	0.25	0.29	0.29	0.32	0.34	0.35	0.37	0.19	0.16	0.27	0.19	0.13	0.07	-0.02	-0.06	-0.12	-0.98		
F			-0.19	0.32	0.26	0.28	0.26	0.29	0.11	0.12	0.00	-0.03	0.01	-0.05	0.07	-0.01	-0.04	-0.10	-0.07	-0.61		
G		-0.67	0.19	0.33	0.24	0.27	0.22	0.26	0.18	0.19	0.18	0.14	0.08	0.00	0.02	-0.06	-0.06	-0.13	-0.07	-0.24	-1.13	
H		-0.20	0.30	0.36	0.23	0.27	0.28	0.31	0.23	0.22	0.22	0.18	0.11	0.05	0.07	-0.01	-0.07	-0.15	-0.06	-0.14	-0.66	
J	-0.61	0.15	0.30	0.36	0.23	0.19	0.23	0.25	0.25	0.26	0.23	0.20	0.14	0.07	0.01	-0.07	-0.16	-0.16	-0.06	-0.15	-0.32	-1.10
K	-0.47	0.20	0.27	0.34	0.13	0.09	0.24	0.27	0.28	0.28	0.20	0.16	0.16	0.09	0.02	-0.07	-0.27	-0.27	-0.09	-0.18	-0.28	-0.96
L	-0.58	0.15	0.25	0.33	0.24	0.20	0.24	0.27	0.28	0.29	0.15	0.11	0.17	0.09	0.02	-0.07	-0.15	-0.16	-0.10	-0.21	-0.33	-1.07
M	-0.59	0.14	0.24	0.31	0.22	0.18	0.21	0.25	0.26	0.28	0.14	0.10	0.16	0.08	0.00	-0.09	-0.18	-0.18	-0.12	-0.22	-0.33	-1.07
N	-0.50	0.16	0.24	0.29	0.19	0.14	0.18	0.22	0.23	0.23	0.09	0.05	0.12	0.04	-0.02	-0.12	-0.20	-0.20	-0.13	-0.21	-0.30	-0.98
O	-0.66	0.10	0.24	0.29	0.26	0.21	0.14	0.17	0.18	0.18	0.16	0.12	0.07	0.00	-0.06	-0.15	-0.13	-0.12	-0.12	-0.20	-0.36	**-1.13**
P		-0.28	0.22	0.26	0.11	0.14	0.18	0.20	0.12	0.11	0.11	0.07	0.01	-0.05	-0.02	-0.10	-0.18	-0.25	-0.14	-0.20	-0.72	
Q		-0.78	0.09	0.24	0.08	0.11	0.12	0.13	0.04	0.04	0.04	0.00	-0.05	-0.12	-0.08	-0.14	-0.20	-0.26	-0.13	-0.31	-1.20	
R			-0.30	0.23	0.06	0.08	0.16	0.15	-0.04	-0.05	-0.11	-0.14	-0.14	-0.19	-0.05	-0.09	-0.20	-0.26	-0.13	-0.69		
S			-0.71	0.15	0.04	0.05	0.19	0.19	0.17	0.18	-0.01	-0.03	0.09	0.04	0.00	-0.03	-0.21	-0.26	-0.19	-1.07		
T				-0.49	0.12	0.17	0.15	0.12	0.09	0.09	-0.09	-0.12	0.01	-0.03	-0.05	-0.06	-0.08	-0.16	-0.80			
U					-0.59	0.03	0.07	0.05	0.03	0.01	-0.20	-0.22	-0.06	-0.08	-0.11	-0.12	-0.20	-0.85				
V						-0.86	-0.62	-0.50	-0.13	-0.08	-0.16	-0.18	-0.14	-0.24	-0.64	-0.80	-1.08					
W									-0.91	-0.77	-0.91	-0.93	-0.83	-1.00								

The maximum percent change is shown in bold character

Figure 2.2: Relative percent change of channel power introduced by mesh spacing (104 x104 x 48 vs 52 x 52 x 24)

	1	2	3	4	5	6	7	8	9	10	11	12	13	14	15	16	17	18	19	20	21	22
A									-0.48	-0.21	-0.70	-0.74	-0.31	-0.65								
B						-0.58	0.01	0.43	1.45	1.40	1.07	1.03	1.29	1.27	0.18	-0.30	-0.94					
C					0.06	1.65	1.61	1.53	1.48	1.35	1.12	1.08	1.22	1.29	1.26	1.28	1.27	-0.38				
D				0.08	1.74	1.66	1.50	1.40	1.29	1.16	0.80	0.75	1.03	1.08	1.12	1.15	1.25	1.28	-0.42			
E			-0.61	1.64	1.60	1.38	1.32	1.27	1.18	1.07	0.65	0.60	0.93	0.96	0.97	0.95	0.95	1.11	1.11	-1.17		
F			0.26	1.47	1.22	0.98	0.69	0.46	-0.36	-0.58	-0.92	-0.97	-0.72	-0.59	0.15	0.30	0.53	0.71	0.92	-0.33		
G		-1.17	1.16	1.27	0.98	0.69	0.07	-0.09	-0.47	-0.56	-0.59	-0.64	-0.71	-0.72	-0.42	-0.33	0.22	0.46	0.69	0.54	**-1.80**	
H		0.12	1.18	1.00	0.59	0.26	-0.10	-0.21	-0.61	-0.74	-0.82	-0.87	-0.90	-0.86	-0.55	-0.52	-0.23	0.05	0.41	0.55	-0.53	
J	-0.88	1.04	1.06	0.85	0.44	-0.33	-0.63	-0.72	-0.89	-0.98	-1.13	-1.18	-1.14	-1.15	-1.07	-1.06	-0.83	-0.12	0.24	0.41	0.36	-1.56
K	-0.61	0.98	0.88	0.63	-0.07	-0.82	-0.76	-0.81	-1.03	-1.15	-1.39	-1.45	-1.32	-1.29	-1.16	-1.20	-1.32	-0.64	0.02	0.23	0.30	-1.30
L	-0.94	0.85	0.86	0.77	0.46	-0.26	-0.62	-0.80	-1.08	-1.24	-1.56	-1.62	-1.41	-1.35	-1.16	-1.06	-0.77	-0.11	0.15	0.21	0.16	-1.63
M	-0.93	0.87	0.89	0.78	0.41	-0.31	-0.62	-0.79	-1.09	-1.26	-1.63	-1.68	-1.43	-1.35	-1.14	-1.06	-0.81	-0.15	0.16	0.24	0.19	-1.61
N	-0.57	1.04	0.99	0.81	0.38	-0.36	-0.62	-0.76	-1.05	-1.24	-1.66	-1.71	-1.40	-1.31	-1.10	-1.05	-0.85	-0.18	0.21	0.35	0.38	-1.26
O	-0.88	1.07	1.13	0.99	0.81	0.06	-0.55	-0.73	-0.94	-1.01	-1.06	-1.12	-1.17	-1.19	-1.06	-0.96	-0.43	0.27	0.40	0.50	0.42	-1.54
P		0.04	1.09	0.87	0.37	-0.01	-0.29	-0.37	-0.76	-0.88	-0.96	-1.01	-1.03	-1.00	-0.69	-0.69	-0.47	-0.15	0.30	0.48	-0.59	
Q		-1.40	0.88	0.93	0.49	0.06	-0.31	-0.40	-0.72	-0.81	-0.92	-0.97	-0.95	-0.94	-0.70	-0.69	-0.38	-0.01	0.38	0.30	-2.00	
R			-0.13	1.04	0.68	0.22	0.23	0.09	-0.64	-0.78	-0.92	-0.97	-0.91	-0.85	-0.19	-0.12	-0.19	0.22	0.52	-0.68		
S			-1.03	1.16	0.93	0.50	0.85	0.90	0.87	0.80	0.45	0.40	0.68	0.67	0.63	0.53	0.12	0.49	0.67	-1.54		
T				-0.13	1.63	1.48	1.22	1.09	0.97	0.85	0.50	0.46	0.74	0.79	0.84	0.91	1.12	1.22	-0.58			
U					-0.21	1.41	1.34	1.23	1.15	0.94	0.45	0.41	0.83	0.98	1.00	1.05	1.07	-0.59				
V						-0.89	-0.29	0.14	1.18	1.19	1.05	1.02	1.10	1.02	-0.07	-0.55	-1.20					
W									-0.74	-0.42	-0.84	-0.87	-0.51	-0.88								

The maximum percent change is shown in bold character

Figure 2.3: Relative percent change of channel power introduced by mesh spacing (26 x 26 x 24 vs 104 x104 x 48)

	1	2	3	4	5	6	7	8	9	10	11	12	13	14	15	16	17	18	19	20	21	22
A									-1.05	-0.77	-1.24	-1.28	-0.88	-1.22								
B						-1.12	-0.55	-0.13	0.90	0.87	0.56	0.52	0.75	0.70	-0.39	-0.87	-1.51					
C					-0.45	1.13	1.08	1.00	0.97	0.87	0.69	0.65	0.74	0.77	0.72	0.73	0.72	-0.91				
D				-0.38	1.27	1.18	1.02	0.93	0.84	0.76	0.46	0.42	0.62	0.62	0.63	0.65	0.75	0.78	-0.91			
E			-1.03	1.22	1.19	0.97	0.91	0.87	0.82	0.75	0.40	0.35	0.61	0.58	0.56	0.52	0.51	0.67	0.65	-1.63		
F			-0.12	1.11	0.88	0.66	0.37	0.16	-0.62	-0.79	-1.08	-1.13	-0.95	-0.86	-0.17	-0.04	0.18	0.34	0.52	-0.75		
G		-1.51	0.83	0.98	0.74	0.48	-0.14	-0.29	-0.63	-0.68	-0.67	-0.72	-0.84	-0.89	-0.63	-0.56	-0.02	0.19	0.36	0.18	**-2.18**	
H		-0.19	0.90	0.78	0.46	0.17	-0.20	-0.29	-0.65	-0.75	-0.81	-0.87	-0.92	-0.92	-0.66	-0.64	-0.35	-0.12	0.15	0.23	-0.88	
J	-1.17	0.76	0.82	0.69	0.39	-0.33	-0.63	-0.70	-0.82	-0.88	-1.01	-1.07	-1.05	-1.10	-1.07	-1.08	-0.86	-0.21	0.04	0.14	0.05	-1.90
K	-0.87	0.74	0.69	0.52	-0.07	-0.76	-0.68	-0.69	-0.86	-0.95	-1.15	-1.21	-1.12	-1.15	-1.07	-1.14	-1.29	-0.68	-0.14	-0.01	0.01	-1.61
L	-1.18	0.63	0.70	0.68	0.47	-0.18	-0.49	-0.61	-0.84	-0.94	-1.21	-1.27	-1.12	-1.12	-0.99	-0.95	-0.72	-0.14	0.02	0.00	-0.09	-1.92
M	-1.13	0.69	0.76	0.72	0.45	-0.20	-0.44	-0.54	-0.78	-0.90	-1.20	-1.27	-1.07	-1.07	-0.92	-0.91	-0.74	-0.16	0.06	0.07	-0.03	-1.86
N	-0.74	0.90	0.90	0.80	0.45	-0.20	-0.40	-0.48	-0.71	-0.84	-1.21	-1.27	-1.01	-0.99	-0.85	-0.86	-0.73	-0.14	0.15	0.22	0.19	-1.47
O	-1.01	0.98	1.09	1.03	0.94	0.26	-0.29	-0.42	-0.58	-0.61	-0.63	-0.69	-0.78	-0.85	-0.78	-0.74	-0.26	0.36	0.40	0.42	0.28	-1.71
P		0.00	1.11	0.97	0.59	0.27	-0.01	-0.06	-0.40	-0.49	-0.54	-0.59	-0.65	-0.66	-0.40	-0.43	-0.22	0.03	0.36	0.46	-0.67	
Q		-1.39	0.96	1.09	0.77	0.38	-0.01	-0.08	-0.37	-0.43	-0.52	-0.57	-0.58	-0.61	-0.41	-0.41	-0.09	0.24	0.51	0.34	-2.02	
R			-0.02	1.24	0.99	0.56	0.53	0.39	-0.31	-0.41	-0.51	-0.56	-0.55	-0.54	0.09	0.15	0.12	0.49	0.69	-0.60		
S			-0.89	1.37	1.23	0.81	1.12	1.17	1.16	1.14	0.85	0.81	1.01	0.95	0.88	0.77	0.40	0.76	0.85	-1.44		
T				0.07	1.87	1.72	1.45	1.32	1.23	1.16	0.88	0.84	1.04	1.03	1.05	1.12	1.33	1.42	-0.41			
U					-0.02	1.61	1.53	1.43	1.38	1.22	0.79	0.75	1.10	1.20	1.19	1.23	1.24	-0.42				
V						-0.72	-0.12	0.32	1.39	1.43	1.32	1.29	1.33	1.22	0.10	-0.40	-1.05					
W									-0.55	-0.22	-0.62	-0.66	-0.31	-0.70								

The maximum percent change is shown in bold character

Figure 2.4: Relative percent change of channel power introduced by mesh spacing (26 x 26 x 12 vs 104 x104 x 48)

CHAPTER 3
NUMERICAL CONSIDERATIONS OF THE ANALYTIC NODAL METHOD

3.1 Introduction

In chapter 1, the spatially-discretized static nodal diffusion equations for Analytic Nodal Method were derived from the solution of the multigroup diffusion equations, based on the single assumption that the transverse leakage shape is spatially flat across each node. The flux and coupling coefficients were obtained by solving analytic difference equations. For the difficulty in evaluation of spatial coupling matrix, the number of neutron energy groups is restricted to two. In this chapter, we analyze the numerical properties of the Analytic Nodal Diffusion equations, then a multi-level iterative scheme for solving the resulting analytic nodal diffusion equations is presented.

3.2 Numerical Properties of the Analytic Nodal Diffusion Equations

The equation for which a solution is sought in the Analytic Nodal Method is given in Chapter 1, by equation 1.40. The super-matrix equation is a set of linear equations in the four vector unknowns, $[\bar{\phi}], [\bar{L}_x], [\bar{L}_y]$ *and* $[\bar{L}_z]$. In its present form, equation 1.40 has very little spatial coupling in the nodal-averaged flux terms and most of the coupling in the face-averaged net leakage terms. It is known from physical principles that the net leakage will be small compared to the average fluxes in a large number of reactor configurations. Therefore, equation 1.40 has the undesirable characteristic that the spatial coupling is dominated by the net leakage equations. This situation is altered by substituting the last three blocks of equations into the first block of equations to obtain (Smith, 1979)

$$[H]\,[\varphi]=\frac{1}{\gamma}[P]\,[\varphi] \tag{3.1}$$

where

$$[\varphi]\equiv col\left\{[\bar{\phi}],\ [\bar{L}_x],\ [\bar{L}_y],\ [\bar{L}_z]\right\}$$

$$[H]\equiv\begin{bmatrix} [F] & (h_z^k[G_y]+h_y^j[G_z]) & (h_z^k[G_x]+h_x^i[G_z]) & (h_y^j[G_x]+h_x^i[G_y]) \\ [F_x] & -[I] & \frac{1}{h_y^j}[G_x] & \frac{1}{h_z^k}[G_x] \\ [F_y] & \frac{1}{h_x^i}[G_y] & -[I] & \frac{1}{h_z^k}[G_y] \\ [F_z] & \frac{1}{h_x^i}[G_z] & \frac{1}{h_y^j}[G_z] & -[I] \end{bmatrix}$$

$$[F]\equiv[\Sigma_T]+h_y^j h_z^k[F_x]+h_x^i h_z^k[F_y]+h_x^i h_y^j[F_Z]$$

$$[P]\equiv\begin{bmatrix} [M] & [0] & [0] & [0] \\ [0] & [0] & [0] & [0] \\ [0] & [0] & [0] & [0] \\ [0] & [0] & [0] & [0] \end{bmatrix}$$

Since each of the matrices $[F_u]$ is a (2 x 2) tridiagonal block, equation 3.1 has substantially more spatial coupling in node-averaged flux terms than does equation 1.40. Equation 3.1 is clearly an eigenvalue problem in which the elements of the matrix [H] depend on the eigenvalue.

Any iterative scheme that is used to solve equation 3.1 will require that the matrices [H] and [P] have certain properties in order to guarantee successful convergence. It is very useful to examine the properties of the matrices in equation 3.1.

The matrix [P] is quite simple. The only non-zero submatrix of the matrix [P] is [M], and the matrix [M] is block diagonal with non-negative components (all fission cross sections are nonnegative). Unfortunately, the matrix [H] is not nearly as simple. In the

general case, the only property of the matrix [H] that can be guaranteed is that all of its components are real (Smith, 1979).

The expression of matrix $[F_u]$ (Smith, 1979) reveals that the matrices, $[F_u]$ are

1. Real
2. Irreducible
3. Symmetric
4. Diagonally dominant.

From these properties, it can be proved that equation 3.1 has the following properties (Wachspress, 1966):

There exists a unique positive real eigenvalue, $\tilde{a}_1$, which is greater in modulus than all other eigenvalues, and the eigenvector corresponding to the eigenvalue $\tilde{a}_1$ is unique and positive.

These properties and others derived from them will be used in the next section to demonstrate that the numerical schemes chosen to solve the Analytic Nodal Diffusion equations can be guaranteed to work.

3.3 Iterative Strategy for Solving the Static Nodal Diffusion Equations

3.3.1 The General Iterative

The general scheme for solving equation 3.1 is as following:

1. An initial guess for γ (usually γ=1.5) is used to evaluate the components of the matrix [H].
2. An accelerated fission source (outer) iteration is employed to determine iteratively the maximum eigenvalue and corresponding eigenvector (γ and $[\varphi]$).

3. After several outer iterations (usually 5-10), the latest estimate of ã is used to update the components of the matrix [H].
4. Use "modified" block Gauss-Seidel iteration method to perform the inner iteration.
5. Cyclic Chebyshev Semi(CCSI) iteration method or Gauss-Seidel iteration method is used for flux iteration.

3.3.2 Eigenvalue Updating

The fact that the submatrix [H] depends on the eigenvalue of the global static reactor problem gives the outer iterations a nonlinear character. However, the effects of updating the matrices on the outer iterations are generally quite negligible, especially when a reasonable estimate of the eigenvalue is available. Another characteristic of the outer iterations which helps to mitigate nonlinear effects is that a very good estimate of the eigenvalue (accurate to about 0.5%) can be obtained in relatively few (3 to 5) outer iterations. A general practice of updating the matrices every 5 to 10 outer iterations seems entirely appropriate. In steady-state iterations for problems with feedback, more frequent updating may be required to account for changes in temperatures, densities, etc. No problem has failed to converge because of the nonlinear nature of the outer iterations (Smith, 1979), and this also maintains for our CANDU cases.

3.3.3 Outer Iteration

The fission source iteration (Wachspress, 1966) is applied to equation 3.1 to determine the maximum eigenvalue and corresponding eigenvector. If p is used as the index of the outer iterations, equation 3.1 can be expressed as

$$[\varphi]_{p+1} = \frac{1}{\gamma_{p+1}} [H]_p^{-1} [P]\ [\varphi]_p \ ; \qquad p=0,1,\ldots,\infty \qquad 3.2$$

where γ_{p+1} is an estimate of the globe static eigenvalue and the matrix [H] is given a subscript p to indicate that its components are updated during the outer iterations. The maximum eigenvalue can be estimated by the ratio of the vector norms from successive solution vectors,

$$\gamma_{p+1} = \frac{\left\| [\varphi]_{p+1} \right\|}{\left\| [\varphi]_p \right\|} \qquad 3.3$$

The fission source iteration is guaranteed to converge if the eigenvalue with the largest modulus is unique (Varga, 1962). This property exists in the case of infinitely fine mesh spacing, but cannot be demonstrated in the general case. Nevertheless, this property is assumed to exist in the general case, and no problem has failed to converge because of eigenvalues with degenerate maximum moduli.

The rate at which the outer iterations converge is determined by the ratio of the moduli of the two maximum eigenvalues, usually called the dominance ratio, defined by

$$d = \frac{|\gamma_2|}{|\gamma_1|} \qquad 3.4$$

where γ_1, γ_2 are the eigenvalues with the largest and second largest moduli, respectively. For most problems, the dominance ratio is very close to unity and convergence is very slow; hence, many methods have been developed to increase the convergence rate of the fission source iterations. One of the most direct methods of altering the convergence rate is "eigenvalue shifting" or Wielandt's fractional iteration (Wachspress, 1966). In Wielandt's method, equation 3.1 is modified to obtain

$$\left\{ [H]-\frac{1}{\gamma_s}[P] \right\} [\varphi]=\left(\frac{1}{\gamma}-\frac{1}{\gamma_s}\right)[P]\ [\varphi] \qquad 3.5$$

where γ_s is arbitrarily selected but subject to certain restrictions discussed below.

Equation 3.5 is a new eigenvalue problem with much different properties than equation 3.5. It is easily demonstrated that the eigenvector associated with the maximum value of $\left(\frac{1}{\gamma}-\frac{1}{\gamma_s}\right)^{-1}$ is identical to the eigenvector associated with the maximum value of γ in equation 3.1, provided γ_s is larger in modulus than γ (Wachspress,1966). The dominance ratio of the new eigenvalue problem is

$$d_s=\frac{\left(\frac{1}{\gamma_1}-\frac{1}{\gamma_s}\right)}{\left(\frac{1}{\gamma_2}-\frac{1}{\gamma_s}\right)} \qquad 3.6$$

Since γ_s must be chosen such that the modulus of γ_s exceeds the modulus of γ_1, which in turn exceeds the modulus of γ_2, the dominance ratio, d_s, is less than unity and less than the unshifted dominance ratio, d. Naturally, the convergence rate of the outer iterations is maximized by the eigenvalue shift, γ_s, to be equal to the true static eigenvalue γ_1. Unfortunately, this choice makes the flux iteration matrix nearly singular, as is pointed out in the next section. Nevertheless, an optimum value of γ_s may exist, and the problem of determining it is addressed in section 4.4. Using the eigenvalue shift, the outer iteration is defined by

$$[\varphi]_{p+1}=\left(\frac{1}{\gamma_{p+1}}-\frac{1}{\gamma_{s_p}}\right)\left\{[H]_p-\frac{1}{\gamma_{s_p}}[P]\right\}^{-1}[P]\ [\varphi]_P \qquad p=0,1,\ldots,8 \qquad 3.7$$

where $[\varphi]_0$ is arbitrary (Wachspress.1966). The new eigenvalue estimate can be determined using any vector norm. For simplicity, the l_1 norm of the first block of vector $[\varphi]$ is chosen (Wachspress,1966)

$$\left(\frac{1}{\gamma_{p+1}}-\frac{1}{\gamma_{sp}}\right)^{-1}=\frac{\left\|[\bar{\phi}]_{p+1}\right\|_1}{\left\|[\bar{\phi}]_p\right\|_1} \tag{3.8}$$

The first block of equation 3.7 can be written as

$$\left\{\,[F]_p-\frac{1}{\gamma_{S_p}}[M]\,\right\}[\bar{\phi}]_{p+1}=\left(\frac{1}{\gamma_{p+1}}-\frac{1}{\gamma_{s_p}}\right)[M]\,[\bar{\phi}]_p-[S]_{p+1} \tag{3.9}$$

where [S] is the leakage source term

$$\begin{aligned}[S]_{p+1}=&(h_z^k[G_y]_p+h_y^j[G_z]_p)[\bar{L}_x]_{p+1}+(h_z^k[G_x]_p+h_x^i[G_z]_p)[\bar{L}_y]_{p+1}\\&+(h_x^i[G_y]_p+h_y^j[G_x]_p)[\bar{L}_z]_{p+1}\end{aligned}$$

Because the detailed calculations using nodal methods show that the transverse leakage is comparatively small in comparison to the fluxes, we can assume that the leakage source terms of adjacent outer iteration are equal. The outer iteration can be written as

$$\begin{aligned}[\bar{\phi}]_{p+1}=&\left\{\,[F]_p-\frac{1}{\gamma_{S_p}}[M]\,\right\}^{-1}\left(\frac{1}{\gamma_{p+1}}-\frac{1}{\gamma_{s_p}}\right)[M]\,[\bar{\phi}]_p\\&-\left\{\,[F]_p-\frac{1}{\gamma_{S_p}}[M]\,\right\}^{-1}[S]_p\end{aligned} \tag{3.10}$$

It is recognized that if γ_{s_p} is fixed throughout the outer iteration process, most other conventional methods of accelerating the outer iteration convergence can also be applied. For reasons detailed in the section 3.3.3, there seems to be several advantages to altering the eigenvalue shift during the outer iterations. Also, the convergence rate of the outer iterations can be significantly increased by eigenvalue shifting, such that additional acceleration schemes are not required.

3.3.4 Inner Iteration

The method used to perform the inner iteration is a "modified" block Gauss-Seidel iteration, where each block is a square matrix whose order is the number of energy groups times the number of spatial mesh points. With q as the index of the inner iteration, this "modified" Gauss-Seidel iteration is defined by

$$\begin{aligned}[\bar{\phi}]_{p,q+1} = \{\,[F]_p - \frac{1}{\gamma_{s_p}}[M]\,\}^{-1}\langle \left(\frac{1}{\gamma_p}-\frac{1}{\gamma_{s_p}}\right)[M]\,[\bar{\phi}]_p \\ -(h_z^k[G_y]_p + h_y^j[G_z]_p)[\bar{L}_x]_{p,q} - (h_z^k[G_x]_p + h_x^i[G_z]_p)[\bar{L}_y]_{p,q} \\ -(h_y^j[G_x]_p + h_x^i[G_y]_p)[\bar{L}_z]_{p,q}\ \rangle \end{aligned} \qquad 3.11a$$

$$\begin{aligned}[\bar{L}_x]_{p,q+1} &= [F_x]_p[\bar{\phi}]_{p,q+1} + \frac{1}{h_y^j}[G_x]_p[\bar{L}_y]_{p,q} + \frac{1}{h_z^k}[G_x]_p[\bar{L}_z]_{p,q} \\ [\bar{L}_y]_{p,q+1} &= [F_y]_p[\bar{\phi}]_{p,q+1} + \frac{1}{h_x^i}[G_y]_p[\bar{L}_x]_{p,q} + \frac{1}{h_z^k}[G_y]_p[\bar{L}_z]_{p,q} \\ [\bar{L}_z]_{p,q+1} &= [F_z]_p[\bar{\phi}]_{p,q+1} + \frac{1}{h_x^i}[G_z]_p[\bar{L}_z]_{p,q} + \frac{1}{h_y^j}[G_z]_p[\bar{L}_y]_{p,q} \end{aligned} \qquad 3.11b$$

p=0,1,2,3,....,∞

q=0,1,2,3,....,∞

This iterative scheme would be a true block Gauss-Seidel iteration if the latest values of the face-averaged net leakage were used.

This particular scheme is chosen for two reasons. First, it eliminates the need to calculate both $[G_u]_p[L_u]_{p,q}$ and $[G_u]_p[L_u]_{p,q+1}$, which saves computational effort. Second, this scheme does not "favor" any one direction in the calculation of leakages. The inner iteration, defined by equation 3.11, consists of two distinct steps. First, the new node-averaged fluxes are determined from the old fission source and the old leakages. The second step is the determination of the new net leakages from the new

fluxes and the old leakages. This step is not iterative, but requires a number of matrix multiplication, since the matrices $[G_u]_p$ are block tridiagonal.

In most cases, there is no reason to coverage the fluxes and leakages completely at every inner iteration, since the fission source is computed from fluxes at the last outer iteration. In problems where the net leakages are small compared to the average fluxes, it seems reasonable to perform only one inner iteration per outer iteration and continue the outer iterations until the fluxes are converged. In some cases, however, the net leakages can be fairly large compared to the average fluxes, and it may be more efficient to perform additional inner iterations to converge the net leakages more rapidly than would otherwise be possible.

3.3.5 Flux Iteration

In three-dimensional case, $[F]_p$ is a block diagonal matrix, each block being 2 x 2. Since primary consideration in this work is with two-group methods, both groups will be solved simultaneously. We use Cyclic Chebyshev Semi-Iteration (CCSI) method (Varga, 1962) or Gauss-Seidel iteration method as the flux iteration method.

If the matrix $\left\{ [F]_p - \frac{1}{\gamma_{s_p}}[M] \right\}$ is split into strictly lower block triangular matrix, a block diagonal matrix, and a strictly upper block triangular matrix such that

$$\left\{ [F]_p - \frac{1}{\gamma_{s_p}}[M] \right\} \equiv [L]_p + [D]_p + [U]_p \qquad 3.12$$

The CCSI method with iterative index r is defined by

$$[\bar{\phi}]_{p,q,r+1} = (1-\omega_{r+1})[\bar{\phi}]_{p,q,r} + \omega_{r+1}\left\{ [D]_p + [L]_p \right\}^{-1}\left\{ [Q]_{p,q} - [U]_p[\bar{\phi}]_{p,q,r} \right\} \qquad 3.13$$

where

$$[Q]_{p,q} \equiv \{ \left(\frac{1}{\gamma_p} - \frac{1}{\gamma_{s_p}} \right) [M] \, [\bar{\phi}]_p - (h_z^k [G_y]_p + h_y^j [G_z]_p)[\bar{L}_x]_{p,q}$$
$$- (h_z^k [G_x]_p + h_x^i [G_z]_p)[\bar{L}_y]_{p,q} - (h_y^j [G_x]_p + h_x^i [G_y]_p)[\bar{L}_z]_{p,q} \}$$

$$\omega_{r+1} \equiv \frac{1}{1 - (\frac{\rho^2 \omega_r}{4})} \quad ; \qquad r = 1 \qquad = 1.0 \; ; \qquad r = 0,$$

with ρ^2 defined below.

The Gauss-Seidel iteration method with iterative index r is defined by

$$[\bar{\phi}]_{p,q,r+1} = \{ [D]_p + [L]_p \}^{-1} \{ [Q]_{p,q} - [U]_p [\bar{\phi}]_{p,q,r} \} \qquad 3.14$$

It is as same as the CCSI when the relaxation factor is equal to unity. Mathematically, the CCSI is a permutation transformation of the conventional Gauss-Seidel iteration. This transformation can be thought of as a reordering of equations and unknowns. The permutation transformation does not change the properties of the flux iteration matrix.

Strictly speaking, to guarantee that the CCSI method will converge, the flux iteration matrix must possess several properties. First, the flux iteration matrix must be an irreducible, consistently ordered weakly cyclic matrix of order 2, which it is. The flux iteration matrix must also be convergent, which can be guaranteed if the flux coefficient matrix is diagonally dominant. Lastly it must be assumed that all eigenvalues of the flux iteration matrix are real (Clark, 1964).

The CCSI method is related to the block successive overrelaxation (SOR) methods and can be thought of as SOR method in which the relaxation parameter is varied from iteration to iteration in such a way as to increase the average rate of convergence. For SOR methods, the optimum choice for the relaxation factor is defined to be the

relaxation factor that gives the greatest asymptotic convergence rate and is given by (Varga,1962)

$$\omega_b = \frac{2}{1+\sqrt{1-\rho^2}} \qquad 3.15$$

where ρ is the spectral radius of the Jacobi iteration matrix. The relaxation factors in the CCSI method are chosen to give the greatest average convergence rate; hence, the relaxation factors change from iteration to iteration. Asymptotically, the CCSI relaxation factor must equal the SOR relaxation factor, and indeed

$$\omega_\infty = \frac{2}{1+\sqrt{1-\rho^2}} \qquad 3.16$$

It is apparent from equation 3.13 that the spectral radius of the Jacobi flux iteration matrix must be known in order to actually use the CCSI method. Since the flux coefficient matrix is to be inverted by the CCSI method, it would be useful to be able obtain ρ^2 by using this same method. It is easily shown that ρ^2 is equal to the spectral radius of the Gauss-Seidel iteration matrix. Thus, ρ^2 can be determined by performing a series of flux iterations with unity (Gauss-Seidel iterations) and estimating the spectral radius, $\rho(G^{-}S)$, by

$$\rho_{r+1}(G-S) = \frac{\left\| [\bar{\phi}]_{r+1} - [\bar{\phi}]_r \right\|_1}{\left\| [\bar{\phi}]_r - [\bar{\phi}]_{r-1} \right\|_1} = \rho^2 \qquad r=0,1,\ldots,8 \qquad 3.17$$

It is recognized that better estimates of ρ^2 are possible. However, the flux coefficient matrix depends on the true static eigenvalue which is not known when ρ^2 is estimated; thus, there seems to be little value in obtaining the "exact" spectral radius of the "wrong" matrix.

3.4 Summary

In this chapter, the properties of the nodal diffusion equations were examined. The numerical methods used to solve the nodal diffusion equations were also detailed in this chapter.

In chapter 4, applications of the Analytic Nodal Method and the numerical methods described in present chapter will be presented.

CHAPTER 4
STATIC APPLICATION OF THE ANALYTIC NODAL METHOD

4.1 Induction

In chapter 1, the static nodal diffusion equations of the Analytic Nodal Method, based on the single assumption that the transverse leakage shape is spatially flat across each node, were derived. The flux and leakage coupling coefficients were obtained by solving analytic difference equations. A multi-level iterative scheme for solving the resulting analytic nodal diffusion equations was detailed in chapter 3.

In this chapter, results from applications of the Analytic Nodal Method to a two-dimensional, two-group static PWR reactor problem and to two three-dimensional, two-group, static CANDU reactor problems are presented. The Xenon effect for a typical CANDU-6 problem is also discussed in this chapter. Throughout this chapter, the accuracy and computational efficiency of the Analytic Nodal Method are compared to those of Coarse Mesh Finite Difference Method.

4.2 Foreword to Static Results

4.2.1 Computer Code

The method developed in chapter 1 and the numerical techniques detailed in chapter 3 are incorporated into a series of program modules of the NDF (Kaveh, et al., 1999) code, which has been originally developed to simulate CANDU reactor transients. All these modules are written in FORTRAN 77. The code was compiled under the Visual

Fortran 5.0 compiler with full optimization and in single precision. All computations reported in this chapter are performed on an IBM PC computer.

NDF is capable of handling non-uniform mesh spacing and irregular geometric boundaries. The generalized albedo boundary conditions described in chapter 1 are incorporated into NDF, but no attempt has been made as yet to utilize the albedos except to model zero flux, zero incoming current and zero current boundary conditions.

4.2.2 Convergence Criteria

The convergence criterion on the node-averaged fluxes which is employed in the code NDF is

$$\left(\frac{\left| \overline{\phi}(g)^{q}_{i,j,k} - \overline{\phi}(g)^{q-1}_{i,j,k} \right|}{\overline{\phi}(g)^{q-1}_{i,j,k}} \right) < \varepsilon$$

where $\overline{\phi}(g)^{q-1}_{i}$ is the average flux and ε is the outer iteration convergence criterion. In the IAEA 2-D PWR benchmark problem, we used the convergence criterion of 10^{-6}. In the CANDU benchmark problem, we used an outer iteration convergence criterion of 10^{-6}. For the typical CANDU-6 problem which is a large 3-D problem, it is not always easy to obtain convergence to 10^{-6}. Therefore, we used an outer iteration convergence criterion of 10^{-5}.

4.2.3 Errors in Power Distributions

The static solutions to problems presented in this chapter are compared to reference solutions, which are spatially converged. For purposes of summarizing the results, some tables are used to present the maximum and average errors in nodal power densities. With the power density in the (i, j, k) node defined as $P_{i,j,k}$, and the

reference power density represented as $P^{ref}_{i,j,k}$, the maximum error in nodal power density is defined to be

$$\varepsilon_{\max}(I,J,K) \equiv \max imum \quad over \quad all \quad i,j,k \quad \left\{ \frac{\left| P_{i,j,k} - P^{ref}_{i,j,k} \right|}{P^{ref}_{i,j,k}} \right\}$$

and the average error is

$$\bar{\varepsilon} \equiv \frac{1}{V_t} \sum_i \sum_j \sum_k \frac{\left| P_{i,j,k} - P^{ref}_{i,j,k} \right|}{P^{ref}_{i,j,k}} V_{i,j,k}$$

where $V_{i,j,k}$ is the node $(i,j,k)$and V_t is the total volume of the reactor core. The maximum nodal power densities defined as $P_{\max}(I,J,K)$ are also presented in the tables too. All nodal powers are normalized such that the total reactor power is unity.

4.2.4 Execution Times

In order to establish comparisons between methods, we use the same computer (IBM PC) and the same compiler (Visual Fortran 5.0) to perform the calculations. In this thesis, the execution times reported are the total CPU time consumed from the point at which the computer begins to read the input files to the point at which solution editing begins.

4.3 Static Results

4.3.1 The 2-D IAEA PWR Benchmark Problem

In this section, results from 2-D IAEA PWR benchmark problem are presented. The benchmark problem is a highly simplified two-dimensional, two-group static benchmark problem (Muller et al., 1991), as described in Section A1.1 of Appendix 1. The reactor consists of a two-zone core containing 177 fuel assemblies each having a

width of 20 cm. The core is reflected radially and axially by 20 cm of water, and the active core height is 340 cm. Each of nine fully inserted control rods is represented as smeared absorbers in a single fuel assembly. The existence of inserted control rods and a water reflector gives this problem severe local flux perturbation, which make the problem quite challenging.

The 2-D problem was solved with 5cm spatial meshes. Table 4.1 summarizes the results of Analytic Nodal Method and Coarse Mesh Finite Difference Method. The normalized assembly power densities are given in Figure 4.1. The reference solution is a 3-1/3 cm nodal calculation by Wagner (Finnemann et al., 1977), which is spatially converged. The assembly with the largest percentage error in power densities is one of the lower assemblies adjacent to the reflector. These results indicate that the Analytic Nodal Method with flat leakage approximation is more accurate than Coarse Mesh Finite Difference Method for PWR calculation, but the execution time is longer for the same mesh size.

4.3.2 The 3-D CANDU Benchmark Problem

In this section, the static results from 3-D CANDU benchmark problem are presented. The CANDU benchmark problem (ANL, 1985) is a simplified three-dimensional, two-group kinetics benchmark problem as described in Section A1.2 of Appendix 1. The kinetics results will be presented in chapter 6. This benchmark has been proven to be a very important standard by which progress in CANDU reactor calculation methods have been measured. Following the introduction of this problem, many solutions were obtained (ANL, 1985), but most of these solutions were calculated by Coarse Mesh Finite Difference Method.

The reactor core of this benchmark has 88 channels that are divided into inner and outer fuel regions. Each channel is assumed to have 10 fuel bundles each having a length 60cm. The cell-averaged cross sections for each region are provided as part of the benchmark specification.

The solution of the 3-D CANDU benchmark problem with 18 x 18 x 10 spatial mesh is summarized in Table 4.2. A comparison of Analytic Nodal Method (ANM) with Coarse Mesh Finite Difference Method (CMFD) for this problem is given in Table 4.2 also. The reference case for this benchmark is the solution of a fine mesh CMFD calculation split to 72 x 72 x 40, obtained by using the NDF code.

The following results are given:

- Figure 4.2: Normalized channel power densities.
- Figure 4.3: Normalized bundle power densities on plane 1.
- Figure 4.4: Normalized bundle power densities on plane 5.
- Figure 4.5: Comparison of percent errors in power densities from CMFD and ANM method.
- Figure 4.6: Graph of normalized bundle power density distributions on plane 5.
- Figure 4.7: Graph of absolute percent errors in bundle power densities on plane 5.
- Figure 4.8: Graph of transverse leakages of thermal group on plane 5.

Compared with the reference values, the maximum error of bundle power densities for ANM and CMFD are about 4.3% and 5.9% respectively, and located in the node (5,5,2), near the boundary of Z axial; the maximum error of channel power densities for ANM and CMFD are about 4.3% and 5.9% respectively, located near the reflector. These results indicate that all the nodes with larger percent errors of power densities are in lower power regions, near the reflector. Because the core of the CANDU benchmark is essentially homogenous in the axial direction for the static calculation,

the percent errors of bundle power densities are identical on each plane. The comparison of solutions from CMFD method and ANM method illustrates that with the same mesh size, the ANM can get more accurate solution.

4.3.3 The Typical CANDU-6 without Xenon Effect Problem

In this section, the static results of a typical CANDU-6 problem are presented. The typical CANDU-6 problem (Koclas, 1998 and Navarro Arias, 1996) is a simplified 3-D full core, 2 energy group model of CANDU reactor, with main reactivity devices, such as liquid zone controllers and adjuster rods are presented in the core. This problem has 380 fuel channels with 12 bundles in each channel. The core is divided into three fuel regions. The lattice pitch is 28.575 cm and the bundle length is 49.53 cm. This problem is much like the true CANDU-6 reactor core, in contrast to the CANDU benchmark problem. This problem is introduced on purpose of full-core dynamic simulation. The problem is somewhat simplified, as the axial notch in the reflector is not present in this model, and Xenon is not taken into account. The fuel and reactivity device macroscopic cross-sections were calculated using the DRAGON/DONJON chain code (Marleau et al., 1993,1994; Roy et al., 1993). Section A1.3 of Appendix 1 gives the detailed description of this problem.

The reference solution for this problem is the result of a fine mesh CMFD calculation with 104 x 104 x 48 spatial meshes obtained by the NDF code. The main results without Xenon effect from CMFD and ANM calculations with the same coarse meshes (26 x 26 x 12) are summarized and compared in Table 4.3. The more detailed results are given as following:

- Figure 4.9: Normalized channel power densities (without Xenon).
- Figure 4.10: Normalized bundle power densities on plane 1 (without Xenon).
- Figure 4.11: Normalized bundle power densities on plane 6 (without Xenon).

- Figure 4.12: Normalized bundle power densities on plane 8 (without Xenon).
- Figure 4.13: Comparison of percent errors in channel power densities from CMFD and ANM Method (without Xenon).
- Figure 4.14: Graph of normalized bundle power density distributions on plane 6 (without Xenon).
- Figure 4.15: Graph of absolute percent errors in bundle power densities on plane 6 (without Xenon).
- Figure 4.16: Graph of the transverse leakages of thermal group on plane 6 (without Xenon).

Table 4.3 indicates that both CMFD- and ANM-derived eigenvalues, maximum channel power and maximum bundle power agree well with the reference values. Compared with the reference values, the average and maximum errors in ANM-predicted channel and bundle power densities are all smaller than those predicted with CMFD. The maximum error of bundle power densities for ANM and CMFD are about 2.8% and 6.0% respectively; the maximum error of channel power densities for ANM and CMFD are about 1.6% and 2.2% respectively. For ANM calculations, the maximum percent errors of channel and bundle power densities are located at W13 and (W14, 4) respectively, which is in the core periphery region adjacent to the reflector. Overall, comparison between CMFD and ANM shows that the ANM results are more accurate as expected.

4.3.4 The Typical CANDU-6 with Xenon Effect Problem

In this section the results with Xenon effect for the typical CANDU-6 problem are presented. The reactivity effect that due to the concentration of this fission product Xenon is a particularly important aspect of thermal-reactor operation. We shall use the premise that the effect of Xenon is limited to neutron absorption. The change in the

absorption cross section due to the presence of Xenon is calculated by DRAGON/DONJON chain code (Marleau et al., 1993,1994; Roy et al., 1993).

The reactivity of Xenon can be expressed as

$$\rho_{Xenon} = \frac{\gamma_X - \gamma}{\gamma_X \gamma}$$

where γ_X is the eigenvalue with Xenon effect, γ is the eigenvalue without Xenon effect.

Table 4.4 summaries the results of typical CADU-6 with Xenon effect problem from Analytic Nodal Method and Coarse Mesh Finite Difference Method. It indicates that the difference of Xenon reactivity is about 0.038 mk. The Xenon effect on the power density distribution is shown by Figures 4.17 and 4.18. The power density distributions tend towards flat in account of the Xenon effect.

4.4 Summary

Although the Analytic Nodal Method has been demonstrated to be a superior and more accurate method than Coarse Mesh Finite Difference Method for solving PWR problems, nodal methods such as the Analytic Nodal Method are seldom used for CANDU system. In this chapter, the static Analytic Nodal Method results of one PWR problem and two CANDU problems were presented and compared with the results calculated with the Coarse Mesh Finite Difference Method.

Comparison of 2-D IAEA PWR problem shows that the Analytic Nodal Method is a much more accurate method than Coarse Mesh Finite Difference Method for light-water system as expected. However, because of the large migration area in a heavy-water system, the Coarse Mesh Finite Difference Method is found to be generally

adequate for CANDU problems. Although the advantage of Analytic Nodal Method with flat transverse leakage approximation in the calculation accuracy is illustrated, the improvement is not as obvious as shown for PWR problem. For the static 3-D CANDU benchmark problem, by using the Analytic Nodal Method instead of the Coarse Mesh Finite Difference Method, the maximum error in the channel power densities can be improved from about 5.9% to 4.3%; and the average error in the channel power densities can be improved from about 1.4% to 0.8%. However, the computational efficiency of the Analytic Nodal Method is lower than that of the Coarse Mesh Finite Difference Method with the same spatial meshes.

From the calculation results shown in this chapter, we conclude that the derivation of the Analytic Nodal Diffusion Equations in Chapter 1 is correct, the implementation of the iterative procedures and the development of the Analytic Nodal Method within the NDF code is successful. It is demonstrated that the Analytic Nodal Method is not only applicable for PWR, but also good for CANDU reactor. With the increasing accuracy requirements of current and future CANDU analysis, the Analytic Nodal Method is expected to act as an alternative tool for CANDU analysis.

Table 4.1: Summary of results for the 2-D IAEA PWR benchmark problem

	Coarse Finite Difference Method (CMFD)	Analytic Nodal Method (ANM)
Outer iterations	100	187
Eigenvalue	1.02922	1.02972
$\varepsilon_{max}(I,J)(assembly,\%)$	14.200 (3,8)	3.699 (3,8)
$\bar{\varepsilon}$ $(assembly,\%)$	5.341	1.291
$P_{max}(I,J)$	1.567 (3,2),(2,3)	1.496 (3,2),(2,3)
Execution time (s)	0.77	2.82

Reference eigenvalue: 1.02959

Reference maximum nodal power density: 1.480

Outer iteration convergence criterion: 10^{-6}

Flux iteration convergence criterion: 10^{-6}

Table 4.2: Summary of results for the 3-D CANDU benchmark problem

	Coarse Finite Difference Method (CMFD)	Analytic Nodal Method (ANM)
Outer iterations	32	132
Eigenvalue	1.00355	1.00318
$\varepsilon_{max}(I,J)(channel,\%)$	5.889 (14,5)	4.252 (5,5)
$\bar{\varepsilon}$ $(channel,\%)$	1.419	0.847
$P_{max}(I,J)$ $(channel)$	1.252 (10,13),(9,13)	1.239 (10,13),(13,10)
$\varepsilon_{max}(I,J,K)(bundle,\%)$	5.889 (14,5,5)	4.253 (5,5,2)
$\bar{\varepsilon}$ $(bundle,\%)$	1.419	0.847
$P_{max}(I,J,K)$ $(bundle)$	1.934 (10,13,5),(9,13,5)	1.914
Execution time (s)	1.32	12.26

Reference eigenvalue: 1.00338

Reference maximum channel power density: 1.228

Reference maximum bundle power density: 1.897

Outer iteration convergence criterion: 10^{-6}

Flux iteration convergence criterion: 10^{-6}

Table 4.3: Summary of results for the 3-D typical CANDU-6 without Xenon effect problem

	Coarse Finite Difference Method (CMFD)	Analytic Nodal Method (ANM)
Outer iterations	91	93
Eigenvalue	1.03067	1.03047
$\varepsilon_{max}(I,J)(channel,\%)$	2.176 (G21)	1.606 (W11)
$\bar{\varepsilon}$ $(channel,\%)$	0.735	0.516
$P_{max}(I,J)$ $(channel)$	1.249 (E14)	1.246 (F15)
$\varepsilon_{max}(I,J,K)(bundle,\%)$	6.045 (K12,8)	2.792 (W12,4)
$\bar{\varepsilon}$ $(bundle,\%)$	1.552	0.646
$P_{max}(I,J,K)$ $(bundle)$	1.853 (E12,6)	1.843 (E12,6)
Execution time (s)	13.74	42.85

Reference eigenvalue: 1.03057

Reference maximum channel power density: 1.250

Reference maximum bundle power density: 1.846

Outer iteration convergence criterion: 10^{-6}

Flux iteration convergence criterion: 10^{-5}

Table 4.4: Summary of results for the 3-D typical CANDU-6 with Xenon effect problem

	Coarse Finite Difference Method (CMFD)	Analytic Nodal Method (ANM)
Eigenvalue	1.00275	1.00258
Xenon Reactivity (mk)	-26.952	-26.990
$P_{max}(I,J,K)$ *(bundle)*	1.845 (E11,6)	1.835 (E12,6)

Total reactor power is 2.154×10^9 w

	1	2	3	4	5	6	7	8
1	0.746	1.310	1.454	1.211	0.610	0.935	0.935	0.755
	2.780	7.642	6.109	6.157	-0.775	1.104	-3.070	-9.714
	-0.588	2.071	1.279	1.741	-1.298	0.808	-0.670	-2.054
2	1.310	1.435	**1.480**	1.315	1.070	1.036	0.950	0.736
	7.642	6.728	5.867	5.135	3.876	0.326	-3.370	-10.025
	2.071	1.334	1.095	1.013	1.330	0.076	-0.829	-2.164
3	1.454	**1.480**	1.469	1.354	1.179	1.071	0.975	0.692
	6.109	5.867	5.213	3.504	2.331	-0.677	-4.098	-14.188
	1.279	1.095	0.886	0.091	0.537	-0.219	-0.797	-3.685
4	1.211	1.315	1.345	1.193	0.967	0.906	0.846	
	6.157	5.135	4.196	3.480	2.283	-1.800	-9.085	
	1.741	1.013	0.761	0.690	1.014	-0.331	-2.223	
5	0.610	1.070	1.179	0.967	0.471	0.686	0.597	
	-0.775	3.876	2.331	2.283	-4.646	-3.183	-13.938	
	-1.298	1.330	0.537	1.014	-2.053	0.398	-3.346	
6	0.935	1.036	1.071	0.906	0.686	0.585		
	1.104	0.326	-0.677	-1.800	-3.183	-13.173		
	0.808	0.076	-0.219	-0.331	0.398	-3.372		
7	0.934	0.950	0.975	0.846	0.597			
	-3.019	-3.370	-4.098	-9.085	-13.938			
	-0.617	-0.829	-0.797	-2.223	-3.346			
8	0.755	0.736	0.692					
	-9.714	-10.013	**-14.200**					
	-2.054	-2.150	**-3.699**					

Reference normalized power densities

Percent errors for CMFD (5cm x 5cm)

Percent errors for ANM (5cm x 5cm)

Reference is the result of 3-1/3 cm nodal calculation by Wagner

The maximum assembly power density and the maximum percent errors are shown in bold character

Figure 4.1: Normalized assembly power densities and percent errors of the 2-D IAEA PWR benchmark problem

	3	4	5	6	7	8	9	10	11	12	13	14	15	16
3					0.64	0.81	0.89	0.89	0.81	0.64				
					-2.83	-1.52	-1.29	-1.29	-1.52	-2.83				
4					0.82	0.99	1.07	1.07	0.99	0.82				
					-1.56	0.22	0.45	0.45	0.22	-1.56				
5			0.66	0.81	0.97	1.13	1.21	1.21	1.13	0.97	0.81	0.66		
			-4.25	-3.36	-0.60	0.58	0.83	0.83	0.58	-0.59	-3.36	-4.25		
6			0.81	0.92	1.06	1.17	1.23	1.23	1.17	1.06	0.92	0.81		
			-3.36	-1.33	-0.10	0.65	0.89	0.90	0.66	-0.10	-1.33	-3.36		
7	0.64	0.82	0.97	1.06	1.04	1.06	1.08	1.08	1.06	1.04	1.06	0.97	0.82	0.64
	-2.83	-1.56	-0.59	-0.10	0.26	0.55	0.78	0.78	0.56	0.26	-0.09	-0.59	-1.56	-2.83
8	0.81	0.99	1.13	1.17	1.06	1.00	0.98	0.98	1.00	1.06	1.17	1.13	0.99	0.81
	-1.52	0.22	0.59	0.66	0.55	0.31	0.32	0.32	0.32	0.56	0.66	0.59	0.23	-1.51
9	0.89	1.07	1.21	1.23	1.08	0.98	0.94	0.94	0.98	1.08	1.23	1.21	1.07	0.89
	-1.29	0.46	0.83	0.90	0.78	0.32	0.14	0.14	0.33	0.78	0.90	0.84	0.46	-1.28
10	0.89	1.07	1.21	1.23	1.08	0.98	0.94	0.94	0.98	1.08	**1.23**	1.21	1.07	0.89
	-1.29	0.46	0.83	0.90	0.78	0.32	0.14	0.14	0.33	0.78	0.90	0.84	0.46	-1.28
11	0.81	0.99	1.13	1.17	1.06	1.00	0.98	0.98	1.00	1.06	1.17	1.13	0.99	0.81
	-1.51	0.22	0.59	0.66	0.56	0.31	0.33	0.33	0.32	0.56	0.66	0.59	0.23	-1.51
12	0.64	0.82	0.97	1.06	1.04	1.06	1.08	1.08	1.06	1.04	1.06	0.97	0.82	0.64
	-2.83	-1.56	-0.59	-0.09	0.26	0.56	0.78	0.78	0.56	0.27	-0.09	-0.59	-1.55	-2.82
13			0.81	0.92	1.06	1.17	1.23	1.23	1.17	1.06	0.92	0.81		
			-3.36	-1.33	-0.09	0.66	0.90	0.90	0.66	-0.09	-1.32	-3.35		
14			0.66	0.81	0.97	1.13	1.21	1.21	1.13	0.97	0.81	0.66		
			-4.25	-3.36	-0.59	0.59	0.83	0.83	0.59	-0.59	-3.35	-4.24		
15					0.82	0.99	1.07	1.07	0.99	0.82				
					-1.55	0.22	0.46	0.46	0.23	-1.55				
16					0.64	0.81	0.89	0.89	0.81	0.64				
					-2.83	-1.51	-1.28	-1.28	-1.51	-2.83				

Reference channel power densities

Percent errors for ANM (18 x 18 x 10)

Reference is the result of CMFD (72 x 72 x 40)

The maximum normalized channel power density and the maximum percent error are shown in bold character

Figure 4.2: Normalized channel power densities and percent errors of the CANDU benchmark problem for ANM (18 x 18 x 10)

	3	4	5	6	7	8	9	10	11	12	13	14	15	16
3					0.16	0.20	0.22	0.22	0.20	0.16				
					-2.83	-1.52	-1.29	-1.29	-1.52	-2.83				
4					0.20	0.24	0.26	0.26	0.24	0.20				
					-1.56	0.22	0.45	0.45	0.22	-1.56				
5			0.16	0.20	0.24	0.28	0.30	0.30	0.28	0.24	0.20	0.16		
			-4.25	-3.36	-0.60	0.58	0.83	0.83	0.59	-0.59	-3.36	-4.25		
6			0.20	0.22	0.26	0.29	0.30	0.30	0.29	0.26	0.22	0.20		
			-3.36	-1.33	-0.10	0.65	0.89	0.89	0.66	-0.10	-1.33	-3.35		
7	0.16	0.20	0.24	0.26	0.25	0.26	0.26	0.26	0.26	0.25	0.26	0.24	0.20	0.16
	-2.83	-1.56	-0.59	-0.10	0.26	0.55	0.78	0.78	0.55	0.26	-0.09	-0.59	-1.56	-2.83
8	0.20	0.24	0.28	0.29	0.26	0.24	0.24	0.24	0.24	0.26	0.29	0.28	0.24	0.20
	-1.52	0.22	0.59	0.66	0.55	0.31	0.32	0.32	0.31	0.56	0.66	0.59	0.23	-1.51
9	0.22	0.26	0.30	0.30	0.26	0.24	0.23	0.23	0.24	0.26	0.30	0.30	0.26	0.22
	-1.29	0.46	0.83	0.90	0.78	0.32	0.14	0.14	0.33	0.78	0.90	0.84	0.46	-1.28
10	0.22	0.26	0.30	0.30	0.26	0.24	0.23	0.23	0.24	0.26	0.30	**0.30**	0.26	0.22
	-1.29	0.46	0.83	0.90	0.78	0.32	0.14	0.14	0.33	0.78	0.90	0.84	0.46	-1.28
11	0.20	0.24	0.28	0.29	0.26	0.24	0.24	0.24	0.24	0.26	0.29	0.28	0.24	0.20
	-1.51	0.22	0.59	0.66	0.56	0.31	0.33	0.33	0.32	0.56	0.66	0.59	0.23	-1.51
12	0.16	0.20	0.24	0.26	0.25	0.26	0.26	0.26	0.26	0.25	0.26	0.24	0.20	0.16
	-2.83	-1.56	-0.59	-0.09	0.26	0.56	0.78	0.78	0.56	0.27	-0.09	-0.59	-1.55	-2.82
13			0.20	0.22	0.26	0.29	0.30	0.30	0.29	0.26	0.22	0.20		
			-3.36	-1.33	-0.09	0.66	0.90	0.90	0.66	-0.09	-1.32	-3.35		
14			0.16	0.20	0.24	0.28	0.30	0.30	0.28	0.24	0.20	0.16		
			-4.25	-3.36	-0.59	0.59	0.83	0.83	0.59	-0.59	-3.35	-4.24		
15					0.20	0.24	0.26	0.26	0.24	0.20				
					-1.56	0.22	0.46	0.46	0.23	-1.55				
16					0.16	0.20	0.22	0.22	0.20	0.16—*Reference channel power densities*				
					-2.83	-1.51	-1.28	-1.28	-1.51	-2.83—*Percent errors for ANM (18 x 18 x 10)*				

Reference is the result of CMFD (72 x 72 x 40)

The maximum normalized bundle power density and the maximum percent error are shown in bold character

Figure 4.3: Normalized bundle power densities and percent errors on plane 1 of the CANDU benchmark problem for ANM (18 x 18 x 10)

	3	4	5	6	7	8	9	10	11	12	13	14	15	16
3					0.99	1.25	1.37	1.37	1.25	0.99				
					-2.83	-1.52	-1.29	-1.29	-1.52	-2.83				
4					1.27	1.53	1.66	1.66	1.53	1.27				
					-1.56	0.22	0.45	0.45	0.22	-1.56				
5			1.02	1.25	1.50	1.75	1.86	1.86	1.75	1.50	1.25	1.02		
			-4.25	-3.36	-0.60	0.58	0.83	0.83	0.59	-0.59	-3.36	-4.25		
6			1.25	1.42	1.63	1.81	1.90	1.90	1.81	1.63	1.42	1.25		
			-3.36	-1.33	-0.10	0.65	0.89	0.89	0.66	-0.10	-1.33	-3.35		
7	0.99	1.27	1.50	1.63	1.60	1.64	1.66	1.66	1.64	1.60	1.63	1.50	1.27	0.99
	-2.83	-1.56	-0.59	-0.10	0.26	0.55	0.78	0.78	0.55	0.26	-0.09	-0.59	-1.56	-2.83
8	1.25	1.53	1.75	1.81	1.64	1.54	1.51	1.51	1.54	1.64	1.81	1.75	1.53	1.25
	-1.52	0.22	0.59	0.66	0.55	0.31	0.32	0.32	0.31	0.56	0.66	0.59	0.23	-1.51
9	1.37	1.66	1.86	1.90	1.66	1.51	1.45	1.45	1.51	1.66	1.90	1.86	1.66	1.37
	-1.29	0.46	0.83	0.90	0.78	0.32	0.14	0.14	0.33	0.78	0.90	0.84	0.46	-1.28
10	1.37	1.66	1.86	1.90	1.66	1.51	1.45	1.45	1.51	1.66	**1.90**	1.86	1.66	1.37
	-1.29	0.46	0.83	0.90	0.78	0.32	0.14	0.14	0.33	0.78	0.90	0.84	0.46	-1.28
11	1.25	1.53	1.75	1.81	1.64	1.54	1.51	1.51	1.54	1.64	1.81	1.75	1.53	1.25
	-1.51	0.22	0.59	0.66	0.56	0.31	0.33	0.33	0.32	0.56	0.66	0.59	0.23	-1.51
12	0.99	1.27	1.50	1.63	1.60	1.64	1.66	1.66	1.64	1.60	1.63	1.50	1.27	0.99
	-2.83	-1.56	-0.59	-0.09	0.26	0.56	0.78	0.78	0.56	0.27	-0.09	-0.59	-1.55	-2.82
13			1.25	1.42	1.63	1.81	1.90	1.90	1.81	1.63	1.42	1.25		
			-3.36	-1.33	-0.09	0.66	0.90	0.90	0.66	-0.09	-1.32	-3.35		
14			1.02	1.25	1.50	1.75	1.86	1.86	1.75	1.50	1.25	1.02		
			-4.25	-3.36	-0.59	0.59	0.83	0.83	0.59	-0.59	-3.35	-4.24		
15					1.27	1.53	1.66	1.66	1.53	1.27				
					-1.56	0.22	0.46	0.46	0.23	-1.55				
16					0.99	1.25	1.37	1.37	1.25	0.99				
					-2.83	-1.51	-1.28	-1.28	-1.51	-2.83				

Reference channel power densities

Percent errors for ANM (18 x 18 x 10)

Reference is the result of CMFD (72 x 72 x 40)

The maximum normalized bundle power density and the maximum percent error are shown in bold character

Figure 4.4: Normalized bundle power densities and percent errors on plane 5 of the CANDU benchmark problem for ANM (18 x 18 x 10)

	3	4	5	6	7	8	9	10	11	12	13	14	15	16
3					-1.97 -2.83	-1.65 -1.52	-1.83 -1.29	-1.83 -1.29	-1.65 -1.52	-1.97 -2.83				
4					0.59 -1.56	1.53 0.22	1.48 0.45	1.48 0.45	1.53 0.22	0.59 -1.56				
5			-5.89 **-4.25**	-2.87 -3.36	1.42 -0.60	1.76 0.58	1.78 0.83	1.78 0.83	1.76 0.58	1.42 -0.59	-2.87 -3.36	-5.89 -4.25		
6			-2.87 -3.36	0.06 -1.33	1.58 -0.10	1.89 0.65	1.97 0.89	1.97 0.90	1.89 0.66	1.58 -0.10	0.06 -1.33	-2.87 -3.36		
7	-1.97 -2.83	0.59 -1.56	1.42 -0.59	1.58 -0.10	-1.10 0.26	-1.11 0.55	-1.12 0.78	-1.12 0.78	-1.11 0.56.26	-1.10 -0.09	1.58 -0.59	1.42 -1.56	0.59 -2.83	-1.97
8	-1.65 -1.52	1.54 0.22	1.76 0.59	1.89 0.66	-1.11 0.55	-0.90 0.31	-0.84 0.32	-0.84 0.32	-0.90 0.32	-1.11 0.56	1.89 0.66	1.76 0.59	1.54 0.23	-1.65 -1.51
9	-1.83 -1.29	1.49 0.46	1.78 0.83	1.97 0.90	-1.11 0.78	-0.84 0.32	-0.71 0.14	-0.71 0.14	-0.84 0.33	-1.11 0.78	1.97 0.90	1.78 0.84	1.49 0.46	-1.83 -1.28
10	-1.83 -1.29	1.49 0.46	1.78 0.83	1.97 0.90	-1.11 0.78	-0.84 0.32	-0.71 0.14	-0.71 0.14	-0.84 0.33	-1.11 0.78	1.97 0.90	1.78 0.84	1.49 0.46	-1.83 -1.28
11	-1.65 -1.51	1.54 0.22	1.76 0.59	1.89 0.66	-1.11 0.56	-0.90 0.31	-0.84 0.33	-0.84 0.33	-0.90 0.32	-1.11 0.56	1.89 0.66	1.76 0.59	1.54 0.23	-1.65 -1.51
12	-1.97 -2.83	0.59 -1.56	1.42 -0.59	1.58 -0.09	-1.10 0.26	-1.11 0.56	-1.12 0.78	-1.12 0.78	-1.11 0.56	-1.10 0.27	1.58 -0.09	1.42 -0.59	0.59 -1.55	-1.97 -2.82
13			-2.87 -3.36	0.06 -1.33	1.58 -0.09	1:89 0.66	1.97 0.90	1.97 0.90	1.89 0.66	1.58 -0.09	0.06 -1.32	-2.87 -3.35		
14			**-5.89** -4.25	-2.87 -3.36	1.42 -0.59	1.76 0.59	1.78 0.83	1.78 0.83	1.76 0.59	1.42 -0.59	-2.87 -3.35	-5.89 -4.24		
15					0.59 -1.56	1.53 0.22	1.48 0.46	1.48 0.46	1.53 0.23	0.59 -1.55				
16					-1.97 -2.83	-1.65 -1.51	-1.83 -1.28	-1.83 -1.28	-1.65 -1.51	-1.97--*Percent errors for CMFD (18 x 18 x 10)* -2.83--*Percent errors for ANM (18 x 18 x 10)*				

Reference is the result of CMFD (72 x 72 x 40)
The maximum percent errors are shown in bold character

Figure 4.5: Comparison of percent errors in channel power densities from CMFD (18 x 18 x 10) and ANM (18 x 18 x 10) for the CANDU benchmark problem

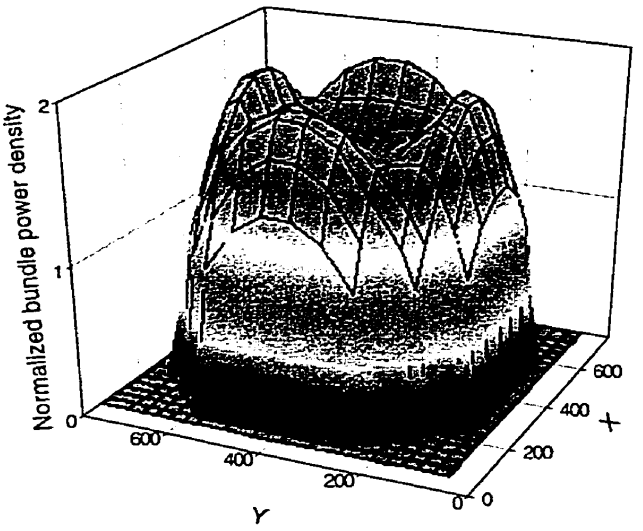

Figure 4.6: Normalized bundle power density distributions on plane 5 of the CANDU benchmark problem for ANM (18 x 18 x 10)

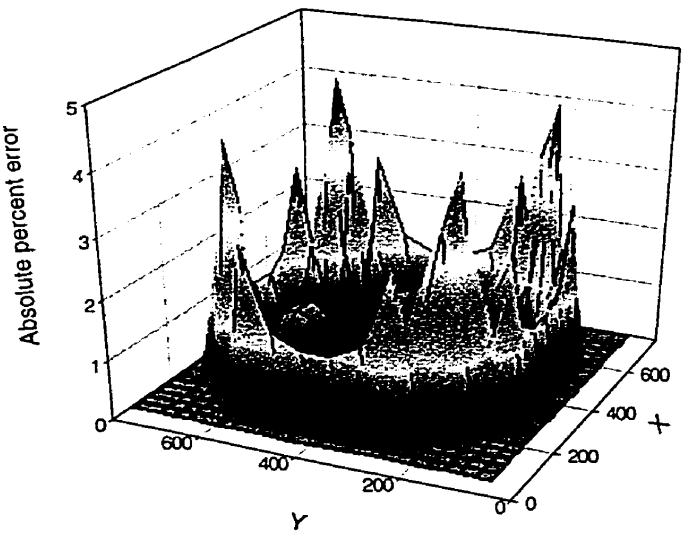

Figure 4.7: Absolute percent errors of bundle power densities on plane 5 of the CANDU benchmark problem for ANM (18 x 18 x10)

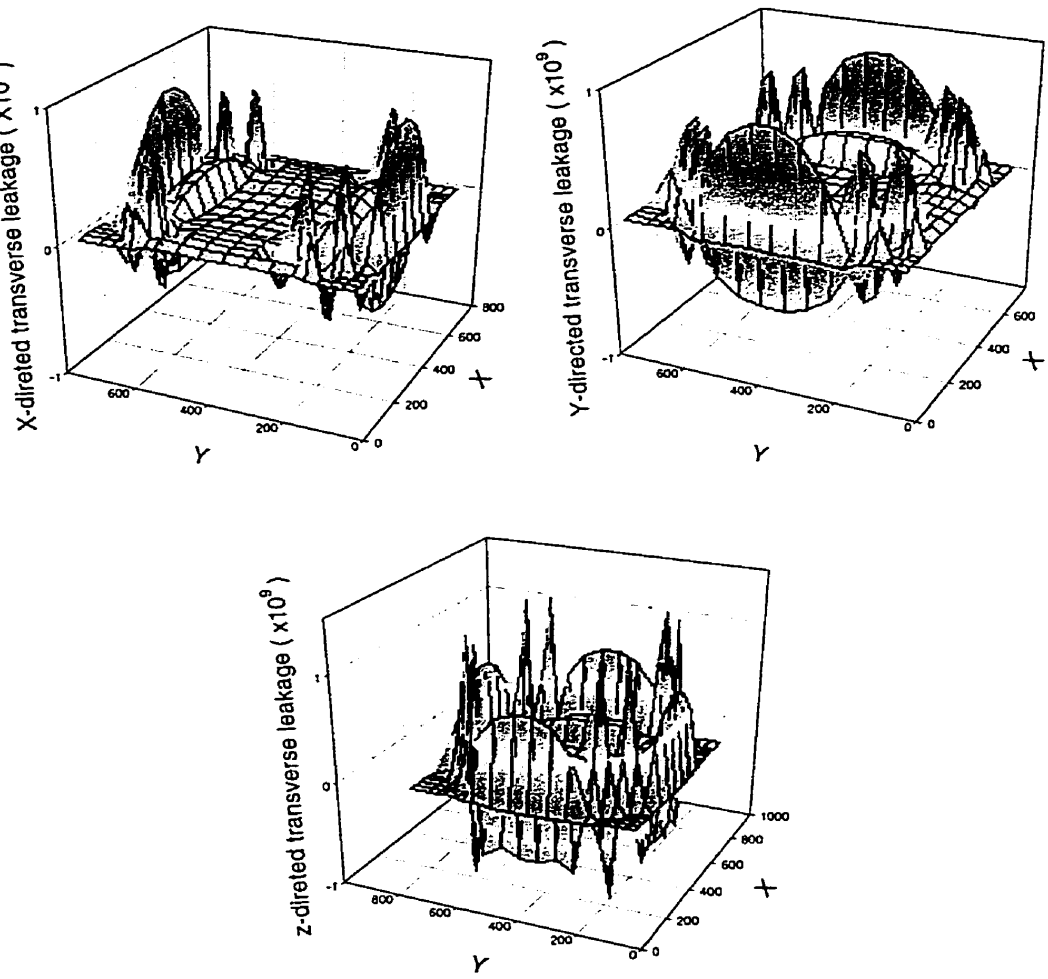

Figure 4.8: Transverse leakages of thermal group on plane 5 of the CANDU benchmark problem for ANM (18 x 18 x10)

	1	2	3	4	5	6	7	8	9	10	11	12	13	14	15	16	17	18	19	20	21	22
A									0.57	0.62	0.64	0.64	0.62	0.57								
									0.12	1.01	1.25	1.22	0.93	-0.01								
B						0.51	0.63	0.73	0.80	0.85	0.87	0.87	0.85	0.81	0.73	0.63	0.51					
						-0.30	0.06	-0.17	0.56	0.73	0.99	0.96	0.65	0.42	-0.36	-0.18	-0.59					
C					0.57	0.71	0.85	0.95	1.02	1.05	1.05	1.05	1.05	1.02	0.95	0.85	0.72	0.58				
					-0.34	0.86	0.72	0.65	0.55	0.45	0.83	0.80	0.36	0.40	0.44	0.47	0.56	-0.68				
D				0.59	0.75	0.90	1.03	1.12	1.17	1.18	1.16	1.16	1.18	1.17	1.12	1.04	0.91	0.75	0.59			
				-0.63	0.83	0.84	0.59	0.52	0.41	0.19	0.66	0.62	0.09	0.25	0.30	0.32	0.52	0.47	-1.02			
E			0.56	0.74	0.91	1.05	1.16	1.22	1.24	1.24	1.21	1.21	1.24	1.24	1.22	1.16	1.06	0.92	0.75	0.56		
			-0.69	0.51	0.80	0.65	0.43	0.27	0.20	-0.10	0.25	0.21	-0.21	0.03	0.04	0.15	0.32	0.42	0.10	-1.12		
F			0.69	0.88	1.03	1.14	1.21	1.24	1.22	1.20	1.18	1.18	1.20	1.22	**1.25**	1.22	1.15	1.04	0.89	0.70		
			-0.43	0.46	0.63	0.41	0.28	-0.03	0.04	-0.25	-0.09	-0.13	-0.36	-0.14	-0.27	-0.01	0.07	0.24	0.03	-0.89		
G		0.60	0.81	0.99	1.11	1.19	1.21	1.22	1.20	1.18	1.17	1.17	1.18	1.20	1.23	1.22	1.19	1.11	0.99	0.81	0.60	
		-0.96	0.26	0.31	0.60	0.32	0.02	-0.34	-0.22	-0.42	-0.48	-0.52	-0.54	-0.41	-0.59	-0.28	-0.04	0.20	-0.14	-0.22	-1.46	
H		0.70	0.91	1.06	1.14	1.19	1.20	1.20	1.18	1.16	1.16	1.16	1.16	1.18	1.21	1.21	1.20	1.15	1.07	0.91	0.71	
		-0.30	0.38	0.15	0.64	0.26	-0.25	-0.56	-0.47	-0.61	-0.75	-0.79	-0.73	-0.66	-0.82	-0.57	-0.12	0.22	-0.31	-0.11	-0.81	
J	0.56	0.78	0.99	1.12	1.16	1.17	1.18	1.17	1.15	1.14	1.13	1.13	1.14	1.16	1.18	1.18	1.18	1.17	1.13	0.99	0.79	0.57
	0.18	0.54	0.38	0.03	0.51	0.04	-0.41	-0.64	-0.70	-0.85	-0.99	-1.03	-0.97	-0.90	-0.90	-0.74	-0.35	0.07	-0.44	-0.11	0.02	-0.36
K	0.62	0.85	1.04	1.16	1.18	1.16	1.17	1.15	1.13	1.11	1.09	1.09	1.11	1.14	1.16	1.17	1.17	1.18	1.17	1.05	0.85	0.62
	1.06	0.79	0.43	-0.02	0.51	0.04	-0.49	-0.69	-0.85	-1.03	-0.97	-1.02	-1.16	-1.05	-0.96	-0.83	-0.35	0.06	-0.49	-0.07	0.26	0.51
L	0.65	0.88	1.07	1.18	1.20	1.18	1.17	1.15	1.12	1.09	1.06	1.06	1.10	1.13	1.15	1.17	1.19	1.21	1.19	1.08	0.88	0.65
	1.08	0.84	0.46	0.07	0.47	0.04	-0.41	-0.69	-0.91	-1.14	-0.85	-0.90	-1.26	-1.11	-0.96	-0.75	-0.36	0.03	-0.40	-0.02	0.31	0.52
M	0.65	0.88	1.07	1.19	1.21	1.19	1.17	1.15	1.12	1.09	1.06	1.06	1.09	1.12	1.15	1.18	1.20	1.22	1.20	1.08	0.88	0.65
	1.08	0.86	0.53	0.17	0.50	0.08	-0.30	-0.63	-0.88	-1.14	-0.91	-0.95	-1.27	-1.08	-0.90	-0.64	-0.32	0.06	-0.30	0.03	0.33	0.53
N	0.61	0.84	1.04	1.17	1.21	1.19	1.17	1.15	1.13	1.10	1.07	1.07	1.10	1.13	1.16	1.18	1.20	1.21	1.18	1.05	0.85	0.62
	1.08	0.83	0.54	0.25	0.54	0.10	-0.20	-0.54	-0.76	-0.98	-0.83	-0.87	-1.11	-0.96	-0.81	-0.54	-0.28	0.10	-0.21	0.05	0.31	0.54
O	0.56	0.78	0.98	1.12	1.18	1.19	1.18	1.16	1.14	1.12	1.11	1.11	1.12	1.14	1.17	1.18	1.20	1.19	1.13	0.99	0.78	0.56
	0.21	0.60	0.51	0.31	0.54	0.11	-0.12	-0.47	-0.56	-0.70	-0.71	-0.75	-0.82	-0.76	-0.73	-0.44	-0.26	0.12	-0.14	0.02	0.10	-0.31
P		0.69	0.89	1.05	1.12	1.17	1.18	1.18	1.15	1.14	1.13	1.14	1.14	1.16	1.18	1.19	1.18	1.13	1.05	0.90	0.70	
		-0.23	0.48	0.27	0.68	0.29	-0.12	-0.40	-0.29	-0.41	-0.53	-0.57	-0.53	-0.47	-0.65	-0.43	-0.07	0.27	-0.17	0.01	-0.72	
Q		0.58	0.78	0.95	1.04	1.12	1.17	1.18	1.17	1.15	1.15	1.15	1.16	1.17	1.19	1.17	1.13	1.05	0.95	0.79	0.59	
		-0.89	0.30	0.26	0.82	0.43	0.00	-0.21	-0.01	-0.18	-0.32	-0.36	-0.28	-0.18	-0.44	-0.29	0.09	0.43	-0.16	-0.15	-1.36	
R			0.66	0.83	0.95	1.06	1.15	1.20	1.18	1.17	1.16	1.16	1.17	1.18	1.20	1.16	1.07	0.95	0.83	0.66		
			-0.44	0.33	0.96	0.56	0.20	0.09	0.27	0.08	0.18	0.15	-0.02	0.11	-0.13	-0.07	0.24	0.60	-0.07	-0.87		
S			0.53	0.69	0.83	0.97	1.09	1.16	1.19	1.20	1.17	1.17	1.20	1.20	1.17	1.10	0.98	0.84	0.69	0.53		
			-0.74	0.37	1.10	0.76	0.40	0.42	0.46	0.25	0.68	0.65	0.16	0.31	0.22	0.15	0.47	0.76	0.00	-1.14		
T				0.55	0.70	0.85	0.98	1.07	1.12	1.14	1.12	1.12	1.14	1.13	1.07	0.98	0.85	0.70	0.55			
				-0.65	0.95	0.96	0.72	0.71	0.69	0.48	0.96	0.93	0.39	0.54	0.52	0.49	0.68	0.64	-1.00			
U					0.54	0.68	0.81	0.91	0.98	1.01	1.00	1.00	1.01	0.98	0.91	0.81	0.68	0.55				
					-0.29	0.99	0.97	0.89	0.85	0.74	1.24	1.21	0.66	0.72	0.72	0.75	0.73	-0.59				
V						0.49	0.60	0.70	0.77	0.82	0.83	0.83	0.82	0.77	0.70	0.60	0.49					
						-0.15	0.34	0.12	0.88	1.12	1.44	1.41	1.04	0.76	-0.05	0.13	-0.39					
W									0.55	0.60	0.62	0.62	0.60	0.55	---------*Reference channel power densities*							
									0.45	1.43	**1.61**	1.58	1.36	0.34	---------*Percent errors for ANM (26 x 26 x 12)*							

Reference is the result of CMFD (104 x 104 x 48)

The maximum normalized channel power density and the maximum percent error are shown in bold character

Figure 4.9: Normalized channel power densities and percent errors of the typical CANDU-6 without Xenon effect problem for ANM (26 x 26 x 12)

	1	2	3	4	5	6	7	8	9	10	11	12	13	14	15	16	17	18	19	20	21	22
A									0.13	0.14	0.14	0.14	0.14	0.13								
									-0.93	0.04	0.13	0.14	0.07	-0.89								
B						0.11	0.14	0.16	0.18	0.19	0.20	0.20	0.19	0.18	0.16	0.14	0.11					
						-1.36	-0.91	-1.16	-0.38	-0.05	0.09	0.10	-0.02	-0.33	-1.10	-0.84	-1.27					
C					0.13	0.16	0.19	0.21	0.23	0.24	0.25	0.25	0.24	0.23	0.21	0.19	0.16	0.13				
					-1.38	-0.12	-0.14	-0.27	-0.28	-0.14	0.01	0.02	-0.11	-0.23	-0.20	-0.05	-0.03	-1.27				
D				0.13	0.17	0.21	0.24	0.26	0.27	0.28	0.29	0.29	0.28	0.27	0.26	0.24	0.21	0.17	0.13			
				-1.41	-0.08	-0.03	-0.16	-0.29	-0.31	-0.19	-0.05	-0.04	-0.16	-0.26	-0.22	-0.07	0.07	0.04	-1.28			
E			0.12	0.17	0.21	0.24	0.27	0.29	0.30	0.31	0.31	0.31	0.31	0.30	0.29	0.27	0.24	0.21	0.17	0.12		
			-1.50	-0.16	0.00	-0.09	-0.22	-0.37	-0.41	-0.30	-0.16	-0.15	-0.26	-0.35	-0.29	-0.12	0.03	0.12	-0.02	-1.36		
F			0.15	0.20	0.24	0.27	0.30	0.31	0.32	0.32	0.32	0.32	0.32	0.32	0.31	0.30	0.27	0.24	0.20	0.15		
			-1.11	-0.05	0.00	-0.10	-0.26	-0.44	-0.52	-0.44	-0.32	-0.31	-0.41	-0.46	-0.36	-0.16	0.02	0.13	0.09	-0.96		
G		0.13	0.18	0.23	0.27	0.29	0.31	0.32	0.33	0.33	0.33	0.33	0.33	0.33	0.32	0.31	0.29	0.27	0.23	0.18	0.13	
		-1.71	-0.29	0.01	0.07	-0.04	-0.30	-0.54	-0.63	-0.59	-0.51	-0.50	-0.55	-0.57	-0.46	-0.19	0.08	0.21	0.16	-0.13	-1.55	
H		0.15	0.20	0.25	0.28	0.31	0.32	0.33	0.33	0.34	0.34	0.34	0.34	0.34	0.33	0.32	0.31	0.28	0.25	0.20	0.15	
		-0.94	-0.02	0.11	0.15	0.01	-0.31	-0.60	-0.70	-0.69	-0.64	-0.62	-0.65	-0.64	-0.51	-0.20	0.14	0.29	0.26	0.14	-0.77	
J	0.12	0.17	0.22	0.27	0.30	0.31	0.32	0.33	0.34	0.34	0.34	0.34	0.34	0.34	0.33	0.32	0.31	0.30	0.27	0.22	0.17	0.12
	-0.51	-0.01	0.11	0.20	0.21	0.03	-0.29	-0.58	-0.72	-0.71	-0.66	-0.64	-0.67	-0.65	-0.49	-0.18	0.16	0.36	0.36	0.27	0.17	-0.33
K	0.13	0.19	0.24	0.28	0.30	0.32	0.33	0.34	0.34	0.34	0.34	0.34	0.34	0.34	0.34	0.33	0.32	0.30	0.28	0.24	0.19	0.13
	0.46	0.32	0.23	0.25	0.22	0.04	-0.27	-0.55	-0.68	-0.66	-0.58	-0.57	-0.61	-0.61	-0.45	-0.15	0.17	0.37	0.42	0.40	0.50	0.64
L	0.14	0.19	0.24	0.28	0.31	0.32	0.33	0.34	0.34	0.34	0.34	0.34	0.34	0.34	0.34	0.33	0.32	0.31	0.28	0.24	0.19	0.14
	0.55	0.45	0.33	0.29	0.22	0.05	-0.23	-0.48	-0.59	-0.54	-0.45	-0.43	-0.50	-0.52	-0.38	-0.11	0.19	0.37	0.45	0.50	0.63	0.74
M	0.14	0.19	0.24	0.28	0.31	0.32	0.33	0.34	0.34	0.34	0.34	0.34	0.34	0.34	0.34	0.33	0.32	0.31	0.28	0.24	0.19	0.14
	0.62	0.53	0.40	0.34	0.25	0.10	-0.15	-0.36	-0.46	-0.40	-0.30	-0.28	-0.36	-0.39	-0.27	-0.03	0.23	0.40	0.50	0.58	0.71	0.81
N	0.13	0.19	0.24	0.28	0.30	0.31	0.33	0.33	0.34	0.34	0.34	0.34	0.34	0.34	0.33	0.33	0.32	0.30	0.28	0.24	0.19	0.13
	0.67	0.55	0.45	0.42	0.36	0.21	-0.01	-0.21	-0.30	-0.25	-0.15	-0.14	-0.20	-0.23	-0.12	0.10	0.34	0.50	0.58	0.62	0.73	0.85
O	0.12	0.17	0.22	0.26	0.29	0.31	0.32	0.33	0.33	0.33	**0.34**	0.34	0.33	0.33	0.33	0.32	0.31	0.29	0.26	0.22	0.17	0.12
	-0.18	0.36	0.48	0.54	0.54	0.41	0.18	-0.03	-0.11	-0.07	0.01	0.02	-0.03	-0.04	0.06	0.29	0.54	0.69	0.70	0.64	0.53	
P		0.15	0.20	0.24	0.28	0.30	0.31	0.32	0.33	0.33	0.33	0.33	0.33	0.33	0.32	0.31	0.30	0.28	0.24	0.20	0.15	
		-0.46	0.51	0.68	0.76	0.67	0.40	0.17	0.11	0.15	0.22	0.23	0.19	0.17	0.26	0.51	0.79	0.90	0.83	0.67	-0.29	
Q		0.13	0.17	0.22	0.25	0.28	0.30	0.31	0.32	0.32	0.32	0.32	0.32	0.32	0.31	0.30	0.28	0.25	0.22	0.17	0.13	
		-1.14	0.39	0.81	0.98	0.91	0.65	0.41	0.35	0.42	0.51	0.53	0.46	0.41	0.49	0.75	1.03	1.12	0.96	0.55	-0.98	
R			0.15	0.19	0.23	0.26	0.28	0.30	0.31	0.31	0.31	0.31	0.31	0.31	0.30	0.28	0.26	0.23	0.19	0.15		
			-0.34	0.92	1.11	1.05	0.86	0.66	0.61	0.73	0.87	0.88	0.76	0.67	0.74	0.96	1.16	1.24	1.06	-0.19		
S			0.12	0.16	0.20	0.23	0.26	0.28	0.29	0.30	0.30	0.30	0.30	0.29	0.28	0.26	0.23	0.20	0.16	0.12		
			-0.70	0.86	1.16	1.12	0.98	0.85	0.86	1.03	1.20	1.21	1.06	0.91	0.92	1.08	1.23	1.28	0.99	-0.56		
T				0.12	0.16	0.19	0.22	0.24	0.26	0.27	0.27	0.27	0.27	0.26	0.24	0.22	0.19	0.16	0.12			
				-0.45	1.04	1.17	1.07	1.00	1.07	1.28	1.48	1.49	1.31	1.12	1.07	1.16	1.27	1.15	-0.33			
U					0.12	0.15	0.18	0.20	0.22	0.23	0.24	0.24	0.23	0.22	0.20	0.18	0.15	0.12				
					-0.34	1.04	1.13	1.10	1.20	1.44	1.65	1.66	1.47	1.25	1.17	1.21	1.14	-0.24				
V						0.11	0.13	0.15	0.17	0.18	0.19	0.19	0.18	0.17	0.15	0.13	0.11					
						-0.19	0.40	0.26	1.17	1.58	1.77	1.78	1.61	1.21	0.32	0.47	-0.11					
W									0.12	0.13	0.14	0.14	0.13	0.12	----------	*Reference bundle power densities*						
									0.63	1.66	1.77	**1.78**	1.69	0.67	----------	*Percent errors for ANM (26 x 26 x 12)*						

Reference is the result of CMFD (104 x 104 x 48)

The maximum normalized bundle power density and the maximum percent error are shown in bold character

Figure 4.10: Normalized bundle power densities and percent errors on plane 1 of the typical CANDU-6 without Xenon effect problem for ANM (26 x 26 x 12)

	1	2	3	4	5	6	7	8	9	10	11	12	13	14	15	16	17	18	19	20	21	22
A									0.89	0.97	1.01	1.01	0.97	0.89								
									-0.51	0.43	0.51	0.52	0.46	-0.47								
B						0.79	0.97	1.13	1.24	1.32	1.37	1.37	1.32	1.24	1.13	0.97	0.79					
						-1.18	-0.66	-0.84	-0.03	0.26	0.38	0.39	0.29	0.02	-0.78	-0.58	-1.09					
C					0.90	1.11	1.30	1.45	1.56	1.63	1.66	1.66	1.63	1.56	1.45	1.30	1.11	0.90				
					-1.32	-0.03	0.04	-0.01	0.01	0.10	0.22	0.23	0.14	0.07	0.06	0.12	0.07	-1.21				
D				0.92	1.17	1.40	1.57	1.69	1.76	1.81	1.83	1.83	1.81	1.76	1.69	1.57	1.40	1.17	0.92			
				-1.39	-0.11	-0.01	-0.05	-0.09	-0.05	-0.01	0.05	0.06	0.03	0.00	-0.02	0.04	0.09	0.01	-1.27			
E			0.87	1.15	1.42	1.61	1.73	1.79	1.81	1.83	1.85	**1.85**	1.83	1.81	1.80	1.73	1.61	1.42	1.15	0.87		
			-1.40	-0.19	-0.08	-0.16	-0.11	-0.26	-0.12	-0.12	-0.20	**-0.18**	-0.08	-0.06	-0.18	-0.01	-0.04	0.05	-0.05	-1.26		
F			1.08	1.37	1.60	1.75	1.78	1.78	1.70	1.69	1.72	1.72	1.69	1.70	1.78	1.79	1.75	1.61	1.37	1.08		
			-1.07	-0.12	-0.13	-0.30	-0.04	-0.42	-0.03	-0.07	-0.44	-0.43	-0.03	0.04	-0.34	0.06	-0.18	0.00	0.02	-0.92		
G		0.93	1.25	1.54	1.73	1.81	1.76	1.70	1.61	1.58	1.61	1.61	1.58	1.61	1.70	1.76	1.81	1.73	1.54	1.25	0.93	
		-1.60	-0.32	-0.13	-0.14	-0.35	-0.11	-0.61	-0.16	-0.26	-0.84	-0.83	-0.22	-0.09	-0.52	0.01	-0.22	0.01	0.02	-0.16	-1.44	
H		1.08	1.40	1.66	1.80	1.82	1.71	1.63	1.53	1.50	1.52	1.52	1.50	1.53	1.63	1.71	1.82	1.80	1.66	1.41	1.09	
		-0.91	-0.14	-0.13	-0.11	-0.39	-0.16	-0.70	-0.36	-0.45	-1.09	-1.08	-0.41	-0.28	-0.60	-0.04	-0.26	0.04	0.03	0.02	-0.74	
J	0.86	1.21	1.52	1.73	1.81	1.76	1.64	1.54	1.47	1.43	1.45	1.45	1.44	1.47	1.54	1.64	1.76	1.81	1.73	1.52	1.21	0.86
	-0.41	-0.04	-0.10	-0.16	-0.03	-0.44	-0.10	-0.56	-0.53	-0.56	-1.12	-1.10	-0.51	-0.46	-0.46	0.03	-0.30	0.13	0.01	0.07	0.14	-0.23
K	0.95	1.29	1.59	1.76	1.78	1.70	1.58	1.49	1.42	1.39	1.40	1.40	1.39	1.42	1.49	1.58	1.70	1.78	1.76	1.59	1.30	0.95
	0.53	0.26	-0.02	-0.25	0.13	-0.30	-0.15	-0.49	-0.59	-0.55	-1.01	-0.99	-0.51	-0.51	-0.38	-0.02	-0.15	0.29	-0.08	0.15	0.44	0.71
L	0.99	1.34	1.62	1.77	1.77	1.67	1.55	1.46	1.39	1.36	1.37	1.37	1.36	1.39	1.46	1.55	1.67	1.77	1.78	1.62	1.34	0.99
	0.61	0.38	0.05	-0.28	0.16	-0.24	-0.15	-0.41	-0.52	-0.45	-0.83	-0.81	-0.41	-0.44	-0.30	-0.02	-0.09	0.32	-0.11	0.23	0.56	0.79
M	0.99	1.34	1.62	1.77	1.77	1.67	1.55	1.45	1.39	1.36	1.37	1.37	1.36	1.39	1.45	1.55	1.67	1.77	1.77	1.62	1.34	0.99
	0.68	0.46	0.14	-0.20	0.22	-0.17	-0.04	-0.27	-0.37	-0.29	-0.64	-0.63	-0.24	-0.29	-0.17	0.09	-0.03	0.38	-0.03	0.32	0.64	0.86
N	0.94	1.29	1.58	1.75	1.77	1.69	1.57	1.47	1.40	1.37	1.38	1.38	1.37	1.40	1.47	1.57	1.69	1.77	1.75	1.58	1.29	0.94
	0.74	0.50	0.23	-0.02	0.31	-0.09	0.17	-0.08	-0.15	-0.08	-0.49	-0.47	-0.03	-0.07	0.02	0.29	0.05	0.47	0.15	0.41	0.68	0.92
O	0.85	1.19	1.50	1.70	1.78	1.73	1.61	1.52	1.44	1.41	1.42	1.42	1.41	1.44	1.52	1.61	1.74	1.79	1.71	1.50	1.19	0.85
	-0.06	0.36	0.33	0.26	0.36	-0.01	0.46	0.10	0.17	0.19	-0.34	-0.33	0.23	0.25	0.20	0.58	0.13	0.51	0.42	0.50	0.53	0.12
P		1.06	1.37	1.62	1.75	1.77	1.67	1.58	1.49	1.46	1.48	1.48	1.46	1.49	1.59	1.67	1.77	1.75	1.62	1.38	1.06	
		-0.39	0.44	0.51	0.58	0.35	0.66	0.19	0.58	0.53	-0.10	-0.08	0.57	0.65	0.28	0.78	0.49	0.73	0.67	0.61	-0.22	
Q		0.90	1.21	1.49	1.67	1.74	1.69	1.64	1.56	1.53	1.56	1.56	1.53	1.56	1.64	1.69	1.75	1.67	1.49	1.22	0.90	
		-0.96	0.42	0.72	0.85	0.70	0.95	0.47	0.98	0.92	0.34	0.35	0.96	1.05	0.56	1.06	0.83	0.99	0.87	0.57	-0.80	
R			1.03	1.31	1.53	1.67	1.71	1.71	1.64	1.63	1.65	1.65	1.63	1.64	1.71	1.71	1.67	1.53	1.31	1.03		
			-0.23	0.90	1.06	0.96	1.19	0.82	1.29	1.29	0.91	0.92	1.33	1.36	0.91	1.29	1.08	1.20	1.04	-0.08		
S			0.82	1.09	1.34	1.53	1.65	1.71	1.73	1.75	1.77	1.77	1.75	1.74	1.71	1.65	1.53	1.34	1.10	0.83		
			-0.48	0.92	1.20	1.19	1.23	1.12	1.33	1.39	1.33	1.34	1.43	1.39	1.20	1.33	1.30	1.33	1.05	-0.34		
T				0.87	1.11	1.32	1.49	1.60	1.68	1.73	1.75	1.75	1.73	1.68	1.60	1.49	1.32	1.11	0.87			
				-0.28	1.14	1.32	1.36	1.39	1.51	1.63	1.73	1.75	1.66	1.56	1.46	1.45	1.43	1.26	-0.15			
U					0.85	1.05	1.23	1.38	1.48	1.55	1.58	1.58	1.55	1.48	1.38	1.23	1.05	0.85				
					-0.10	1.31	1.50	1.56	1.66	1.83	2.01	2.02	1.86	1.71	1.63	1.59	1.41	0.01				
V						0.75	0.92	1.07	1.18	1.26	1.30	1.30	1.26	1.18	1.07	0.92	0.75					
						0.21	0.86	0.77	1.68	2.03	2.18	2.19	2.06	1.72	0.84	0.94	0.30					
W									0.85	0.92	0.96	0.96	0.92	0.85								
									1.21	2.21	2.28	**2.29**	2.23	1.25								

Reference bundle power densities

Percent errors for ANM (26 x 26 x 12)

Reference is the result of CMFD (104 x 104 x 48)

The maximum normalized bundle power density and the maximum percent error are shown in bold character

Figure 4.11: Normalized bundle power densities and percent errors on plane 6 of the typical CANDU-6 without Xenon effect problem for ANM (26 x 26 x 12)

	1	2	3	4	5	6	7	8	9	10	11	12	13	14	15	16	17	18	19	20	21	22
A									0.83	0.89	0.93	0.93	0.89	0.83								
									-0.58	0.28	0.37	0.38	0.31	-0.54								
B						0.74	0.90	1.05	1.15	1.22	1.25	1.25	1.22	1.15	1.05	0.90	0.74					
						-1.18	-0.69	-0.88	-0.15	0.01	0.10	0.11	0.04	-0.10	-0.81	-0.61	-1.08					
C					0.83	1.03	1.21	1.35	1.45	1.50	1.51	1.51	1.50	1.45	1.35	1.21	1.03	0.83				
					-1.32	-0.06	-0.02	-0.06	-0.15	-0.27	-0.19	-0.18	-0.24	-0.10	0.01	0.07	0.04	-1.21				
D				0.85	1.08	1.29	1.46	1.58	1.64	1.67	1.66	1.66	1.67	1.64	1.58	1.46	1.30	1.08	0.85			
				-1.44	-0.15	-0.09	-0.15	-0.19	-0.28	-0.54	-0.54	-0.52	-0.50	-0.23	-0.12	-0.05	0.02	-0.03	-1.31			
E			0.80	1.07	1.31	1.49	1.62	1.69	1.70	1.69	1.68	1.68	1.70	**1.70**	1.69	1.62	1.50	1.31	1.07	0.80		
			-1.42	-0.29	-0.18	-0.33	-0.34	-0.56	-0.60	-0.94	-1.09	-1.08	-0.90	-0.54	-0.48	-0.24	-0.21	-0.06	-0.15	-1.28		
F			1.00	1.26	1.47	1.61	1.67	1.68	1.60	1.57	1.58	1.58	1.57	1.60	1.68	1.67	1.62	1.48	1.26	1.00		
			-1.15	-0.32	-0.35	-0.66	-0.51	-1.12	-0.94	-1.27	-1.65	-1.63	-1.23	-0.87	-1.03	-0.40	-0.53	-0.21	-0.17	-0.99		
G		0.86	1.16	1.41	1.58	1.66	1.64	1.61	1.52	1.49	1.51	1.51	1.49	1.53	1.61	1.64	1.67	1.58	1.41	1.16	0.86	
		-1.59	-0.45	-0.46	-0.49	-0.89	-0.79	-1.52	-1.26	-1.53	-2.02	-2.00	-1.48	-1.19	-1.43	-0.67	-0.76	-0.35	-0.31	-0.29	-1.43	
H		1.01	1.30	1.52	1.63	1.66	1.60	1.55	1.47	1.43	1.45	1.45	1.43	1.47	1.55	1.60	1.66	1.63	1.52	1.30	1.01	
		-0.90	-0.32	-0.60	-0.62	-1.15	-1.08	-1.74	-1.47	-1.63	-2.15	-2.14	-1.59	-1.40	-1.64	-0.96	-1.01	-0.47	-0.44	-0.15	-0.73	
J	0.80	1.12	1.40	1.58	1.64	1.61	1.53	1.47	1.41	1.38	1.39	1.39	1.38	1.41	1.47	1.53	1.61	1.64	1.59	1.41	1.12	0.81
	-0.32	-0.02	-0.28	-0.74	-0.74	-1.48	-1.29	-1.79	-1.73	-1.78	-2.28	-2.27	-1.74	-1.66	-1.69	-1.17	-1.34	-0.58	-0.57	-0.11	0.16	-0.14
K	0.88	1.21	1.47	1.62	1.62	1.56	1.48	1.43	1.37	1.34	1.34	1.34	1.34	1.37	1.43	1.48	1.56	1.62	1.63	1.48	1.21	0.88
	0.61	0.29	-0.17	-0.84	-0.67	-1.45	-1.44	-1.76	-1.86	-1.91	-2.34	-2.32	-1.86	-1.78	-1.66	-1.32	-1.31	-0.51	-0.67	0.01	0.47	0.79
L	0.93	1.25	1.51	1.65	1.63	1.55	1.47	1.41	1.35	1.31	1.30	1.30	1.31	1.35	1.41	1.47	1.56	1.63	1.65	1.51	1.25	0.93
	0.68	0.41	-0.03	-0.73	-0.51	-1.26	-1.30	-1.63	-1.83	-1.94	-2.30	-2.28	-1.89	-1.75	-1.53	-1.17	-1.12	-0.35	-0.56	0.15	0.60	0.86
M	0.93	1.25	1.51	1.65	1.64	1.56	1.47	1.40	1.34	1.30	1.29	1.29	1.30	1.34	1.40	1.47	1.56	1.64	1.65	1.51	1.25	0.93
	0.75	0.50	0.10	-0.53	-0.29	-1.03	-1.06	-1.45	-1.69	-1.83	-2.21	-2.20	-1.78	-1.61	-1.34	-0.94	-0.89	-0.13	-0.36	0.28	0.69	0.93
N	0.88	1.20	1.47	1.63	1.64	1.58	1.49	1.42	1.36	1.32	1.31	1.31	1.32	1.36	1.42	1.49	1.58	1.64	1.63	1.47	1.20	0.88
	0.81	0.55	0.20	-0.29	-0.10	-0.85	-0.81	-1.26	-1.44	-1.53	-1.93	-1.92	-1.48	-1.36	-1.15	-0.69	-0.71	0.05	-0.12	0.38	0.73	0.99
O	0.80	1.11	1.39	1.58	1.64	1.61	1.52	1.45	1.39	1.35	1.36	1.36	1.35	1.39	1.45	1.52	1.61	1.65	1.58	1.39	1.11	0.80
	0.01	0.39	0.25	-0.03	-0.02	-0.71	-0.48	-1.06	-1.06	-1.10	-1.55	-1.54	-1.05	-0.99	-0.96	-0.36	-0.58	0.14	0.13	0.42	0.57	0.19
P		0.99	1.27	1.48	1.59	1.62	1.56	1.51	1.43	1.40	1.41	1.41	1.40	1.43	1.51	1.56	1.62	1.59	1.48	1.27	0.99	
		-0.37	0.29	0.07	0.07	-0.41	-0.27	-0.88	-0.56	-0.69	-1.19	-1.18	-0.64	-0.49	-0.78	-0.15	-0.28	0.22	0.22	0.45	-0.20	
Q		0.83	1.11	1.35	1.50	1.58	1.57	1.55	1.47	1.45	1.47	1.47	1.45	1.47	1.55	1.57	1.58	1.50	1.35	1.12	0.84	
		-0.95	0.19	0.13	0.19	-0.18	-0.01	-0.56	-0.15	-0.35	-0.85	-0.84	-0.31	-0.08	-0.47	0.10	-0.05	0.33	0.28	0.35	-0.79	
R			0.94	1.18	1.37	1.50	1.57	1.60	1.53	1.51	1.53	1.53	1.51	1.53	1.60	1.57	1.50	1.37	1.18	0.94		
			-0.48	0.27	0.40	0.11	0.33	-0.04	0.35	0.12	-0.23	-0.22	0.15	0.41	0.05	0.43	0.23	0.53	0.42	-0.33		
S			0.75	0.99	1.20	1.38	1.52	1.60	1.62	1.62	1.62	1.62	1.62	1.62	1.60	1.52	1.39	1.21	0.99	0.75		
			-0.69	0.42	0.71	0.61	0.67	0.68	0.81	0.58	0.49	0.50	0.62	0.87	0.75	0.77	0.72	0.83	0.55	-0.54		
T				0.79	1.00	1.21	1.38	1.49	1.56	1.59	1.58	1.58	1.59	1.56	1.49	1.38	1.21	1.00	0.79			
				-0.52	0.94	1.09	1.12	1.21	1.23	1.02	1.04	1.05	1.05	1.28	1.28	1.21	1.20	1.06	-0.39			
U					0.78	0.97	1.14	1.28	1.37	1.42	1.43	1.43	1.42	1.37	1.28	1.14	0.97	0.78				
					-0.05	1.33	1.46	1.48	1.45	1.35	1.47	1.48	1.38	1.50	1.54	1.54	1.43	0.05				
V						0.69	0.85	0.99	1.09	1.16	1.19	1.19	1.16	1.09	1.00	0.85	0.70					
						0.32	0.90	0.74	1.53	1.76	1.91	1.92	1.79	1.58	0.81	0.98	0.42					
W									0.79	0.85	0.89	0.89	0.85	0.79	----------*Reference bundle power densities*							
									1.16	2.13	2.26	**2.27**	2.16	1.20	---------*Percent errors for ANM (26 x 26 x 12)*							

Reference is the result of CMFD (104 x 104 x 48)

The maximum normalized bundle power density and the maximum percent error are shown in bold character

Figure 4.12: Normalized bundle power densities and percent errors on plane 8 of the typical CANDU-6 without Xenon effect problem for ANM (26 x 26 x 12)

	1	2	3	4	5	6	7	8	9	10	11	12	13	14	15	16	17	18	19	20	21	22
A									-1.05	-0.77	-1.24	-1.28	-0.88	-1.22								
									0.12	1.01	1.25	1.22	0.93	-0.01								
B						-1.12	-0.55	-0.13	0.90	0.87	0.56	0.52	0.75	0.70	-0.39	-0.87	-1.51					
						-0.30	0.06	-0.17	0.56	0.73	0.99	0.96	0.65	0.42	-0.36	-0.18	-0.59					
C					-0.45	1.13	1.08	1.00	0.97	0.87	0.69	0.65	0.74	0.77	0.72	0.73	0.72	-0.91				
					-0.34	0.86	0.72	0.65	0.55	0.45	0.83	0.80	0.36	0.40	0.44	0.47	0.56	-0.68				
D				-0.38	1.27	1.18	1.02	0.93	0.84	0.76	0.46	0.42	0.62	0.62	0.63	0.65	0.75	0.78	-0.91			
				-0.63	0.83	0.84	0.59	0.52	0.41	0.19	0.66	0.62	0.09	0.25	0.30	0.32	0.52	0.47	-1.02			
E			-1.03	1.22	1.19	0.97	0.91	0.87	0.82	0.75	0.40	0.35	0.61	0.58	0.56	0.52	0.51	0.67	0.65	-1.63		
			-0.69	0.51	0.80	0.65	0.43	0.27	0.20	-0.10	0.25	0.21	-0.21	0.03	0.04	0.15	0.32	0.42	0.10	-1.12		
F			-0.12	1.11	0.88	0.66	0.37	0.16	-0.62	-0.79	-1.08	-1.13	-0.95	-0.86	-0.17	-0.04	0.18	0.34	0.52	-0.75		
			-0.43	0.46	0.63	0.41	0.28	-0.03	0.04	-0.25	-0.09	-0.13	-0.36	-0.14	-0.27	-0.01	0.07	0.24	0.03	-0.89		
G		-1.51	0.83	0.98	0.74	0.48	-0.14	-0.29	-0.63	-0.68	-0.67	-0.72	-0.84	-0.89	-0.63	-0.56	-0.02	0.19	0.36	0.18	**-2.18**	
		-0.96	0.26	0.31	0.60	0.32	0.02	-0.34	-0.22	-0.42	-0.48	-0.52	-0.54	-0.41	-0.59	-0.28	-0.04	0.20	-0.14	-0.22	-1.46	
H		-0.19	0.90	0.78	0.46	0.17	-0.20	-0.29	-0.65	-0.75	-0.81	-0.87	-0.92	-0.92	-0.66	-0.64	-0.35	-0.12	0.15	0.23	-0.88	
		-0.30	0.38	0.15	0.64	0.26	-0.25	-0.56	-0.47	-0.61	-0.75	-0.79	-0.73	-0.66	-0.82	-0.57	-0.12	0.22	-0.31	-0.11	-0.81	
J	-1.17	0.76	0.82	0.69	0.39	-0.33	-0.63	-0.70	-0.82	-0.88	-1.01	-1.07	-1.05	-1.10	-1.07	-1.08	-0.86	-0.21	0.04	0.14	0.05	-1.90
	0.18	0.54	0.38	0.03	0.51	0.04	-0.41	-0.64	-0.70	-0.85	-0.99	-1.03	-0.97	-0.90	-0.90	-0.74	-0.35	0.07	-0.44	-0.11	0.02	-0.36
K	-0.87	0.74	0.69	0.52	-0.07	-0.76	-0.68	-0.69	-0.86	-0.95	-1.15	-1.21	-1.12	-1.15	-1.07	-1.14	-1.29	-0.68	-0.14	-0.01	0.01	-1.61
	1.06	0.79	0.43	-0.02	0.51	0.04	-0.49	-0.69	-0.85	-1.03	-0.97	-1.02	-1.16	-1.05	-0.96	-0.83	-0.35	0.06	-0.49	-0.07	0.26	0.51
L	-1.18	0.63	0.70	0.68	0.47	-0.18	-0.49	-0.61	-0.84	-0.94	-1.21	-1.27	-1.12	-1.12	-0.99	-0.95	-0.72	-0.14	0.02	0.00	-0.09	-1.92
	1.08	0.84	0.48	0.07	0.47	0.04	-0.41	-0.69	-0.91	-1.14	-0.85	-0.90	-1.26	-1.11	-0.96	-0.75	-0.36	0.03	-0.40	-0.02	0.31	0.52
M	-1.13	0.69	0.76	0.72	0.45	-0.20	-0.44	-0.54	-0.78	-0.90	-1.20	-1.27	-1.07	-1.07	-0.92	-0.91	-0.74	-0.16	0.06	0.07	-0.03	-1.86
	1.08	0.86	0.53	0.17	0.50	0.08	-0.30	-0.63	-0.88	-1.14	-0.91	-0.95	-1.27	-1.08	-0.90	-0.64	-0.32	0.06	-0.30	0.03	0.33	0.53
N	-0.74	0.90	0.90	0.80	0.45	-0.20	-0.40	-0.48	-0.71	-0.84	-1.21	-1.27	-1.01	-0.99	-0.85	-0.86	-0.73	-0.14	0.15	0.22	0.19	-1.47
	1.08	0.83	0.54	0.25	0.54	0.10	-0.20	-0.54	-0.76	-0.98	-0.83	-0.87	-1.11	-0.96	-0.81	-0.54	-0.28	0.10	-0.21	0.05	0.31	0.54
O	-1.01	0.98	1.09	1.03	0.94	0.26	-0.29	-0.42	-0.58	-0.61	-0.63	-0.69	-0.78	-0.85	-0.78	-0.74	-0.26	0.36	0.40	0.42	0.28	-1.71
	0.21	0.60	0.51	0.31	0.54	0.11	-0.12	-0.47	-0.56	-0.70	-0.71	-0.75	-0.82	-0.76	-0.73	-0.44	-0.26	0.12	-0.14	0.02	0.10	-0.31
P		0.00	1.11	0.97	0.59	0.27	-0.01	-0.06	-0.40	-0.49	-0.54	-0.59	-0.65	-0.66	-0.40	-0.43	-0.22	0.03	0.36	0.46	-0.67	
		-0.23	0.48	0.27	0.68	0.29	-0.12	-0.40	-0.29	-0.41	-0.53	-0.57	-0.53	-0.47	-0.65	-0.43	-0.07	0.27	-0.17	0.01	-0.72	
Q		-1.39	0.96	1.09	0.77	0.38	-0.01	-0.08	-0.37	-0.43	-0.52	-0.57	-0.58	-0.61	-0.41	-0.41	-0.09	0.24	0.51	0.34	-2.02	
		-0.89	0.30	0.26	0.82	0.43	0.00	-0.21	-0.01	-0.18	-0.32	-0.36	-0.28	-0.18	-0.44	-0.29	0.09	0.43	-0.16	-0.15	-1.36	
R			-0.02	1.24	0.99	0.56	0.53	0.39	-0.31	-0.41	-0.51	-0.56	-0.55	-0.54	0.09	0.15	0.12	0.49	0.69	-0.60		
			-0.44	0.33	0.96	0.56	0.20	0.09	0.27	0.08	0.18	0.15	-0.02	0.11	-0.13	-0.07	0.24	0.60	-0.07	-0.87		
S			-0.89	1.37	1.23	0.81	1.12	1.17	1.16	1.14	0.85	0.81	1.01	0.95	0.88	0.77	0.40	0.76	0.85	-1.44		
			-0.74	0.37	1.10	0.76	0.40	0.42	0.46	0.25	0.68	0.65	0.16	0.31	0.22	0.15	0.47	0.76	0.00	-1.14		
T				0.07	1.87	1.72	1.45	1.32	1.23	1.16	0.88	0.84	1.04	1.03	1.05	1.12	1.33	1.42	-0.41			
				-0.65	0.95	0.96	0.72	0.71	0.69	0.48	0.96	0.93	0.39	0.54	0.52	0.49	0.68	0.64	-1.00			
U					-0.02	1.61	1.53	1.43	1.38	1.22	0.79	0.75	1.10	1.20	1.19	1.23	1.24	-0.42				
					-0.29	0.99	0.97	0.89	0.85	0.74	1.24	1.21	0.66	0.72	0.72	0.75	0.73	-0.59				
V						-0.72	-0.12	0.32	1.39	1.43	1.32	1.29	1.33	1.22	0.10	-0.40	-1.05					
						-0.15	0.34	0.12	0.88	1.12	1.44	1.41	1.04	0.76	-0.05	0.13	-0.39					
W									-0.55	-0.22	-0.62	-0.66	-0.31	-0.70	*Percent errors for CMFD (26 x 26 x12)*							
									0.45	1.43	**1.61**	1.58	1.36	0.34	*Percent errors for ANM (26 x 26 x 12)*							

Reference is the result of CMFD (104 x 104 x 48)

The maximum percent errors are shown in bold character

Figure 4.13: Comparison of percent errors of channel power densities from CMFD (26 x 26 x 12) and ANM (26 x 26 x 12) for the typical CANDU-6 without Xenon effect problem

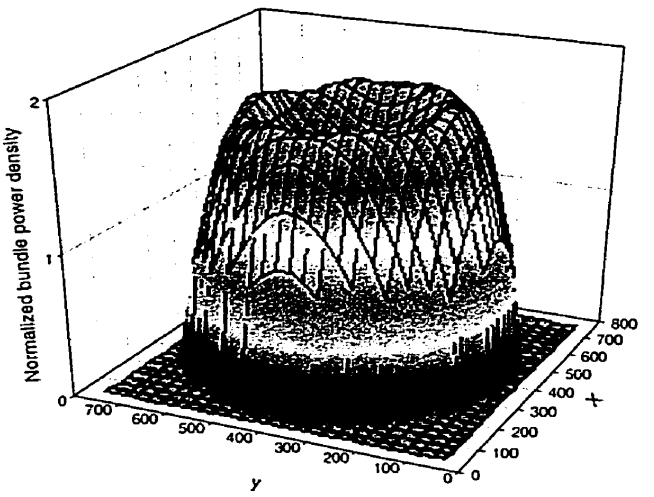

Figure 4.14: Normalized bundle power densities on plane 6 of the typical CANDU-6 without effect Xenon problem for ANM (26 x 26 x12)

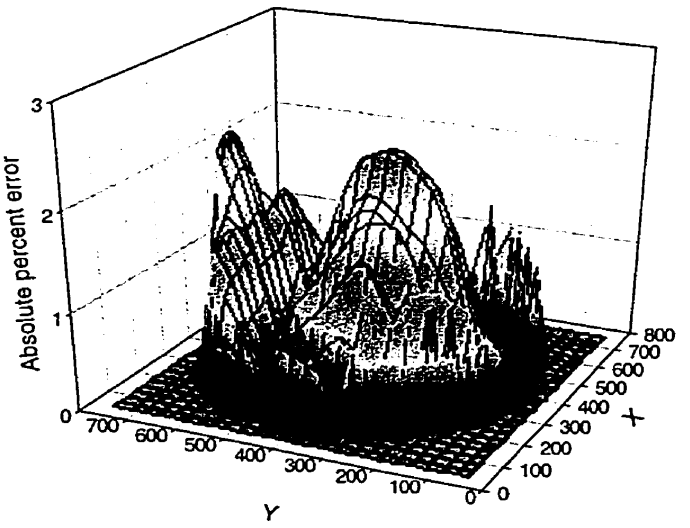

Figure 4.15: Absolute percent errors of bundle power densities on plane 6 of the typical CANDU-6 without Xenon effect problem for ANM (26 x 26 x12)

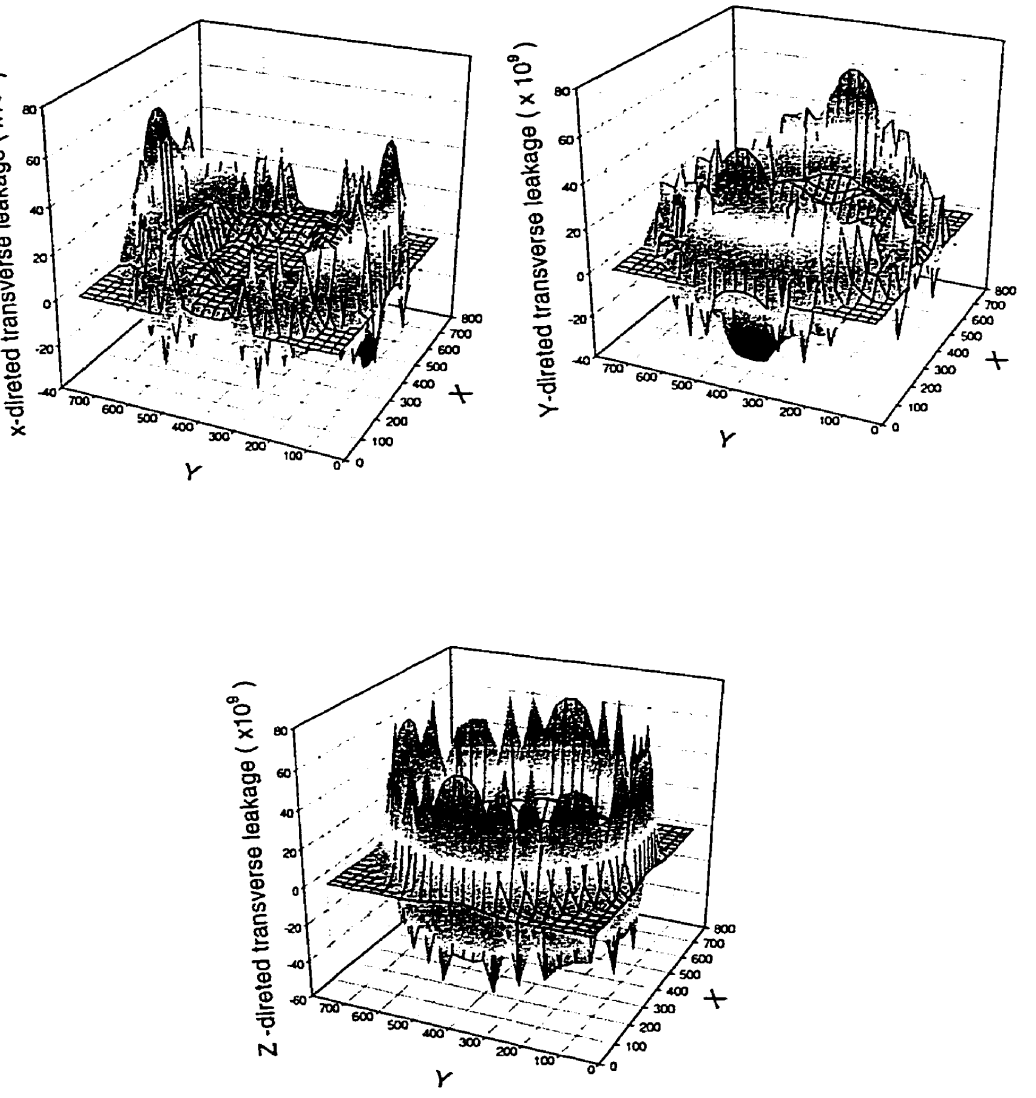

Figure 4.16: Transverse leakages of thermal group on plane 6 of the typical CANDU-6 without Xenon effect problem for ANM (26 x 26 x12)

	1	2	3	4	5	6	7	8	9	10	11	12	13	14	15	16	17	18	19	20	21	22
A									0.87	0.95	0.99	0.99	0.95	0.87								
									0.88	0.95	1.00	1.00	0.95	0.88								
B						0.78	0.95	1.11	1.24	1.32	1.36	1.36	1.32	1.24	1.12	0.95	0.78					
						0.78	0.96	1.12	1.24	1.33	1.37	1.37	1.33	1.24	1.12	0.96	0.78					
C					0.89	1.11	1.30	1.45	1.56	1.63	1.66	1.66	1.63	1.56	1.45	1.30	1.11	0.89				
					0.89	1.11	1.30	1.45	1.56	1.63	1.66	1.66	1.63	1.56	1.45	1.30	1.11	0.89				
D				0.91	1.17	1.40	1.57	1.69	1.76	1.81	1.83	1.83	1.81	1.76	1.69	1.57	1.40	1.17	0.91			
				0.91	1.17	1.40	1.57	1.68	1.76	1.80	1.83	1.83	1.80	1.76	1.68	1.57	1.40	1.17	0.91			
E			0.85	1.16	1.42	1.62	1.74	1.80	1.82	1.84	1.85	**1.85**	1.84	1.82	1.80	1.74	1.62	1.42	1.16	0.85		
			0.85	1.16	1.42	1.61	1.73	1.79	1.82	1.83	**1.85**	1.85	1.83	1.82	1.79	1.73	1.61	1.42	1.16	0.85		
F			1.07	1.37	1.61	1.74	1.78	1.77	1.68	1.67	1.70	1.70	1.67	1.68	1.77	1.78	1.75	1.61	1.37	1.07		
			1.07	1.37	1.60	1.74	1.77	1.76	1.68	1.66	1.69	1.69	1.66	1.68	1.76	1.77	1.74	1.60	1.37	1.07		
G		0.91	1.25	1.54	1.73	1.81	1.74	1.69	1.60	1.57	1.59	1.59	1.57	1.60	1.69	1.75	1.81	1.73	1.54	1.25	0.91	
		0.91	1.25	1.53	1.72	1.80	1.74	1.68	1.59	1.56	1.59	1.59	1.56	1.59	1.68	1.74	1.80	1.72	1.53	1.25	0.91	
H		1.07	1.41	1.66	1.80	1.82	1.71	1.62	1.52	1.49	1.51	1.51	1.49	1.52	1.62	1.71	1.82	1.80	1.66	1.41	1.07	
		1.07	1.40	1.65	1.78	1.81	1.70	1.61	1.52	1.48	1.50	1.50	1.48	1.52	1.61	1.70	1.81	1.78	1.65	1.40	1.07	
J	0.85	1.21	1.52	1.73	1.81	1.75	1.62	1.53	1.45	1.42	1.44	1.44	1.42	1.45	1.53	1.62	1.75	1.81	1.73	1.52	1.21	0.85
	0.85	1.20	1.51	1.72	1.80	1.74	1.61	1.52	1.45	1.42	1.43	1.43	1.42	1.45	1.52	1.61	1.74	1.80	1.72	1.51	1.20	0.85
K	0.93	1.29	1.59	1.76	1.78	1.69	1.57	1.48	1.41	1.38	1.39	1.39	1.38	1.41	1.48	1.57	1.69	1.78	1.76	1.59	1.30	0.93
	0.93	1.29	1.58	1.75	1.76	1.68	1.56	1.47	1.40	1.37	1.38	1.38	1.37	1.40	1.47	1.56	1.68	1.76	1.75	1.58	1.29	0.93
L	0.97	1.34	1.62	1.78	1.77	1.67	1.54	1.45	1.38	1.35	1.36	1.36	1.35	1.38	1.45	1.54	1.67	1.77	1.78	1.62	1.34	0.97
	0.97	1.33	1.61	1.76	1.75	1.65	1.53	1.44	1.37	1.34	1.35	1.35	1.34	1.37	1.44	1.53	1.65	1.75	1.76	1.61	1.33	0.97
M	0.97	1.34	1.62	1.78	1.77	1.67	1.54	1.45	1.38	1.35	1.36	1.36	1.35	1.38	1.45	1.54	1.67	1.77	1.78	1.62	1.34	0.97
	0.97	1.33	1.61	1.76	1.75	1.65	1.53	1.44	1.37	1.34	1.35	1.35	1.34	1.37	1.44	1.53	1.65	1.75	1.76	1.61	1.33	0.97
N	0.93	1.29	1.58	1.76	1.78	1.68	1.56	1.47	1.40	1.37	1.38	1.38	1.37	1.40	1.47	1.56	1.69	1.78	1.76	1.59	1.29	0.93
	0.92	1.28	1.57	1.74	1.76	1.67	1.55	1.46	1.39	1.36	1.37	1.37	1.36	1.39	1.46	1.55	1.67	1.76	1.74	1.57	1.28	0.92
O	0.84	1.20	1.51	1.72	1.80	1.74	1.61	1.52	1.44	1.41	1.42	1.42	1.41	1.44	1.52	1.61	1.74	1.80	1.72	1.51	1.20	0.84
	0.84	1.19	1.49	1.70	1.78	1.72	1.59	1.50	1.42	1.39	1.40	1.40	1.39	1.42	1.50	1.59	1.72	1.78	1.70	1.49	1.19	0.84
P		1.06	1.39	1.63	1.77	1.79	1.68	1.59	1.50	1.46	1.48	1.48	1.46	1.50	1.60	1.68	1.79	1.77	1.63	1.39	1.06	
		1.05	1.37	1.61	1.74	1.76	1.66	1.57	1.48	1.45	1.47	1.47	1.45	1.48	1.57	1.66	1.76	1.74	1.61	1.37	1.05	
Q		0.89	1.22	1.50	1.68	1.76	1.70	1.65	1.56	1.54	1.56	1.56	1.54	1.56	1.65	1.70	1.76	1.68	1.50	1.23	0.89	
		0.88	1.21	1.49	1.66	1.74	1.68	1.63	1.54	1.52	1.54	1.54	1.52	1.54	1.63	1.68	1.74	1.66	1.49	1.21	0.88	
R			1.03	1.33	1.55	1.69	1.72	1.72	1.64	1.63	1.66	1.66	1.63	1.64	1.72	1.72	1.69	1.55	1.33	1.03		
			1.03	1.31	1.53	1.66	1.70	1.70	1.62	1.61	1.63	1.63	1.61	1.62	1.70	1.70	1.66	1.53	1.31	1.03		
S			0.82	1.11	1.37	1.55	1.68	1.74	1.77	1.79	1.81	1.81	1.79	1.77	1.75	1.68	1.56	1.37	1.11	0.82		
			0.81	1.10	1.35	1.54	1.65	1.72	1.74	1.76	1.78	1.78	1.76	1.74	1.72	1.65	1.54	1.35	1.10	0.81		
T				0.87	1.13	1.35	1.51	1.63	1.71	1.76	1.78	1.78	1.76	1.71	1.63	1.52	1.35	1.13	0.87			
				0.86	1.12	1.33	1.49	1.61	1.68	1.73	1.75	1.75	1.73	1.68	1.61	1.49	1.33	1.12	0.86			
U					0.85	1.07	1.25	1.40	1.51	1.58	1.61	1.61	1.58	1.51	1.40	1.25	1.07	0.85				
					0.84	1.06	1.24	1.38	1.49	1.56	1.59	1.59	1.56	1.49	1.38	1.24	1.06	0.84				
V						0.75	0.92	1.08	1.20	1.29	1.33	1.33	1.29	1.20	1.08	0.92	0.75					
						0.74	0.91	1.07	1.19	1.27	1.31	1.31	1.27	1.19	1.07	0.91	0.74					
W									0.85	0.92	0.96	0.96	0.92	0.85	*without Xenon effect*							
									0.84	0.91	0.95	0.95	0.91	0.84	*with Xenon effect*							

The maximum normalized bundle power densities are shown in bold character

Figure 4.17: Xenon effect on normalized bundle power densities at plane 6 of the typical CANDU-6 problem for CMFD (26 x 26 x 12)

	1	2	3	4	5	6	7	8	9	10	11	12	13	14	15	16	17	18	19	20	21	22
A									0.89	0.97	1.02	1.02	0.97	0.89								
									0.89	0.98	1.02	1.02	0.98	0.89								
B						0.78	0.96	1.12	1.24	1.33	1.37	1.37	1.33	1.24	1.12	0.96	0.78					
						0.79	0.96	1.12	1.24	1.33	1.37	1.37	1.33	1.24	1.12	0.96	0.79					
C					0.89	1.11	1.30	1.45	1.56	1.63	1.66	1.66	1.63	1.56	1.45	1.30	1.11	0.89				
					0.89	1.11	1.30	1.45	1.55	1.63	1.66	1.66	1.63	1.55	1.45	1.30	1.11	0.89				
D				0.91	1.17	1.40	1.57	1.68	1.76	1.81	1.83	1.83	1.81	1.76	1.69	1.57	1.40	1.17	0.91			
				0.91	1.17	1.40	1.56	1.68	1.75	1.80	1.82	1.82	1.80	1.75	1.68	1.56	1.40	1.17	0.91			
E			0.85	1.15	1.42	1.61	1.73	1.79	1.81	1.83	1.84	**1.84**	1.83	1.81	1.79	1.73	1.61	1.42	1.15	0.86		
			0.86	1.15	1.41	1.61	1.72	1.78	1.80	1.82	1.83	**1.83**	1.82	1.80	1.78	1.72	1.61	1.41	1.15	0.86		
F			1.06	1.37	1.60	1.74	1.78	1.77	1.70	1.69	1.71	1.71	1.69	1.70	1.77	1.79	1.74	1.61	1.37	1.07		
			1.07	1.37	1.60	1.73	1.78	1.76	1.70	1.68	1.70	1.70	1.68	1.70	1.76	1.78	1.73	1.60	1.37	1.07		
G		0.91	1.25	1.54	1.73	1.80	1.75	1.69	1.61	1.58	1.59	1.59	1.58	1.61	1.69	1.76	1.81	1.73	1.54	1.25	0.92	
		0.92	1.25	1.53	1.72	1.79	1.75	1.68	1.60	1.57	1.59	1.59	1.57	1.60	1.68	1.75	1.79	1.72	1.53	1.25	0.92	
H		1.07	1.40	1.65	1.79	1.81	1.71	1.62	1.53	1.49	1.50	1.50	1.49	1.53	1.62	1.71	1.82	1.80	1.66	1.41	1.08	
		1.07	1.40	1.65	1.78	1.80	1.70	1.61	1.52	1.49	1.50	1.50	1.49	1.52	1.61	1.70	1.80	1.78	1.65	1.40	1.07	
J	0.86	1.21	1.52	1.72	1.81	1.75	1.64	1.53	1.46	1.43	1.43	1.43	1.43	1.46	1.54	1.64	1.76	1.81	1.73	1.52	1.21	0.86
	0.86	1.20	1.51	1.71	1.80	1.74	1.63	1.53	1.45	1.42	1.43	1.43	1.42	1.45	1.53	1.63	1.74	1.80	1.71	1.51	1.20	0.86
K	0.95	1.30	1.59	1.76	1.79	1.70	1.58	1.48	1.41	1.38	1.39	1.39	1.38	1.41	1.48	1.58	1.70	1.79	1.76	1.59	1.30	0.95
	0.95	1.29	1.58	1.74	1.77	1.68	1.57	1.47	1.40	1.37	1.38	1.38	1.37	1.40	1.47	1.57	1.68	1.77	1.75	1.58	1.29	0.95
L	1.00	1.34	1.62	1.77	1.77	1.67	1.55	1.45	1.38	1.36	1.36	1.36	1.36	1.39	1.45	1.55	1.67	1.78	1.78	1.63	1.35	1.00
	1.00	1.34	1.61	1.76	1.76	1.65	1.54	1.44	1.38	1.35	1.35	1.35	1.35	1.38	1.44	1.54	1.65	1.76	1.76	1.61	1.34	1.00
M	1.00	1.34	1.62	1.77	1.77	1.67	1.55	1.45	1.38	1.35	1.36	1.36	1.35	1.38	1.45	1.55	1.67	1.77	1.77	1.63	1.35	1.00
	0.99	1.33	1.61	1.75	1.75	1.65	1.53	1.44	1.37	1.34	1.35	1.35	1.34	1.37	1.44	1.53	1.65	1.75	1.75	1.61	1.33	0.99
N	0.95	1.29	1.58	1.75	1.78	1.69	1.57	1.47	1.40	1.37	1.38	1.38	1.37	1.40	1.47	1.57	1.69	1.78	1.76	1.59	1.30	0.95
	0.94	1.29	1.57	1.73	1.76	1.67	1.55	1.46	1.39	1.36	1.36	1.36	1.36	1.39	1.46	1.56	1.67	1.76	1.73	1.57	1.29	0.94
O	0.85	1.20	1.50	1.71	1.79	1.73	1.62	1.52	1.44	1.41	1.42	1.42	1.41	1.44	1.52	1.62	1.74	1.80	1.71	1.51	1.20	0.86
	0.85	1.19	1.49	1.69	1.77	1.71	1.60	1.50	1.43	1.40	1.40	1.40	1.40	1.43	1.50	1.60	1.71	1.77	1.69	1.49	1.19	0.85
P		1.06	1.38	1.63	1.76	1.78	1.68	1.59	1.50	1.47	1.48	1.48	1.47	1.50	1.59	1.68	1.78	1.77	1.63	1.38	1.06	
		1.05	1.37	1.61	1.74	1.76	1.66	1.57	1.48	1.45	1.46	1.46	1.45	1.48	1.57	1.66	1.76	1.74	1.61	1.37	1.05	
Q		0.89	1.22	1.50	1.68	1.76	1.71	1.65	1.57	1.54	1.56	1.56	1.54	1.57	1.65	1.71	1.76	1.69	1.50	1.22	0.90	
		0.89	1.21	1.48	1.66	1.73	1.69	1.63	1.55	1.52	1.54	1.54	1.52	1.55	1.63	1.69	1.73	1.66	1.48	1.21	0.89	
R			1.03	1.32	1.55	1.68	1.73	1.72	1.66	1.65	1.67	1.67	1.65	1.66	1.72	1.73	1.69	1.55	1.32	1.03		
			1.02	1.31	1.53	1.66	1.70	1.69	1.63	1.62	1.64	1.64	1.62	1.63	1.69	1.70	1.66	1.53	1.31	1.02		
S			0.82	1.10	1.36	1.55	1.67	1.73	1.76	1.78	1.79	1.79	1.78	1.76	1.73	1.67	1.55	1.36	1.11	0.82		
			0.82	1.10	1.35	1.53	1.64	1.71	1.73	1.75	1.76	1.76	1.75	1.73	1.71	1.64	1.53	1.35	1.10	0.82		
T				0.87	1.12	1.34	1.51	1.63	1.70	1.75	1.78	1.78	1.75	1.71	1.63	1.51	1.34	1.12	0.87			
				0.86	1.11	1.32	1.49	1.60	1.68	1.72	1.75	1.75	1.73	1.68	1.60	1.49	1.32	1.11	0.86			
U					0.85	1.06	1.25	1.40	1.51	1.58	1.61	1.62	1.58	1.51	1.40	1.25	1.06	0.85				
					0.84	1.05	1.23	1.38	1.49	1.56	1.59	1.59	1.56	1.49	1.38	1.24	1.05	0.84				
V						0.75	0.92	1.08	1.20	1.29	1.33	1.33	1.29	1.20	1.08	0.93	0.75					
						0.75	0.92	1.07	1.19	1.27	1.31	1.31	1.27	1.19	1.07	0.92	0.75					
W									0.86	0.94	0.99	0.99	0.94	0.86	——————————— *without xenon effect*							
									0.85	0.93	0.98	0.98	0.93	0.85	——————————— *with xenon effect*							

Reference is the result of CMFD (104 x 104 x 48)

The maximum normalized bundle power densities are shown in bold character

Figure 4.18: Xenon effect on normalized bundle power densities at plane 6 of typical CANDU-6 problem for ANM (26 x 26 x 12)

CHAPTER 5
ANALYTIC NODAL METHOD FOR 3-D SPACE-TIME KINETICS NEUTRON DIFFUSION EQUATION

5.1 Introduction

In chapters 1 and 3, the Analytic Nodal Method was derived for the solution of the two-group, static diffusion equations for multi-dimensional reactors consisting of homogenized Cartesian nodes. The only approximation required in the derivation was that the shape of the transverse leakage is spatially flat across each node. Efficient numerical solution procedures were developed and the CANDU benchmark problem and typical CANDU-6 problem were solved. In all of the test cases, the Analytic Nodal Method was shown to have a higher accuracy while employing bundle-sized spatial meshes. Comparison of solutions with Coarse Mesh Finite Difference Method revealed that the nodal method could get more accurate solution for the CANDU reactor problem.

It is possible to take advantage of power of the Analytical Nodal Method with the flat transverse leakage approximation to solve kinetic diffusion problems for the CANDU reactors as well. In this chapter, the three-dimensional, temporally- and spatially-discretized Analytic Nodal diffusion equations are derived. An algorithm for solving these neutronic equations in tandem is presented. Solutions to three-dimensional, time-dependent problems for CANDU reactors are presented in next Chapter.

5.2 Formulation of the Kinetics Nodal Diffusion Equations

The time-dependent nodal balance equations are found by integrating the time- and space-dependent multigroup neutron equations 1.1 over the volume of an arbitrary node (i, j, k) to obtain (Smith, 1979)

$$\frac{1}{v}\frac{\partial}{\partial t}\bar{\phi}_{i,j,k}(t)V_{i,j,k} = -(\bar{J}_{gx,j,k}(x_{i+1},t)-\bar{J}_{gx,j,k}(x_i,t))h_y^j h_z^k - (\bar{J}_{gy,i,k}(y_{j+1},t)-\bar{J}_{gy,i,k}(y_j,t))h_x^i h_z^k$$
$$-(\bar{J}_{gz,i,j}(z_{k+1},t)-\bar{J}_{gz,i,j}(z_k,t))h_x^i h_y^j - \Sigma_{tg,i,j,k}(t)\bar{\phi}_{g,i,j,k}(t)V_{i,j,k}$$
$$+\sum_{g'=1}^{G}\Sigma_{g\leftarrow g',i,j,k}(t)\bar{\phi}_{g',i,j,k}(t)V_{i,j,k}$$
$$+(1-\beta)\frac{1}{\gamma}\chi_g^{\,p}\sum_{g'=1}^{G}\upsilon\Sigma_{fg',i,j,k}(t)\ \bar{\phi}_{g',i,j,k}(t)V_{i,j,k} + \sum_{d=1}^{D}\chi_g^d\lambda_d\bar{C}_{d,i,j,k}(t)V_{i,j,k} \qquad 5.1a$$

$$\frac{\partial}{\partial t}\bar{C}_{d,i,j,k}(t) = \beta_d\sum_{g'=1}^{G}\frac{1}{\gamma}\upsilon\Sigma_{fg',i,j,k}(t)\bar{\phi}_{g',i,j,k}(t) - \lambda_d\bar{C}_{d,i,j,k}(t) \qquad 5.1b$$

where the surface average current over the nodal surface at $x = x_i$ of time t is given by

$$\bar{J}_{gx,j,k}(x_i,t) \equiv \frac{1}{h_y^j}\frac{1}{h_z^k}\int_{y_j}^{y_{j+1}}dy\int_{z_k}^{z_{k+1}}dzJ_{gx}(x_i,y,z,t)$$

with very similar expressions for the other five surface currents. The nodal average flux and node average precursor are

$$\bar{\phi}_{g,i,j,k}(t) = \frac{1}{h_z^k}\frac{1}{h_y^j}\frac{1}{h_x^i}\int_{z_k}^{z_{k+1}}dz\int_{y_j}^{y_{j+1}}dy\int_{x_i}^{x_{i+1}}dx\phi_g(x,y,z,t)$$

$$\bar{C}_{d,i,j,k}(t) = \frac{1}{h_z^k}\frac{1}{h_y^j}\frac{1}{h_x^i}\int_{z_k}^{z_{k+1}}dz\int_{y_j}^{y_{j+1}}dy\int_{x_i}^{x_i}dxC_d(x,y,z,t)$$

Then we integrate equations 1.1 over the direction y and direction z, to obtain a differential equation from which the x-directed spatial coupling of equations 5.1a can be determined for node (i,j,k)

$$\frac{1}{v_g}\frac{\partial}{\partial t}\phi_{gi,j,k}(x,t) = -\frac{\partial}{\partial x}J_{gx,i,j,k}(x,t) - S_{gx,i,j,k}(t) - \Sigma_{tg,i,j,k}(t)\phi_{g,i,j,k}(x,t)$$
$$+\sum_{g'=1}^{G}\Sigma_{g\leftarrow g'}(t)\phi_{g',i,j,k}(x,t) + \chi_g^p(1-\beta)\frac{1}{\gamma}\sum_{g'=1}^{G}\upsilon\Sigma_{fg',i,j,k}(t)\phi_{g',i,j,k}(x,t)$$
$$+\sum_{d=1}^{D}\chi_g^d\lambda_d C_{d,i,j,k}(x,t)$$

5.2a

and

$$\frac{\partial}{\partial t}C_{d,i,j,k}(x,t)=\beta_d\frac{1}{\gamma}\sum_{g'=1}^{G}\upsilon\Sigma_{fg',i,j,k}(t)\phi_{g',i,j,k}(x,t)-\lambda_d C_{d,i,j,k}(x,t) \qquad 5.2b$$

In order to simplify the algebra, we introduce the exponential transform ϖ^p of the flux $\phi_{g,i,j,k}(x,t)$

$$\frac{\partial}{\partial t}\phi_{g,i,j,k}(x,t)=\varpi^p_{g,i,j,k}\phi_{g,i,j,k}(x,t) \qquad 5.3$$

and ϖ^d of the precursor $C_{d,i,j,k}$

$$\frac{\partial}{\partial t}C_{d,i,j,k}(x,t)=\varpi^d_{i,j,k}C_{d,i,j,k}(x,t) \qquad 5.4$$

The precursor equation 5.2b becomes

$$C_{d,i,j,k}(x,t)=\frac{\beta_d}{\varpi^d_{i,j,k}+\lambda_d}\frac{1}{\gamma}\sum_{g'=1}^{G}\upsilon\Sigma_{fg',i,j,k}(t)\phi_{g',i,j,k}(x,t) \qquad 5.5$$

while the transverse integrated flux equation 5.2a becomes

$$\begin{aligned}0=&-\frac{\partial}{\partial x}J_{gx,i,j,k}(x,t)-S_{gx,i,j,k}(x,t)-\Sigma_{tg,i,j,k}(t)\phi_{g,i,j,k}(x,t)\\&+\sum_{g'=1}^{G}\Sigma_{g\leftarrow g'}(t)\phi_{g',i,j,k}(x,t)-\frac{\varpi^p_{g,i,j,k}}{\nu_g}\phi_{g,i,j,k}(x,t)\\&+\chi^p_g(1-\beta)\frac{1}{\gamma}\sum_{g'=1}^{G}\upsilon\Sigma_{fg',i,j,k}(t)\phi_{g',i,j,k}(x,t)\\&+\sum_{d=1}^{D}\chi^d_g\frac{\lambda_d\beta_d}{\varpi^d_{i,j,k}+\lambda_d}\frac{1}{\gamma}\sum_{g'=1}^{G}\upsilon\Sigma_{fg',i,j,k}(t)\phi_{g',i,j,k}(x,t)\end{aligned} \qquad 5.6$$

by introducing matrix notation, this last equation can be written as

$$\frac{\partial}{\partial x}[J_x(x,t)]_{i,j,k} = -[S_x(x,t)]_{i,j,k} - [\Sigma(t)]_{i,j,k}[\phi(x,t)]_{i,j,k}$$
$$+ (1-\beta)[\chi^p]\frac{1}{\gamma}[\upsilon\Sigma_f(t)]^T_{i,j,k}[\phi(x,t)]_{i,j,k}$$
$$+ \sum_{d=1}^{D}[\chi^d]\frac{\lambda_d\beta_d}{\varpi^d_{i,j,k}+\lambda_d}\frac{1}{\gamma}[\upsilon\Sigma_f(t)]^T_{i,j,k}[\phi(x,t)]_{i,j,k} \qquad 5.7$$
$$-\left[\frac{\varpi^p_{i,j,k}}{v}\right][\phi(x,t)]_{i,j,k}$$

We define a new matrix $[\Sigma']$

$$[\Sigma'(t)] \equiv [\Sigma(t)] - (1-\beta)[\chi^p]\frac{1}{\gamma}[\upsilon\Sigma_f(t)]^T - \sum_{d=1}^{D}\frac{\lambda_d\beta_d}{\varpi^d+\lambda_d}[\chi^d]\frac{1}{\gamma}[\upsilon\Sigma_f(t)]^T + diag(\frac{\varpi^p_g}{v_g}) \qquad 5.8$$

to finally write

$$\frac{\partial}{\partial x}[J_x(x,t)]_{i,j,k} + [\Sigma'(t)]_{i,j,k}[\phi(x,t)]_{i,j,k} = -[S_x(x,t)]_{i,j,k} \qquad 5.9$$

Using the Fick's law, an extra relationship is obtained

$$[J_x(x,t)]_{i,j,k} = -[D_x(t)]_{i,j,k}\frac{\partial}{\partial x}[\phi(x,t)]_{i,j,k} \qquad 5.10$$

for a fixed time, t, equation 5.9 and equation 5.10 can be solved analytically (provided the ϖ^p and ϖ^d are known) in the same manner as in Chapter 1, by using the average transverse leakage. Hence, the coupling equation is given by equation analogous to equation 1.39,

$$[\bar{L}_x(t)]_{i,j,k} = [F_x^{i-1}(t)]_{i,j,k}[\bar{\phi}(t)]_{i-1,j,k} + [F_x^{i}(t)]_{i,j,k}[\bar{\phi}(t)]_{i,j,k} + [F_x^{i+1}(t)]_{i,j,k}[\bar{\phi}(t)]_{i+1,j,k}$$
$$+ [G_x^{i-1}(t)]_{i,j,k}[S_x(t)]_{i-1,j,k} + [G_x^{i}(t)]_{i,j,k}[S_x(t)]_{i,j,k} + [G_x^{i+1}(t)]_{i,j,k}[S_x(t)]_{i+1,j,k} \qquad 5.11$$

the matrix elements of equation 5.11 are different depend on the kinetic distortion terms.

A similar approach can be followed for the other two directions. The final three equations for the leakages combine with equation 5.1, we obtain the kinetic Analytic Nodal diffusion equations,

$$\begin{bmatrix} [V]^{-1} & [0] & [0] & [0] \\ [0] & [0] & [0] & [0] \\ [0] & [0] & [0] & [0] \\ [0] & [0] & [0] & [0] \end{bmatrix} \frac{\partial}{\partial t} \begin{bmatrix} [\bar{\phi}(t)] \\ [\bar{L}_x(t)] \\ [\bar{L}_y(t)] \\ [\bar{L}_z(t)] \end{bmatrix} =$$

$$\begin{bmatrix} [F(t)] & -(h_z^k[G_y(t)]+h_y^j[G_z(t)]) & -(h_z^k[G_x(t)]+h_x^i[G_z(t)]) & -(h_x^i[G_y(t)]+h_y^j[G_x(t)]) \\ [F_x(t)] & -[I] & \frac{1}{h_y^j}[G_x(t)] & \frac{1}{h_z^k}[G_x(t)] \\ [F_y(t)] & \frac{1}{h_x^i}[G_y(t)] & -[I] & \frac{1}{h_z^k}[G_y(t)] \\ [F_z(t)] & \frac{1}{h_x^i}[G_z(t)] & \frac{1}{h_y^j}[G_z(t)] & -[I] \end{bmatrix}$$

$$\times \begin{bmatrix} [\bar{\phi}(t)] \\ [\bar{L}_x(t)] \\ [\bar{L}_y(t)] \\ [\bar{L}_z(t)] \end{bmatrix} + \sum_{d=1}^{D} \begin{bmatrix} [V_{i,j,k}[\chi^d]\lambda_d \bar{C}_{d,i,j,k}(t)] \\ [0] \\ [0] \\ [0] \end{bmatrix} \qquad 5.12$$

where

$$[F(t)] \equiv (-[\Sigma_T(t)] - h_y^j h_z^k [F_x(t)] - h_x^i h_z^k [F_y(t)] - h_x^i h_y^j [F_z(t)] + [M(t)]$$

$$[M(t)] \equiv \left\{ (1-\beta) V_{i,j,k} [\chi^p] \frac{1}{\gamma} [\upsilon \Sigma_{f,i,j,k}(t)]^T \right\}$$

$$[V]^{-1} \equiv diag\{V_{i,j,k}[\nu]^{-1}\}$$

Equations 5.12 and 5.1b represent the global system of equations which must be solved to obtain the time- and space-dependent reactor power distributions.

5.3 Time Iteration Method and Solution Techniques

Equations 5.12 represent a system of spatially-discretized, time-dependent ordinary differential equations. Of the four blocks of equation 5.12, only the first involves a temporal operator. The latter three blocks are simply expressions for the transverse leakages at time t and do not involve temporal operators. Hence, any time integration scheme which approximates the temporal derivatives of equation 5.1b and the first block of equation 5.12 can be employed to solve the time-dependent equations. If solutions to the kinetic nodal diffusion equations are desired only at discrete times, a finite difference approximation to the temporal derivatives can be used.

Let it be desired to approximate the solutions to kinetic nodal equations at the times

$$t = t_0, t_1, t_2, \ldots,$$

where time intervals are defined as

$$\Delta t_n \equiv t_{n+1} - t_n$$

Equation 5.1b and the first block of equation 5.12 can be written in a much simpler form as

$$[V]^{-1} \frac{\partial}{\partial t}[\bar{\phi}(t)] = [F(t)]\ [\bar{\phi}(t)] - [S(t)] + \sum_{d=1}^{D} \lambda_d [\bar{C}_d(t)] \qquad 5.13a$$

$$\frac{\partial}{\partial t}[\bar{C}_d(t)] = [M_d(t)]\ [\bar{\phi}(t)] - \lambda_d [\bar{C}_d(t)]; \qquad \text{d=1,2,3,...,D} \qquad 5.13b$$

where

$$[\bar{S}(t)] \equiv (\ h_z^k [G_y(t)] + h_y^j [G_z(t)]\ )[\bar{L}_x(t)] + (\ h_z^k [G_x(t)] + h_x^i [G_z(t)]\ )[\bar{L}_y(t)] + (\ h_x^i [G_y(t)] + h_y^j [G_x(t)]\ )[\bar{L}_z(t)]$$

$$[\bar{C}_d(t)] \equiv col\{V_{i,j,k}[\chi^d]\ \bar{C}_{d,i,j,k}(t)\}$$

$$[M_d] \equiv \left\{ V_{i,j,k} \beta_d [\chi^d] \frac{1}{\gamma} [\upsilon \Sigma_{f,i,j,k}(t)]^T \right\}$$

Equations 5.13 can be differenced using the fully implicit method to obtain the approximations

$$[V]^{-1} \frac{1}{\Delta t_n} \left\{ [\bar{\phi}]^{n+1} - [\bar{\phi}]^n \right\} = [F]^{n+1} [\bar{\phi}]^{n+1} - [\bar{S}]^{n+1} + \sum_{d=1}^{D} \lambda_d [\bar{C}_d]^{n+1} \qquad 5.14a$$

$$\frac{1}{\Delta t_n} \left\{ [\bar{C}_d]^{n+1} - [\bar{C}_d]^n \right\} = [M_d]^{n+1} [\bar{\phi}]^{n+1} - \lambda_d [\bar{C}_d]^{n+1} \qquad 5.14b$$

Equation 5.14b can be rearranged to obtain

$$[\bar{C}_d]^{n+1} = (1 + \lambda_d \Delta t_n)^{-1} ([\bar{C}_d]^n + \Delta t_n [M_d]^{n+1} [\bar{\phi}]^{n+1}) \qquad \text{d=1,2,...,D} \qquad 5.15$$

Equation 5.15 can be substituted into equation 5.14a, and the resulting equation can be solved for $[\bar{\phi}]^{n+1}$. Performing the substitution and some subsequent rearrangement yields

$$\left\{ \frac{1}{\Delta t_n} [V]^{-1} - [F]^{n+1} - \sum_{d=1}^{D} \frac{\lambda_d \Delta t_n}{(1 + \lambda_d \Delta t_n)} [M_d]^{n+1} \right\} [\bar{\phi}]^{n+1} = -[\bar{S}]^{n+1} + \frac{1}{\Delta t_n} [V]^{-1} + \sum_{d=1}^{D} \frac{\lambda_d}{(1 + \lambda_d \Delta t_n)} [\bar{C}_d]^n \qquad 5.16$$

Equations 5.15 and equation 5.16 do not completely specify the temporal integration scheme. In order to advance the node-averaged fluxes from one time step to the next by use of equation 5.16, $[\bar{S}]^{n+1}$ must be known. Since $[\bar{S}]^{n+1}$ depends upon $[\bar{\phi}]^{n+1}$, it is not possible to solve directly for $[\bar{\phi}]^{n+1}$. The full set of kinetic, spatially-discretized Analytic Nodal diffusion equations can be obtained by combining equations 5.12, 5.15, and 5.16.

$$\begin{bmatrix} [P]^{n+1} & -(h_z^k[G_y]^{n+1}+h_y^j[G_z]^{n+1}) & -(h_z^k[G_x]^{n+1}+h_x^i[G_z]^{n+1}) & -(h_x^i[G_y]^{n+1}+h_y^j[G_x]^{n+1}) \\ [F_x]^{n+1} & -[I] & \frac{1}{h_y^j}[G_x]^{n+1} & \frac{1}{h_z^k}[G_x]^{n+1} \\ [F_y]^{n+1} & \frac{1}{h_x^i}[G_y]^{n+1} & -[I] & \frac{1}{h_z^k}[G_y]^{n+1} \\ [F_z]^{n+1} & \frac{1}{h_x^i}[G_z]^{n+1} & \frac{1}{h_y^j}[G_z]^{n+1} & -[I] \end{bmatrix}$$

$$\times \begin{bmatrix} [\bar{\phi}]^{n+1} \\ [\bar{L}_x]^{n+1} \\ [\bar{L}_y]^{n+1} \\ [\bar{L}_z]^{n+1} \end{bmatrix} = \begin{bmatrix} [Q]^n & [0] & [0] & [0] \\ [0] & [0] & [0] & [0] \\ [0] & [0] & [0] & [0] \\ [0] & [0] & [0] & [0] \end{bmatrix} \begin{bmatrix} [\bar{\phi}]^n \\ [\bar{L}_x]^n \\ [\bar{L}_y]^n \\ [\bar{L}_z]^n \end{bmatrix} + \begin{bmatrix} \sum_{d=1}^{D} \left(\frac{\lambda_d}{(1+\lambda_d \Delta t_n)}\right) [\bar{C}_d]^n \\ [0] \\ [0] \\ [0] \end{bmatrix} \qquad 5.17$$

$$[\bar{C}_d]^{n+1} = (1+\lambda_d \Delta t_n)^{-1} ([\bar{C}_d]^n + \Delta t_n [M_d]^{n+1} [\bar{\phi}]^{n+1}) \qquad \text{d=1,2,...,D} \qquad 5.15$$

where

$$[P]^{n+1} \equiv \frac{1}{\Delta t_n}[V]^{-1} - [F]^{n+1} - \sum_{d=1}^{D} \frac{\lambda_d \Delta t_n}{(1+\lambda\ \Delta t_n)} [M_d]^{n+1}$$

$$[Q]^n \equiv \frac{1}{\Delta t_n}[V]^{-1}$$

The details of the iterative process will be provided in the next section.

5.4 Kinetics Solution Techniques

The full set of temporally- and spatially-discretized Analytic Nodal diffusion equations are given by equations 5.15 and 5.17. This section provides the details of a kinetics solution technique required to solve the equations.

5.4.1 Matrix Updating

The complicated matrices in equation 5.16 arise from the analytic solutions to the leakage equation. If these matrices are updated at each time step, the computational effort expended in the updating process will dominate the total solution time. It is unnecessary to recompute these matrices every time step, the complete matrices updating can be performed every 3 to 10 time steps (Smith, 1979).

5.4.2 Frequency Estimations

Since the leakage coupling matrices obtained depend on ϖ_p and ϖ_d, it is necessary to estimate these quantities. We use such approximations as at time step n, the frequencies are assumed to be given by the expressions:

$$\varpi^n_{p,i,j,k} = \frac{1}{\Delta t_{n-1}} \ln\left(\frac{\overline{\phi}^n_{g,i,j,k}}{\overline{\phi}^{n-1}_{g,i,j,k}}\right) \qquad 5.18a$$

$$\varpi^n_{d,i,j,k} = \frac{1}{\Delta t_{n-1}} \ln\left(\frac{\overline{C}^n_{d,i,j,k}}{\overline{C}^{n-1}_{d,i,j,k}}\right). \qquad 5.18b$$

In all but the most rapidly changing kinetics, the frequencies play a very minor role (Smith, 1979).

5.4.3 Iteration

In solving the static problem, it is found that performing one inner iteration per outer iteration was adequate. In the kinetic case, it also appears possible to perform only one inner iteration per time step, provided those reasonable estimates of leakages at the advanced time step are available. These estimates of leakages are obtained by using

the estimated space-dependent frequencies, given by equation 5.18 to extrapolate the leakages. That is, the leakages at time step n+1 are approximated by

$$\left[\bar{L}_{u,i,j,k}\right]^{n+1} = \left[\bar{L}_{u,i,j,k}\right]^{n} \exp(\left[\varpi_{p,i,j,k}\right]^{n} \Delta t_n); \qquad u=x,y,z \tag{5.19}$$

Since the leakages terms in nodal balance equations are generally small in magnitude compared to the flux terms, the errors introduced when only one inner iteration is performed are generally quite acceptable.

The flux iterations performed at each inner iteration are identical with those of the static problem. To facilitate rapid convergence of the node-averaged fluxes at each time step, the fluxes are extrapolated to the advanced time step in the same manner as the leakages,

$$\left[\bar{\phi}_{i,j,k}\right]^{n+1} = \left[\bar{\phi}_{i,j,k}\right]^{n} \exp(\left[\varpi_{p,i,j,k}\right]^{n} \Delta t_n) \tag{5.20}$$

In most kinetics problems, less than five flux iterations are required to achieve an error reduction of 10^{-3} in node-averaged fluxes. A larger number of flux iterations may be required when extrapolated fluxes are poor estimates of the actual fluxes. Such erroneous situations can occur when sudden movements of control rods take place or in time domains near local power extreme. Nevertheless, the extrapolation procedure significantly reduces the computational effort required to solve the kinetic nodal diffusion equations.

The Cyclic Chebyshev Semi-Iterative (CCSI) flux iterations or Gauss-Seidel flux iterations or successive overrelaxation (SOR) flux iterations can be used. At each inner iteration, the convergence is defined as the same as for static calculation.

5.4.4 Kinetics Solution Algorithm

A description of kinetics solution algorithm is outlined below:

1. Choose the times (0,T_1, T2, T3...T_i) which divide the kinetics problem into domains within each Δt, ε is a constant.
2. Assume $[\bar{\phi}]^n, [\bar{L}_u]^n, [\bar{C}_d]^n, [\varpi_p]^n$ *and* $[\varpi_d]^n$ are known at time t_n.
3. If $t_n = T_i$, change Δt and ε to correspond to those of time domain $i+1$. Calculate new CCSI optimization parameters.
4. Alter cross sections to correspond to core status at time t_{n+1}.
5. Calculate matrix elements.
6. Obtain approximations for $[\bar{\phi}]^{n+1}$ *and* $[\bar{L}_u]^{n+1}$ by extrapolating with equations 5.19 and 5.20.
7. Solve equation 5.17 for $[\bar{\phi}]^{n+1}$ *and* $[\bar{L}_u]^{n+1}$.
8. Solve equation 5.15 for $[\bar{C}_d]^{n+1}$.
9. Calculate new frequencies, $[\varpi_p]^{n+1}, [\varpi_d]^{n+1}$ with equation 5.18.
10. Repeat steps 3-9 for each time step until the end of the last time domain.

5.5 Summary

In this chapter, the three-dimensional, temporally- and spatially-discretized Analytic Nodal diffusion equations were derived by employing fully implicit time iteration method. An efficient algorithm for solving the equations in tandem was detailed.

The method described in this chapter will be applied to the CANDU benchmark and the typical CANDU-6 problem in Chapter 6. The accuracy and efficiency of Analytic Nodal Method are presented. Comparisons of Analytic Nodal Method with Coarse Mesh Finite Difference are also presented.

CHAPTER 6
NUMERICAL RESULTS FOR 3D SPACE-TIME KINETICS NEUTRON DIFFUSION CALCULATIONS

6.1 Introduction

In chapter 5, the spatially- and temporally-discretized Analytic Nodal diffusion equations were derived. A method for solving these equations was presented for two-group case.

In this chapter, the kinetic Analytic Nodal Method is applied to 3-D kinetic CANDU benchmark problem and the typical CANDU-6 problem. The results of these two problems are presented, including the comparison to the results from Coarse Mesh Finite Difference Method.

6.2 The 3-D CANDU Kinetics Benchmark Problem

A simplified three-dimensional CANDU benchmark problem (ANL, 1985) with asymmetric reactivity insertion is used for the purpose of checking our implementation of the ANM in the NDF code. A detailed description of the benchmark can be found in section A1.2 of Appendix 1.

This problem is modeled with two neutron groups, six-delayed precursor families. The core has 88 channels divided into inner and outer fuel regions. Each channel is assumed to have 10 fuel bundles. The cell–averaged cross sections for each region, including the reflector are provided by the benchmark specification.

The reactivity insertion in the benchmark problem has two components:

- A component that introduces a negative incremental thermal absorption cross section that varies linearly in time over a fixed volume of the reactor, and is intended to represent a positive reactivity insertion as from a loss-of coolant accident.
- A component that introduces a fixed positive incremental thermal-absorption cross section over a volume that varies with time, to represent the negative reactivity insertion from a shutdown system.

The regions affected by two types of perturbation are showed in Section A1.2. The resulting transient is followed for 2.5 seconds.

The static solution to the 3-D CANDU benchmark problem was described in Section 4.3.2. It is believed that the small errors (less than 4.3%) of the Analytic Nodal Method in predicting the spatial power distribution should have little effect on the kinetic solution presented in this section.

In order to evaluate the accuracy of the different methods, it is necessary to have a reference solution. Unfortunately, all the published solutions for this problem were from Coarse Mesh Finite Difference Method with the coarse spatial meshes (18 x 18 x 10), which is not considered suitable as reference. Hence a Coarse Mesh Finite Difference Method results with 54 x 54 x 30 spatial meshes from NDF calculation is used as the reference in this study. The reference calculations use a time step size of 12.5 ms. These calculations employed convergence criterion of 10^{6}.

The Analytic Nodal Method calculations employed the mesh size (18 x 18 x 10) and the time step of 12.5 ms or 25 ms. The convergence criterion used by ANM was 10^{-6}. Results for the 3-D CANDU benchmark with time step size 12.5ms obtained by Analytic Nodal method and Coarse Mesh Finite Difference Method with the same

spatial meshes are displayed in Figure 6.1. Comparison of the percent errors of total power is contained in Figure 6.2. Results for time step size 25ms obtained by Analytic Nodal method and Coarse Mesh Finite Difference Method are displayed in Figure 6.3. Comparison of the percent errors of total power is contained in Figure 6.4. These results indicate that the time-dependent total power predicted by the Analytic Nodal Method has an excellent agreement with the reference values. The maximum error in total power is of 3 %, and there is no significant loss of accuracy for Analytic Nodal Method during the transient. The difference between Coarse Mesh Finite Difference Method results and the reference values is very small (slightly larger than the ANM results) in the beginning of the transient, but the difference increases quickly in 1.2 seconds and reaches to about 13% after 1.8 seconds, which is not considered negligible. Similar conclusions are observed for the transient channel power and bundle power predictions, as shown in Figures 6.5 to 6.10, separately. This significant decrease in accuracy indicates that the CMFD is not as reliable as the ANM for rapid transient scenario with significant leakage distribution in the core. To improve the calculation accuracy, either the fine mesh with finite difference method or the nodal method must be applied.

The following detailed results are given for this kinetic problem:

- Figure 6.5: Relative channel power density of channel (5,10) versus time.
- Figure 6.6: Percent average error of channel power density versus time.
- Figure 6.7: Relative bundle power density of bundle (6,10,5) versus time.
- Figure 6.9: Relative bundle power density of bundle (7,3,1) versus time.
- Figure 6.10: Relative bundle power density of bundle (9,9,5) versus time.
- Figure 6.11: Relative bundle power distribution on plane 5 versus time.
- Figure 6.12: Relative channel power density distribution at time 0.9s.
- Figure 6.13: Relative bundle power density on plane 5 distribution at time 0.9s.

- Figure 6.14: Comparison of percent errors in bundle power density on plane 5 from CMFD and ANM.

All these results indicate that the Analytic Nodal Method is more accurate than the CMFD for 3-D CANDU kinetic benchmark problem with the bundle-size meshes.

6.3 The Typical CANDU-6 Kinetics Problem

The typical CANDU-6 problem is a full core 3-D, 2-group model, with all reactivity devices, such as liquid zone controllers and adjuster rods. The problem is somewhat simplified, as the axial notch in the reflector is not present in this problem, and Xenon is not taken into account. The fuel and reactivity device macroscopic cross-sections were calculated using the DRAGON/DONJON chain code (Marleau et al. 1993, 1994; Roy et al., 1993). The detailed description of this problem can be found in Section A1.3.

This problem can be used to simulate both normal and abnormal situations. In this thesis, we use it for rod ejection simulation. The transient is initiated by instantaneous withdrawal of the first bank of 5 all-inserted adjuster rods, initially in the core. The resulting transient is followed for 900 seconds.

The static solution to the typical CANDU-6 model was described in Section 4.3.3. It was found that the errors of nodal power were lower, these small errors should have little effect on the kinetics solution.

The reactor regulation system is used in this problem. All the devices are initially set to reference positions. Each device is then moved and set to a new position independently based on the results of the reactor regulating system algorithms. No

reference solution is available for this problem, hence, it is difficult to measure, in absolute sense, the errors in the solution of the Analytic Nodal Method.

The Analytic Nodal Method calculations employed the mesh size (26 x 26 x 12) and the time step size of 25 ms. The convergence criterion used by ANM was 10^{-6}. The Coarse Mesh Finite Difference Method calculations used the same mesh size same time step and same convergence criterion. The resulting plots of total power density as a function of time are shown in Figure 6.15. It indicate that the agreement of Analytic Nodal Method with Coarse Mesh Finite Difference Method is well.

Figure 6.16, Figure 6.17 and Figure 6.18 present the channel power density of a channel as a function of time for channel (E12), (L11) and (L22). Figure 6.19, Figure 6.20 and Figure 6.21 present the bundle power density of a bundle as a function of time for bundles (E12,6), (L11,6) and (S17,6).

All the results exhibit that the curve obtained from Analytic Nodal Method is similar to the curve obtained from Coarse Mesh Finite Difference Method. The Analytic Nodal Method has been demonstrated to be a good method for the simulation of the CANDU reactor.

6.4 Summary

In this chapter, the kinetic Analytic Nodal Method with flat leakage approximation has been applied to two CANDU reactor problems. Results indicate that the accurate time-dependent solutions can be obtained with coarse spatial and temporal meshes. The Analytic Nodal Method with flat transverse leakage approximation was shown to be a very accurate method for solving the multidimensional, two-group kinetics diffusion equation for the CANDU reactor.

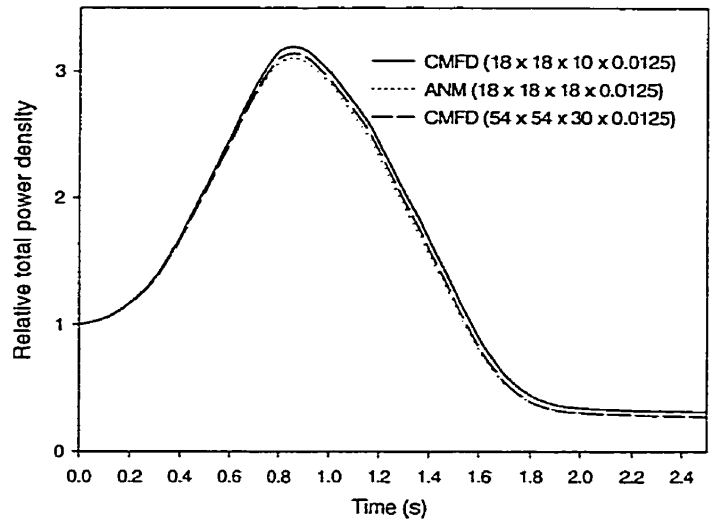

Figure 6.1: Relative total power density versus time for the CANDU benchmark problem (time step = 0.0125s)

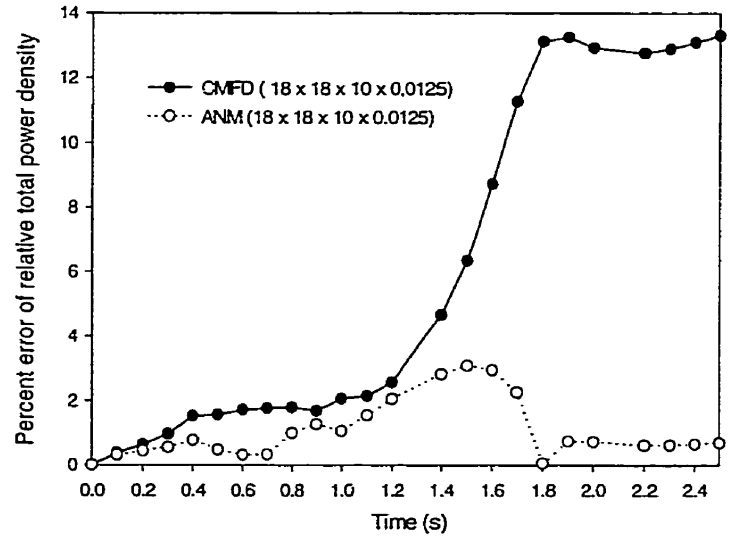

Figure 6.2: Percent error of relative total power density versus time for the CANDU benchmark problem (time step = 0.0125s)

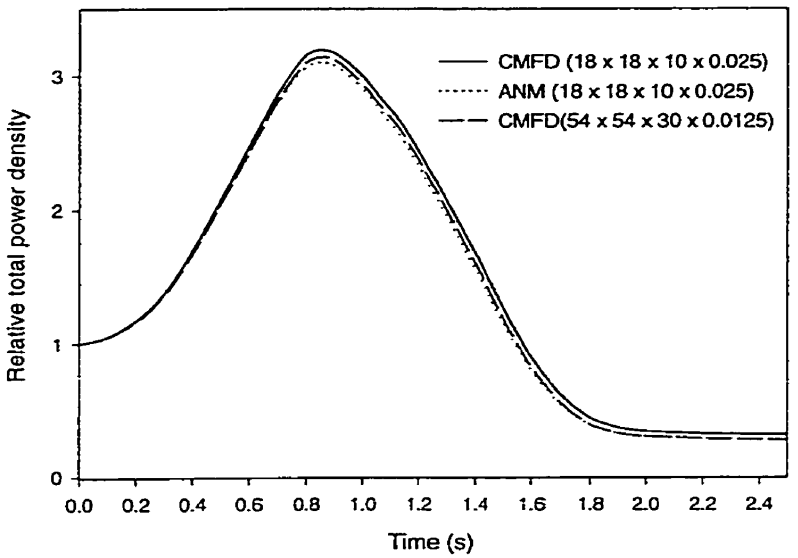

Figure 6.3: Relative total power density versus time for the CANDU benchmark problem (time step =0.025s)

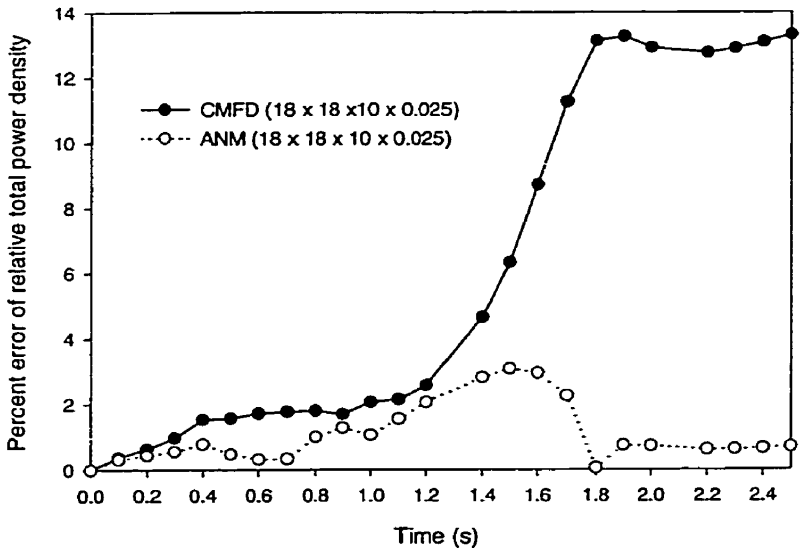

Figure 6.4: Percent error of relative total power density versus time for the CANDU benchmark problem (time step = 0.025s)

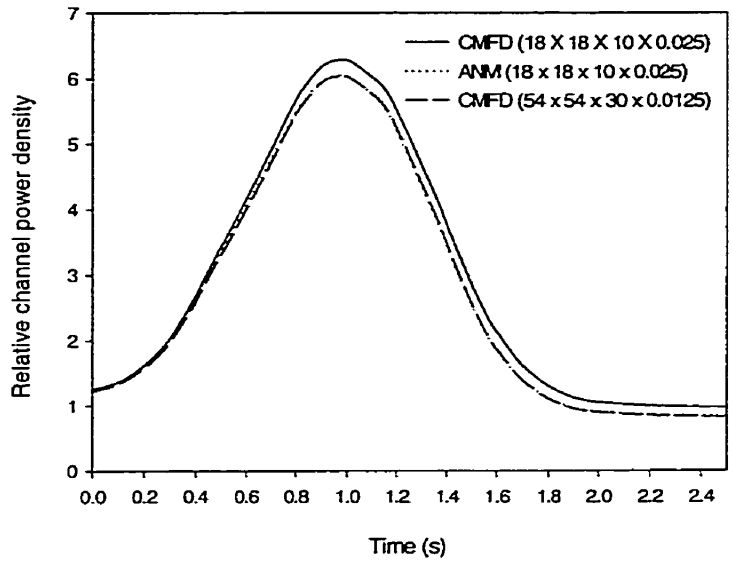

Figure 6.5: Relative channel power density of channel (5,10) versus time for the CANDU benchmark problem (time step = 0.025s)

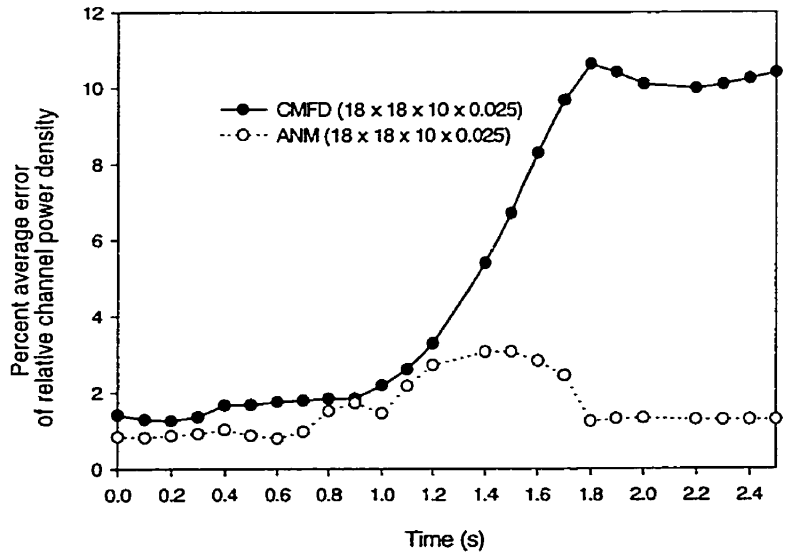

Figure 6.6: Percent average error of relative channel power density versus time for the CANDU benchmark problem (time step =0.025s)

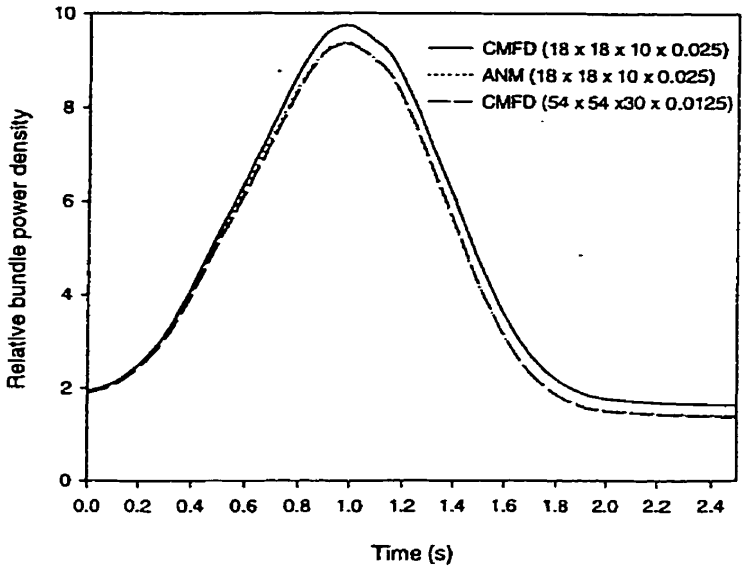

Figure 6.7: Relative bundle power density of bundle (6,10,5) versus time for the CANDU benchmark problem (time step = 0.025s)

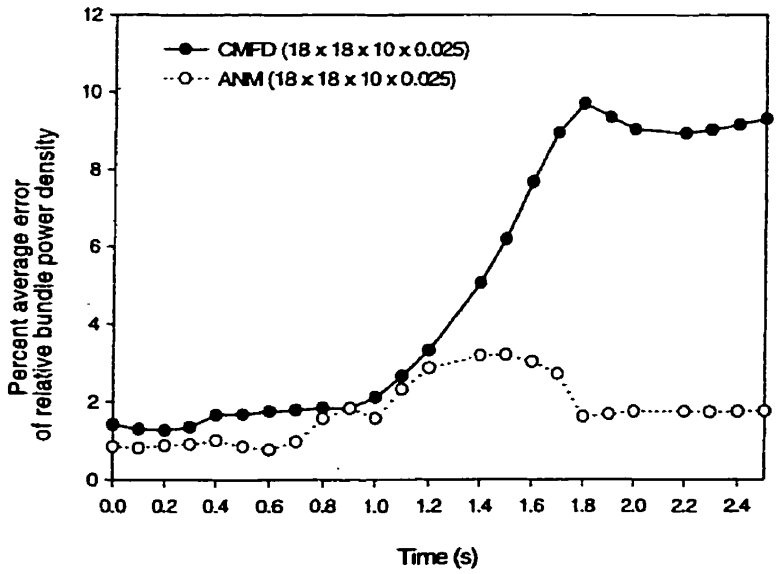

Figure 6.8: Percent average error of relative bundle power density versus time for the CANDU benchmark problem (time step = 0.025s)

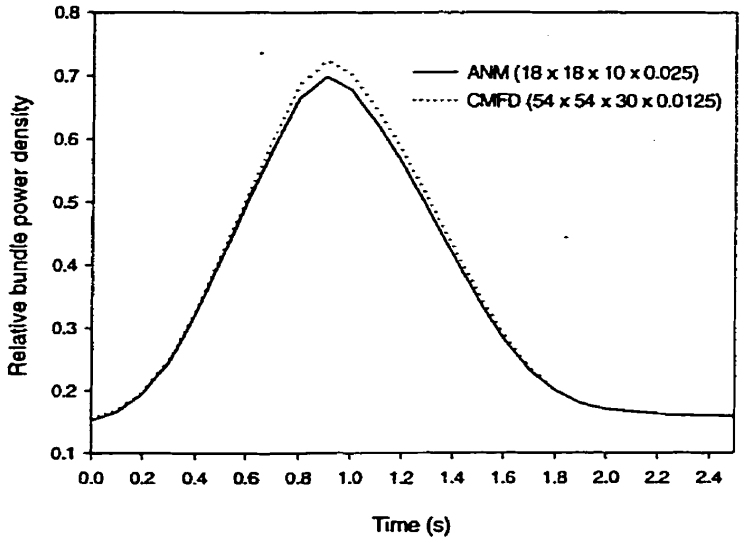

Figure 6.9: Relative bundle power density of bundle (7,3,1) versus time for the CANDU benchmark problem (time step = 0.025s)

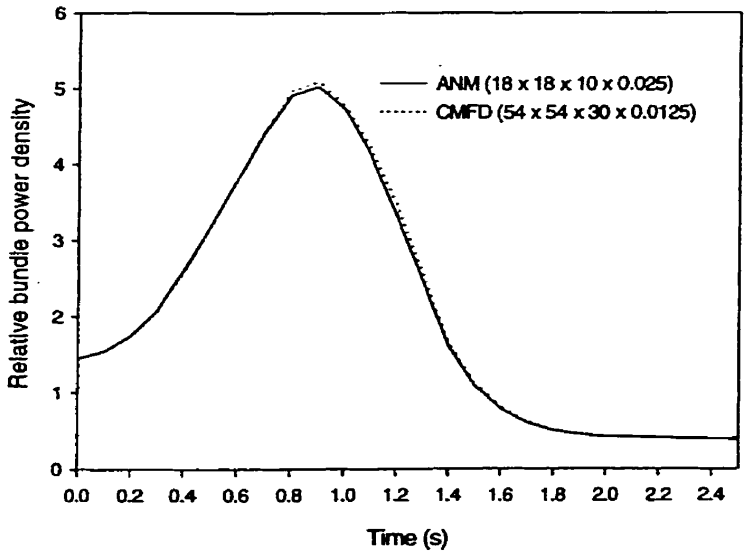

Figure 6.10: Relative bundle power density of bundle (9,9,5) versus time for the CANDU benchmark problem (time step =0.025s)

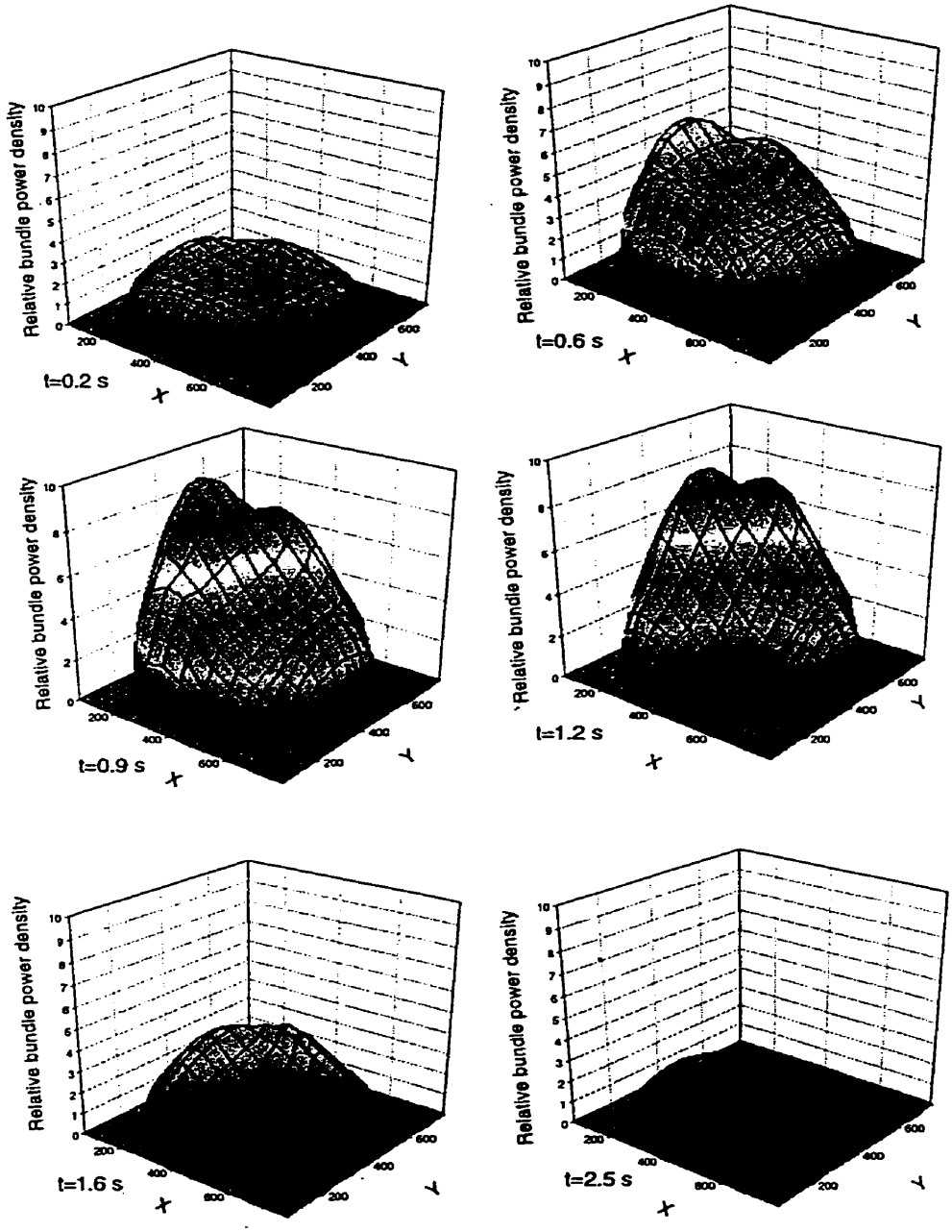

Figure 6.11: Relative bundle power density distributions versus time on plane 5 of the CANDU benchmark problem for ANM (time step = 0.025s)

	3	4	5	6	7	8	9	10	11	12	13	14	15	16
3					1.46	1.52	1.26	0.79	0.56	0.46				
					-3.82	-2.73	-3.22	-3.97	-5.05	-5.45				
4					2.13	2.12	1.79	1.22	0.92	0.77				
					-2.80	-1.33	-1.87	-2.14	-3.18	-4.25				
5			2.42	2.75	2.91	2.83	2.43	1.82	1.44	1.22	1.12	0.99		
			-4.83	-4.35	-2.53	-1.84	-2.41	-3.24	-4.23	-4.92	-6.63	**-6.82**		
6			3.17	3.42	3.54	3.33	2.86	2.26	1.84	1.60	1.45	1.32		
			-4.44	-2.80	-2.13	-1.92	-2.45	-3.16	-3.94	-4.42	-5.13	-6.39		
7	2.85	3.60	4.14	4.33	3.92	3.46	2.93	2.38	2.01	1.84	1.87	1.73	1.48	1.16
	-3.61	-2.75	-1.97	-1.60	-1.45	-1.58	-1.90	-2.17	-2.76	-3.07	-3.46	-3.72	-4.30	-5.08
8	3.79	4.62	5.19	5.24	4.47	3.74	3.11	2.54	2.21	2.13	2.28	2.18	1.90	1.54
	-2.25	-0.85	-0.53	-0.47	-0.74	-1.29	-1.71	-1.81	-2.06	-2.02	-2.04	-2.10	-2.43	-3.70
9	4.29	5.20	5.78	5.78	4.85	3.98	3.29	2.70	2.37	2.33	2.54	2.45	2.16	1.76
	-1.73	-0.33	0.03	0.07	-0.20	-0.87	-1.46	-1.64	-1.73	-1.38	-1.34	-1.39	-1.73	-3.08
10	4.38	5.31	5.93	**5.94**	5.01	4.16	3.47	2.87	2.52	2.46	2.66	2.56	2.24	1.83
	-1.54	-0.14	0.22	0.27	0.00	-0.64	-1.17	-1.32	-1.41	-1.07	-1.01	-1.06	-1.41	-2.76
11	4.04	4.95	5.61	5.72	4.98	4.31	3.71	3.10	2.70	2.54	2.65	2.50	2.15	1.73
	-1.73	-0.27	0.10	0.16	-0.10	-0.51	-0.75	-0.76	-1.03	-1.03	-0.97	-1.05	-1.46	-2.81
12	3.19	4.08	4.78	5.12	4.83	4.56	4.12	3.50	2.98	2.60	2.49	2.23	1.85	1.41
	-2.89	-1.94	-1.04	-0.55	-0.30	-0.08	0.00	-0.04	-0.64	-1.17	-1.62	-2.12	-2.92	-3.85
13			3.90	4.38	4.86	5.01	4.69	4.03	3.37	2.73	2.24	1.90		
			-3.16	-1.37	-0.49	0.22	0.27	0.13	-0.40	-1.42	-2.42	-4.07		
14			3.14	3.79	4.42	4.81	4.60	3.98	3.29	2.56	2.00	1.59		
			-3.60	-3.05	-0.94	0.21	0.26	0.09	-0.46	-1.87	-4.11	-4.56		
15					3.70	4.18	4.08	3.54	2.91	2.20				
					-1.83	-0.10	-0.05	-0.23	-0.81	-2.58				
16					2.84	3.37	3.34	2.92	2.38	1.73—*Reference channel power densities*				
					-2.79	-1.55	-1.47	-1.58	-2.10	-3.41-*Percent errors for ANM (18 x 18 x 10)*				

Reference is the result of CMFD (54 x 54 x 30 x 0.0125)

The maximum relative channel power density and the maximum percent error are shown in bold character

Figure 6.12: Relative channel power densities and percent errors of the CANDU benchmark problem at time 0.9s for ANM (18 x 18 x 10 x 0.025)

	3	4	5	6	7	8	9	10	11	12	13	14	15	16
3					2.61	2.74	2.26	1.30	0.89	0.72				
					-3.72	-2.38	-3.05	-4.16	-5.35	-5.52				
4					3.68	3.71	3.11	1.98	1.44	1.21				
					-2.89	-1.15	-1.90	-2.18	-3.34	-4.29				
5			3.82	4.41	4.77	4.70	3.99	2.91	2.26	1.90	1.74	1.53		
			-4.80	-4.27	-2.11	-1.31	-2.00	-3.08	-4.25	-4.92	-6.66	**-6.84**		
6			4.98	5.40	5.64	5.33	4.56	3.57	2.88	2.49	2.24	2.04		
			-4.36	-2.62	-1.72	-1.46	-2.06	-2.96	-3.88	-4.34	-5.18	-6.40		
7	4.44	5.60	6.45	6.77	6.14	5.44	4.61	3.72	3.13	2.86	2.89	2.68	2.29	1.80
	-3.51	-2.62	-1.73	-1.35	-1.09	-1.24	-1.58	-1.91	-2.49	-2.83	-3.36	-3.70	-4.29	-5.06
8	5.87	7.16	8.05	8.14	6.94	5.81	4.83	3.95	3.43	3.30	3.53	3.37	2.94	2.39
	-2.11	-0.62	-0.33	-0.33	-0.46	-1.00	-1.37	-1.50	-1.77	-1.76	-1.94	-1.97	-2.38	-3.66
9	6.65	8.05	8.96	8.96	7.51	6.17	5.09	4.18	3.67	3.61	3.92	3.79	3.33	2.73
	-1.48	-0.14	0.17	0.19	0.07	-0.60	-1.21	-1.61	-1.70	-1.10	-1.24	-1.27	-1.56	-2.98
10	6.78	8.22	9.17	**9.20**	7.76	6.44	5.37	4.44	3.90	3.81	4.11	3.96	3.47	2.83
	-1.30	0.04	0.36	0.38	0.27	-0.36	-0.91	-1.29	-1.39	-0.78	-0.91	-0.93	-1.23	-2.66
11	6.24	7.66	8.67	8.85	7.70	6.67	5.73	4.80	4.17	3.92	4.09	3.86	3.32	2.67
	-1.62	-0.07	0.24	0.27	0.17	-0.22	-0.39	-0.42	-0.71	-0.72	-0.88	-0.95	-1.41	-2.77
12	4.92	6.30	7.38	7.91	7.47	7.05	6.36	5.41	4.60	4.02	3.85	3.44	2.85	2.19
	-2.82	-1.85	-0.84	-0.36	0.01	0.20	0.26	0.20	-0.30	-0.84	-1.46	-2.08	-2.89	-3.82
13			6.03	6.77	7.51	7.74	7.25	6.23	5.20	4.22	3.46	2.94		
			-3.17	-1.33	-0.31	0.37	0.42	0.26	-0.28	-1.25	-2.47	-4.07		
14			4.85	5.86	6.83	7.43	7.11	6.15	5.08	3.95	3.10	2.45		
			-3.60	-3.06	-0.75	0.39	0.42	0.23	-0.29	-1.82	-4.11	-4.57		
15					5.72	6.46	6.30	5.48	4.49	3.39				
					-1.74	0.12	0.11	-0.08	-0.58	-2.57				
16					4.39	5.20	5.16	4.52	3.68	2.68--*Reference bundle power densities*				
					-2.71	-1.41	-1.35	-1.48	-1.98	-3.37--*Percent errors for ANM (18 x 18 x 10)*				

Reference is the result of CMFD (54 x 54 x 30 x 0.0125)

The maximum relative bundle power density and the maximum percent error are shown in bold character

Figure 6.13: Relative bundle power densities and percent errors on plane 5 of the CANDU benchmark problem at time 0.9s for ANM (18 x 18 x 10 x 0.025)

	3	4	5	6	7	8	9	10	11	12	13	14	15	16
3					5.85	7.13	**9.44**	-2.86	-1.66	-3.80				
					-3.72	-2.38	-3.05	-4.16	-5.35	-5.52				
4					6.26	7.89	9.38	-1.21	-0.90	-2.84				
					-2.89	-1.15	-1.90	-2.18	-3.34	-4.29				
5			-2.46	0.49	5.58	6.30	7.00	1.10	0.83	0.05	-0.91	-3.91		
			-4.80	-4.27	-2.11	-1.31	-2.00	-3.08	-4.25	-4.92	-6.66	**-6.84**		
6			-0.03	2.69	4.70	5.14	5.32	1.40	0.87	0.56	1.00	-1.50		
			-4.36	-2.62	-1.72	-1.46	-2.06	-2.96	-3.88	-4.34	-5.18	-6.40		
7	0.70	3.04	3.72	3.85	1.67	1.72	1.77	-0.35	-0.66	-0.80	2.41	2.24	1.51	-0.88
	-3.51	-2.62	-1.73	-1.35	-1.09	-1.24	-1.58	-1.91	-2.49	-2.83	-3.36	-3.70	-4.29	-5.06
8	0.95	3.79	3.95	4.05	1.36	1.46	1.45	-0.29	-0.56	-0.82	2.52	2.40	2.20	-0.65
	-2.11	-0.62	-0.33	-0.33	-0.46	-1.00	-1.37	-1.50	-1.77	-1.76	-1.94	-1.97	-2.38	-3.66
9	0.81	3.73	3.94	4.07	1.24	1.36	1.41	-0.20	-0.46	-0.80	2.54	2.37	2.11	-0.81
	-1.48	-0.14	0.17	0.19	0.07	-0.60	-1.21	-1.61	-1.70	-1.10	-1.24	-1.27	-1.56	-2.98
10	0.83	3.74	3.95	4.07	1.24	1.37	1.43	-0.14	-0.38	-0.75	2.56	2.38	2.13	-0.78
	-1.30	0.04	0.36	0.38	0.27	-0.36	-0.91	-1.29	-1.39	-0.78	-0.91	-0.93	-1.23	-2.66
11	1.03	3.82	3.96	4.04	1.31	1.40	1.40	-0.18	-0.36	-0.68	2.57	2.44	2.27	-0.51
	-1.62	-0.07	0.24	0.27	0.17	-0.22	-0.39	-0.42	-0.71	-0.72	-0.88	-0.95	-1.41	-2.77
12	0.92	3.13	3.73	3.78	1.43	1.31	1.26	-0.34	-0.45	-0.57	2.46	2.36	1.72	-0.45
	-2.82	-1.85	-0.84	-0.36	0.01	0.20	0.26	0.20	-0.30	-0.84	-1.46	-2.08	-2.89	-3.82
13			-0.36	2.27	4.09	4.27	4.28	2.63	2.43	1.98	1.15	-1.57		
			-3.17	-1.33	-0.31	0.37	0.42	0.26	-0.28	-1.25	-2.47	-4.07		
14			-3.01	-0.39	4.11	4.23	4.17	2.50	2.33	1.88	-1.42	-4.14		
			-3.60	-3.06	-0.75	0.39	0.42	0.23	-0.29	-1.82	-4.11	-4.57		
15					3.56	4.13	3.96	2.29	2.16	1.23				
					-1.74	0.12	0.11	-0.08	-0.58	-2.57				
16					1.49	1.41	1.05	-0.61	-0.70	-1.12				
					-2.71	-1.41	-1.35	-1.48	-1.98	-3.37				

Percent errors for CMFD

Percent errors for ANM

Reference is the result of CMFD (54 x 54 x 30 x 0.0125)

The maximum percent errors are shown in bold character

Figure 6.14: Comparison of percent errors in relative bundle power densities from CMFD (18 x 18 x 10 x 0.025) and ANM (18 x 18 x 10 x 0.025) on plane 5 at time 0.9 s for the CANDU benchmark problem

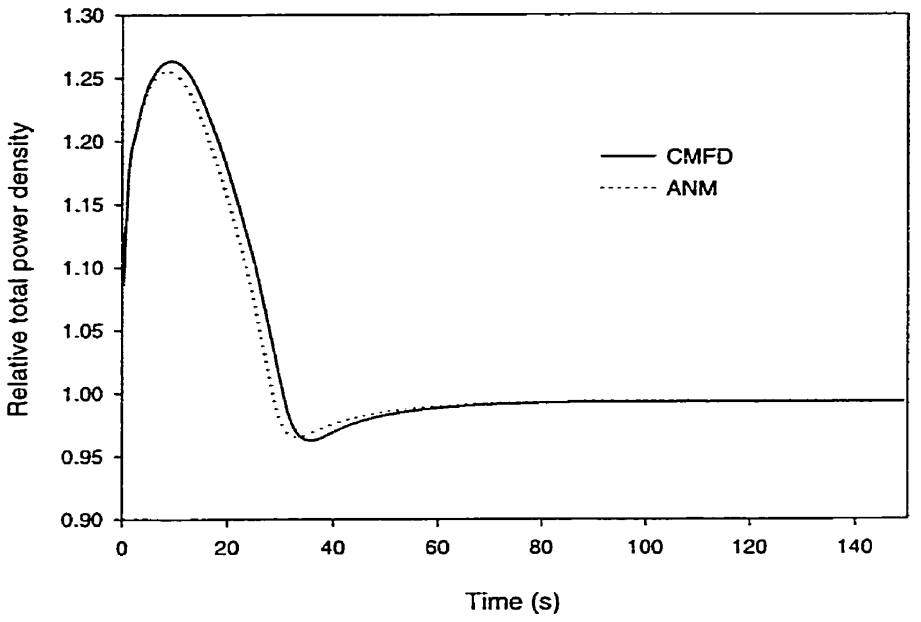

Figure 6.15: Relative total power density versus time for the typical CANDU-6 problem

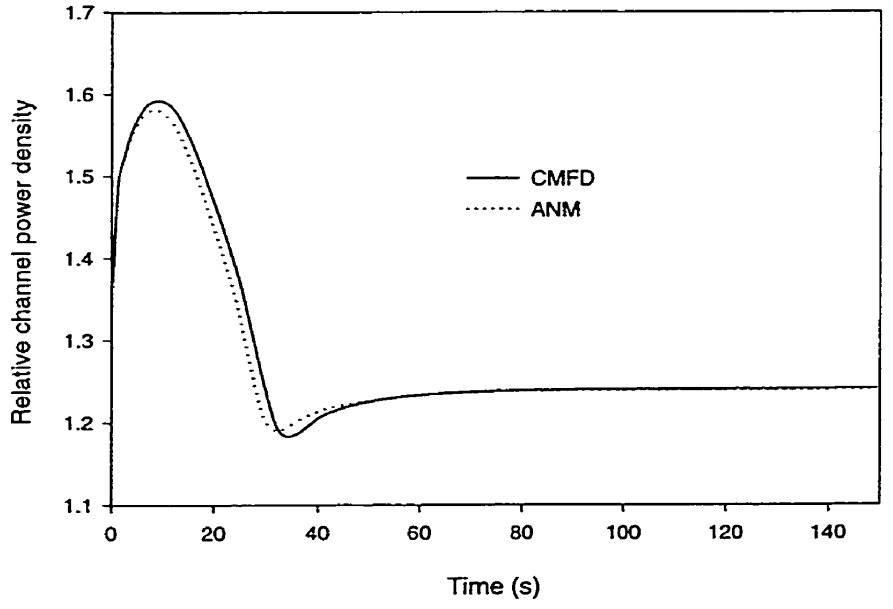

Figure 6.16: Relative channel power density of channel (E12) versus time for the typical CANDU-6 problem

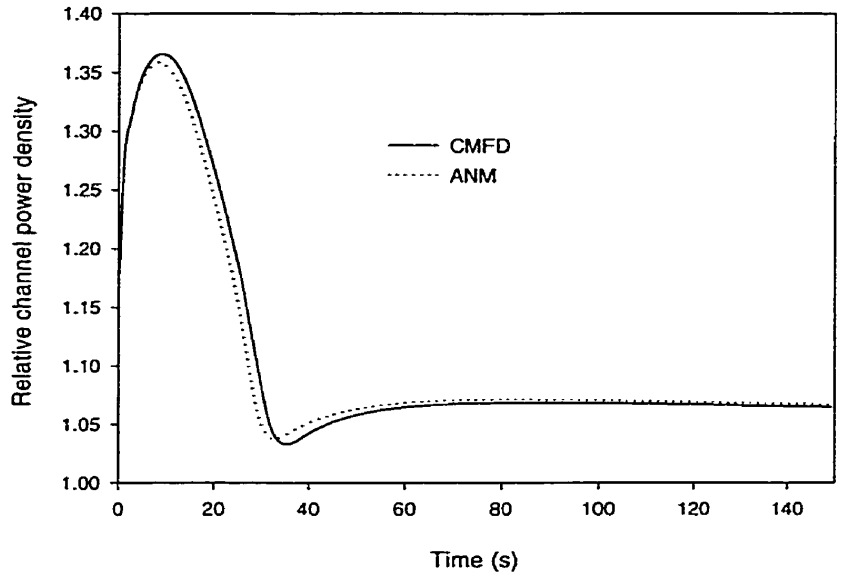

Figure 6.17: Relative channel power density of channel (L11) versus time for the typical CANDU-6 problem

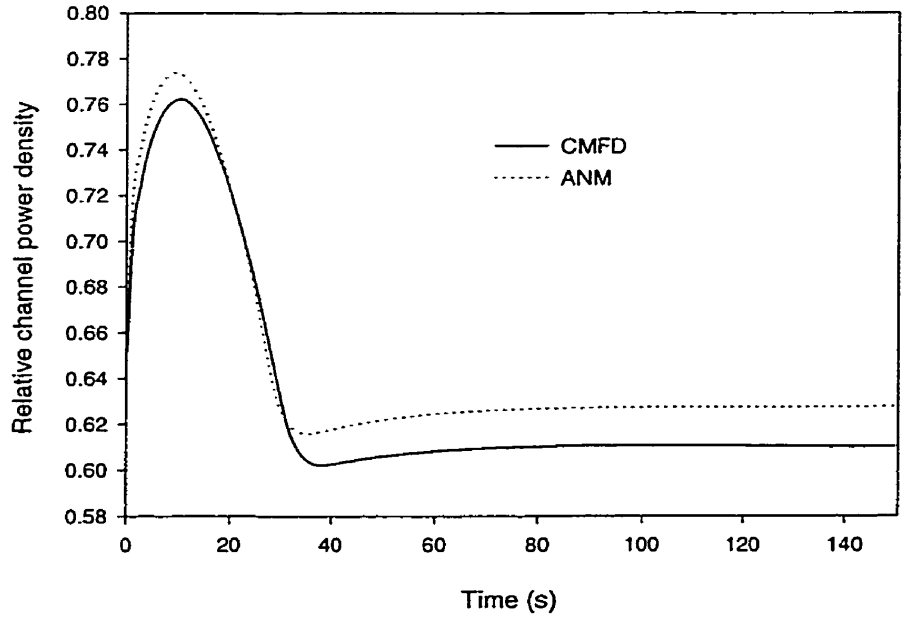

Figure 6.18: Relative channel power density of channel (L22) versus time for the typical CANDU-6 problem

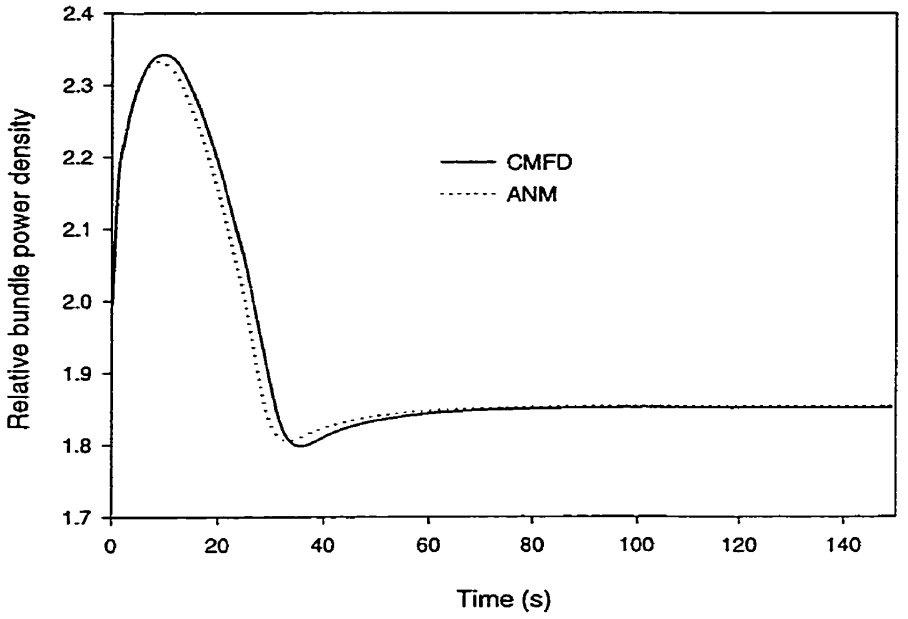

Figure 6.19: Relative bundle power density of bundle (L11,6) versus time for the typical CANDU-6 problem

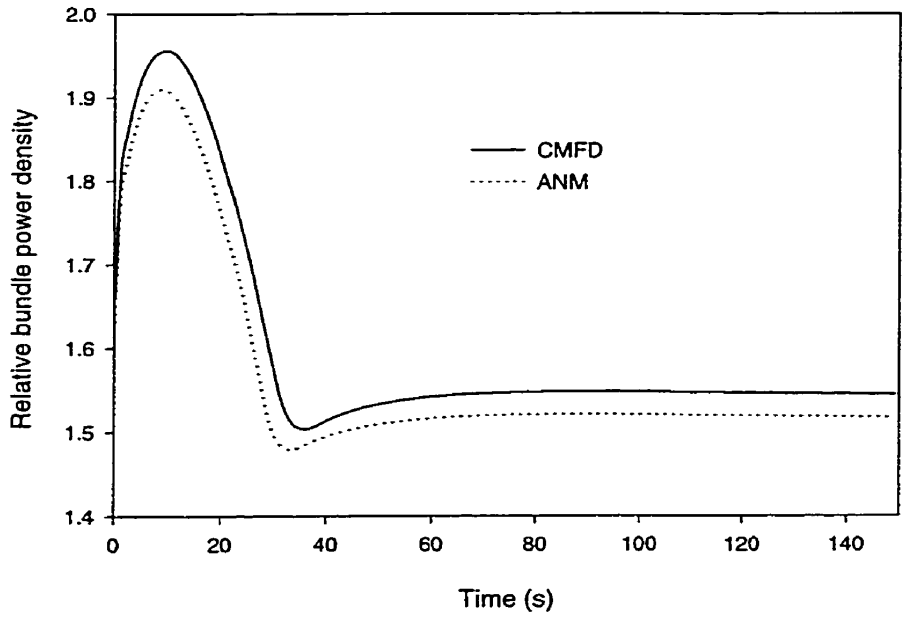

Figure 6.20: Relative bundle power density of bundle (E12,6) versus time for the typical CANDU-6 problem

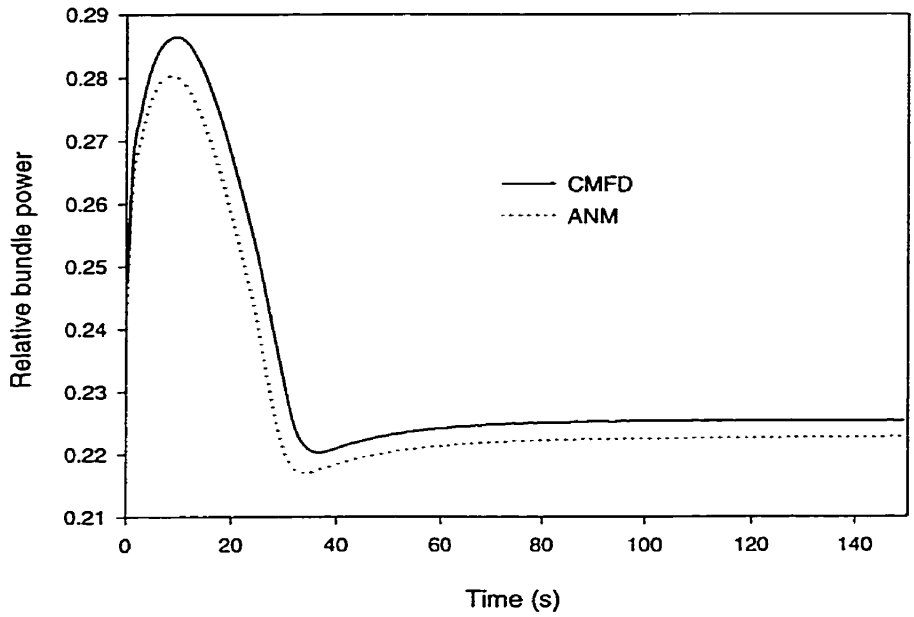

Figure 6.21: Relative bundle power density of bundle (S17,6) versus time for the typical CANDU-6 problem

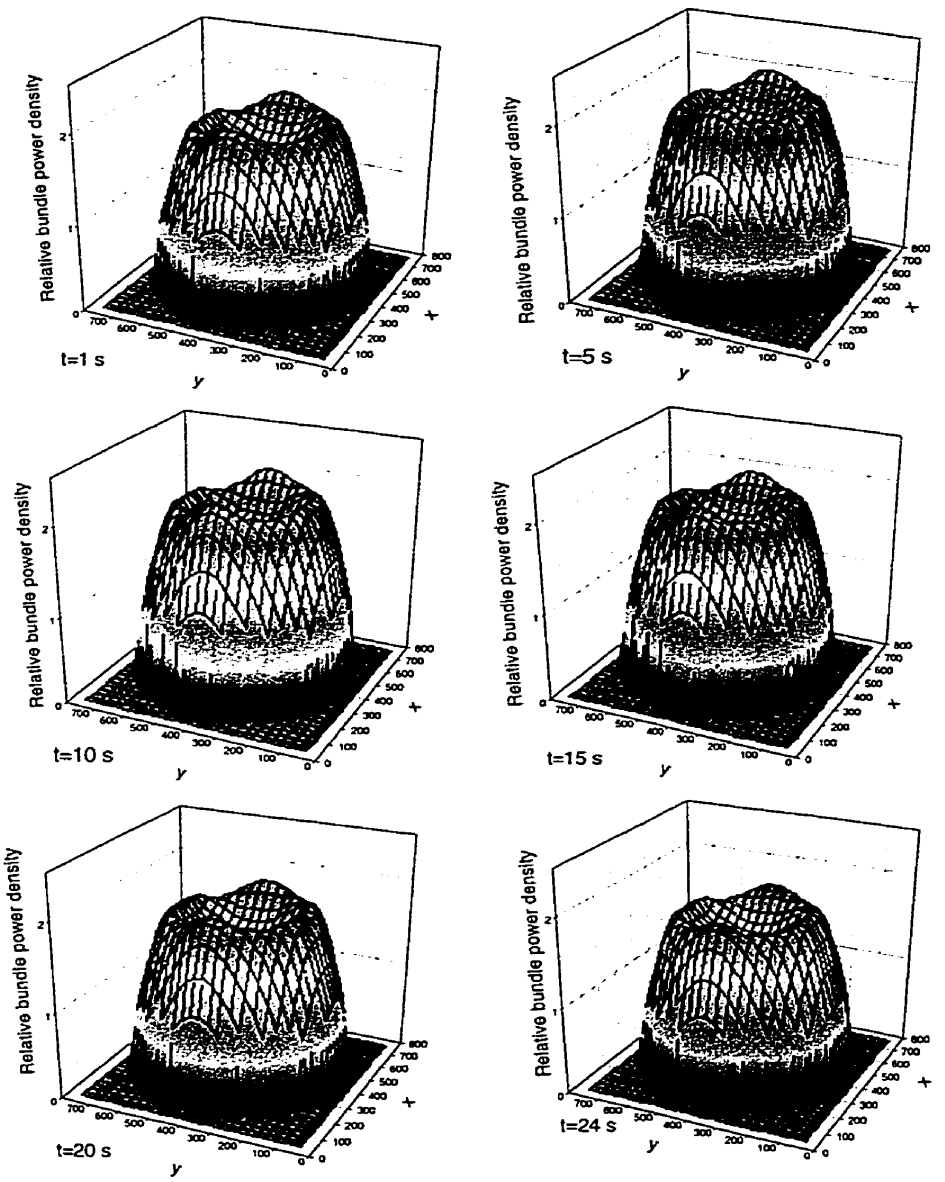

Figure 6.22: Relative bundle power density distributions versus time on plane 6 of the typical CANDU-6 problem for ANM

CHAPTER 7
CONCLUSIONS

7.1 Conclusions

To practically apply ANM for CANDU analysis, a complete derivation of ANM formalism for solving 3-D 2-group static and kinetics diffusion equations were reviewed in this work. The numerical methods used to solve the ANM equations were also examined.

Based on the presented ANM formalism and numerical methods, the modules used for 3-D nodal method module were developed and programmed independently into the NDF code, which was specially designed for 3-D CANDU kinetics calculation.

The Analytic Nodal Method with flat leakage approximation was shown to be a superior method to CMFD for solving the multidimensional two-group static, kinetics diffusion equation of the CANDU reactor. The Analytic Nodal Method with flat leakage is a very accurate method for CANDU reactor analysis and design.

The Coarse Mesh Finite Difference Method is found to be the lowest order nodal method. The calculations show that CMFD is generally adequate for static CANDU analysis. The difference between CMFD and ANM is found to be not important. However, for transient scenarios, with significant leakages, the difference between CMFD and ANM is not considered negligible. With the increased accuracy requirements of current and future analysis, either fine mesh finite difference or higher order nodal methods will have to be applied for CANDU analysis.

It was found that, for the typical static CANDU-6 problem, with the normal coarse mesh size, the Analytic Nodal Method could be expected to yield channel-averaged powers accurate to within about 2% and static reactor eigenvalue accurate to within about 0.02%.

Results from CANDU benchmark and typical CANDU-6 model demonstrate that accurate kinetics solutions could be obtained with bundle size spatial meshes. Comparisons with Coarse Mesh Finite Difference Method indicated that the errors Analytic Nodal Method was lower.

7.2 Recommendations for Future Research

This section contains a description of several items of potential interest that has been left unresolved or untouched.

1. The Transverse Leakage Approximation

As the only approximation in our implementation of the static Analytic Nodal Method is that the transverse leakage is constant, improvements in this approximation would lead to increased accuracy. In particular, it would be very fruitful if a quadratic polynomial could be used for the leakage approximation.

2. Coarse-Grid Acceleration

The philosophy of the coarse-grid acceleration techniques is that the rapid convergence can be maintained by projecting a fine-grid problem to an equivalent coarse grid problem. Nodal equivalence theory can be used as a restriction operator in a multigrid acceleration method for classical iterative procedures. Numerical experiments showed

this employing acceleration technique in Coarse Mesh Finite Difference Method could reduce CPU time efficiently (Kaveh et al., 1999).

REFERENCES

ANL, (1985). National Energy Software Center: Benchmark Problem Book. ANL - 7416, Argonne National Laboratory, United States, pp.699-710.

CLARK, M. Jr. and HANSEN, K. F. (1964). Numerical Methods of Reactor Analysis. Academic Press, New York, N.Y..

FINNEMANN, F. BENNEWITZ, and WAGNER, M. R. (1977). Interface Current Techniques for Multi-dimensional Reactor Calculations. Atomkernenergie, Vol. 30, No.1, pp.123.

HENRY, A. F. (1975). Nuclear Reactor Analysis. M.I.T. Press, Cambridge, Massachusetts.

KAVEH, S., KOCLAS, J. and ROY R. (1999). Simulation of CANDU Reactor Transients Using Hierarchical Supernodal Analysis, CNS Proceedings, Montreal, Canada.

KOCLAS, J. (1998). Comparisons of the Different Approximations Leading to Mesh Centered Finite Differences Starting from the Analytic Nodal Method. Annals of Nuclear Energy, Vol. 25, No.11, pp.821-838.

LAWRENCE, R. D. and DORNING, J. J. (1980). A Nodal Green's Function Method for Multi-dimensional Neutron Diffusion Calculations. Nuclear Science and Engineer, Vol. 76, pp.218.

MARLEAU, G., HEBERT, A. and ROY, R. (1993). New Computational Methods Used in the Lattice Code DRAGON. Topical Meeting on Advances in Reactor Physics, Charleston, SC, pp.8-11.

MARLEAU, G., ROY, R. and ARESENAULT, B. (1994). Simulation of Reactivity Control Devices in a CANDU-6 Reactor using DRAGON. CNS Proceedings, Pembroke, Ontario, Canada.

MARLEAU, G., HÉBERT, A. and ROY, R. (1996). A User's Guide for DRAGON. Report IGE-174 Rev 1, École Polytechnique de Montréal, Canada.

MULLER, E.Z. and WEISS, Z.J. (1991). Benchmarking with the Multi-group Diffusion High-order Response Matrix Method. Annals of Nuclear Energy, Vol. 18, No. 9, pp.535-544.

NAVARRO ARIAS, S. H. (1996). Étude Numérique des Effets de Diffusion Directionnels dan le Cœur du Réacteur GENTILLY-2. MSC. Thesis, Université de Montréal

ROY, R., MARLEAU, G., TAJMOUATI, J. and ROZON, D. (1993). Modeling of CANDU Reactivity Control Devices with the Lattice Code DRAGON. Annals of Nuclear Energy, Vol. 21, No.2, pp115-132.

SMITH, K. S. (1979). An Analytical Nodal Method for Solving the Two-group, Multi-dimensional, Static and Transient Neutron Diffusion Equations. MSC. Thesis, Massachusetts Institute of Technology.

VARGA, R. S. (1962). Matrix Iterative Analysis. Prentice-hall, Englewood Cliffs, N.J..

WACHSPRESS, E.L. (1966). Iterative Solution to Elliptic System and Applications to the Neutron Diffusion Equations of Reactor Physics. Prentice-hall, Englewood Cliffs, N.J..

APPENDIX 1
DESCRIPTION OF TEST PROBLEM

A1.1 The 2-D IAEA PWR Static Benchmark Problem

Geometry

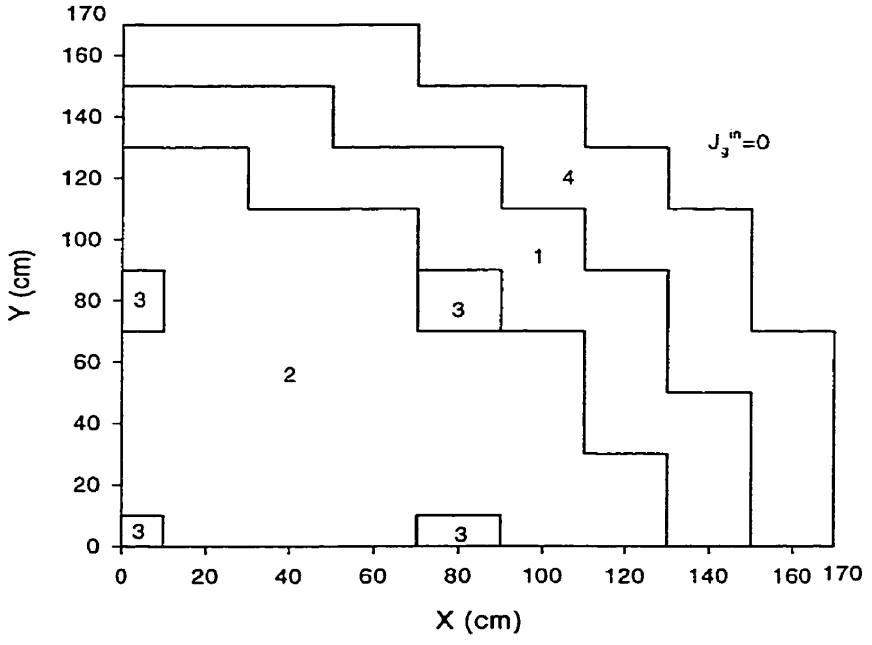

Figure A1.1: Quadrant of reactor horizontal cross section of the 2-D IAEA PWR static benchmark problem

Material Properties

Composition*	Group, g	D_g (cm)	Σ_{ag} (cm^{-1})	$\gamma\Sigma_{fg}$ (cm^{-1})	Σ_{21} (cm^{-1})
1	1	1.5	0.01	0.0	0.02
	2	0.4	0.08	0.135	
2	1	1.5	0.01	0.0	0.02
	2	0.4	0.085	0.135	
3	1	1.5	0.01	0.0	0.02
	2	0.4	0.13	0.135	
4	1	2.0	0.00	0.0	0.04
	2	0.3	0.01	0.0	

* Axial buckling of 0.8×10^{-4} cm^{-2} for all compositions in 2-D problem.

$\chi_1 = 1.0, \quad \chi_2 = 0$

A1.2 The 3-D CANDU Benchmark Problem

Geometry

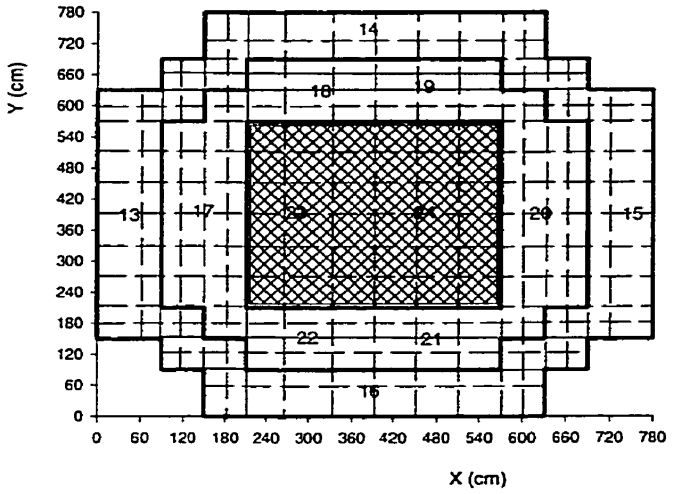

Figure A1.2: Initial back view of reactor for the CANDU benchmark problem

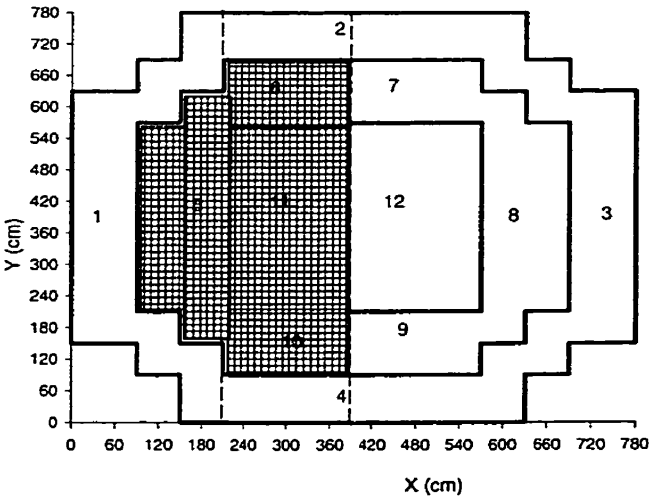

Figure A1.3: Reactor region affected by voiding for the CANDU benchmark problem

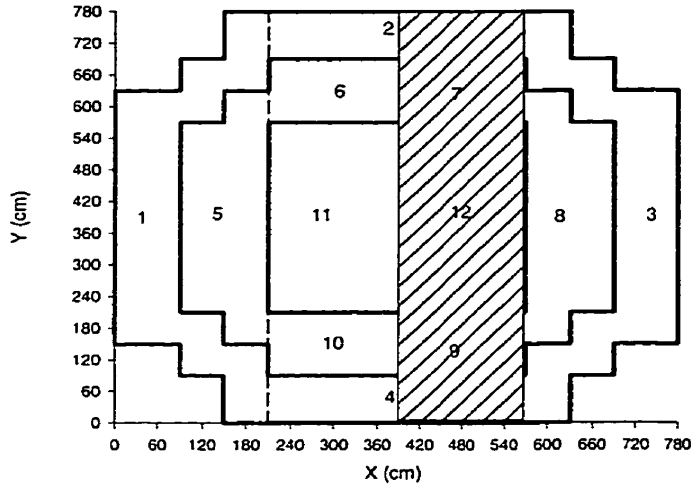

Figure A1.4: Reactor region affected by the shutdown system in front half of the reactor for the CANDU benchmark problem

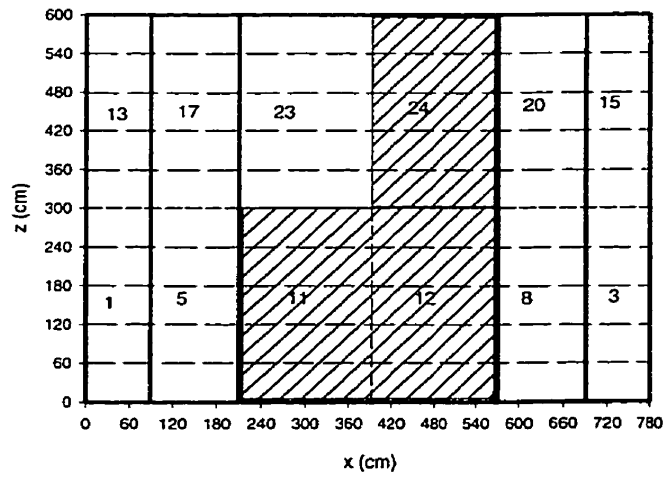

Figure A1.5: Reactor region affected by the shutdown system in horizontal cross-section at Y=390cm for the CANDU benchmark problem

Material Properties

1. Initial two-group constant

Region	Group, g	D_g (cm)	Σ_{tg} (cm^{-1})	$\gamma\Sigma_{fg}$ (cm^{-1})	Σ_{21} (cm^{-1})
1,2,3,4,13,14,15,16	1	1.31	$1.018x10^{-2}$	0.0	$1.018x10^{-2}$
	2	0.8695	$2.117x10^{-4}$	0.0	
5,6,7,8,9,10,17,18,19, 20,21,22	1	1.264	$8.154x10^{-3}$	0.0	$7.368x10^{-3}$
	2	0.9328	$4.014x10^{-3}$	$4.723x10^{-3}$	
11,12,23,24	1	1.264	$8.154x10^{-3}$	0.0	$7.368x10^{-3}$
	2	0.9328	$4.01x10^{-3}$	$4.562x10^{-3}$	

$\chi_1 = 1.0, \quad \chi_2 = 0$

2. Speed: $v_1=10^7$ cm/s $v_2=3x10^5$cm/s

3. Delayed neutron data:

Type	β_i	λ_i
1	$4.170x10^{-4}$	$1.244x10^{-2}$
2	$1.457x10^{-3}$	$3.063x10^{-2}$
3	$1.339x10^{-3}$	$1.139x10^{-1}$
4	$3.339x10^{-3}$	$3.079x10^{-1}$
5	$8.970x10^{-4}$	$1.198x10^{0}$

6	3.200×10^{-4}	3.212×10^{0}

4. Initial perturbations:

Σ_2, Regions 5,6,10,11,17,18,22 and 23, varies linearly in time, with

$$\frac{\partial \Sigma_2}{\partial t} = \begin{cases} -1.0 \times 10^{-4} (cm \cdot s)^{-1}, for\ t \leq 0.4s \\ -8.88889 \times 10^{-6} (cm \cdot s)^{-1}, for\ t > 0.4s \end{cases}$$

5. Absorbers insertions

An incremental cross-section, $\Delta \Sigma_2$, is added to regions 2,4,7,9,14,16,18,19,21,22,23 and 24 to simulate asymmetric insertion of absorbers.

$\Delta \Sigma_2$	6.15×10^{-4} cm^{-1}
Insertion start at	0.6 s
Absorber velocity	520 cm/s

A1.3 The Typical CANDU-6 Problem

Geometry

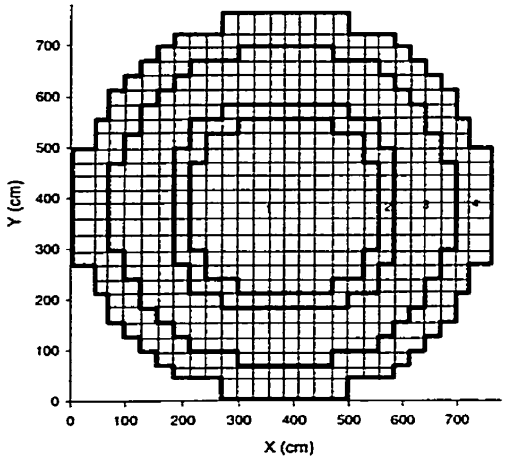

Figure A1.6: Vertical cross-section at Z=0 cm illustrating grid layout in XY plane of the typical CANDU-6 problem

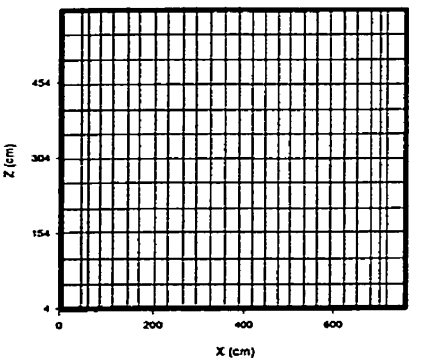

Figure A1.7: Horizontal cross-section at Y = 382.85cm illustrating grid layout in the XZ plane of the typical CANDU-6 problem

Material Properties

1. Initial two-group constant

The initial two-group constant is calculated by DRAGON/DONJON chain code.

2. Delayed neutron data:

Type	β_i	λ_i
1	4.170×10^{-4}	1.244×10^{-2}
2	1.457×10^{-3}	3.063×10^{-2}
3	1.339×10^{-3}	1.139×10^{-1}
4	3.339×10^{-3}	3.079×10^{-1}
5	8.970×10^{-4}	1.198×10^{0}
6	3.200×10^{-4}	3.212×10^{0}

Perturbation:

A group of rods are ejected from the reactor core at beginning. Figure A1.8 shows the location of these rods. The response of the reactor regulation system and the incremental cross-section are calculated by DRAGON/DONJON chain code.

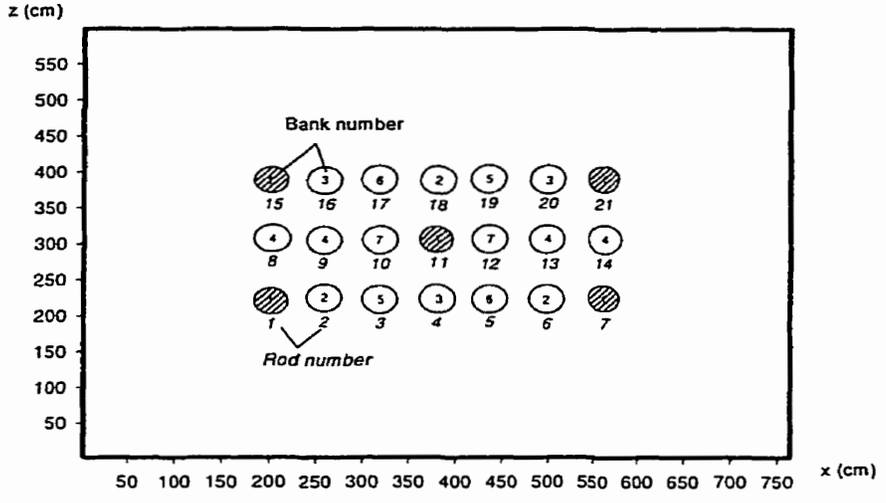

The instantaneous withdrawal rods: No.1, No 7, No.11, No. 15 and No. 21

Figure A1.8: Adjust location in the typical CANDU-6 problem

APPENDIX 2

THE COARSE MESH FINITE DIFFERENCE METHOD WITH FLAT TRANSVERSE LEAKAGE APPROXIMATION

A2.1 Derivation of Equations

The fundamental hypothesis leading to Coarse Mesh Finite Difference Method with flat transverse leakage approximation is to expand matrix exponentials of 1.36 and 1.38 to Taylor's series. When higher order terms approach zero, many of the leading terms cancel, and they become

$$[\bar{\psi}]_{i,j,k} \approx \left\langle [I]-\frac{h_x^i}{2}[N]_{i,j,k} \right\rangle [\psi(x_i)]_{i,j,k} + \left\langle \frac{h_x^i}{2}[I]-\frac{h_x^{i\,2}}{6}[N]_{i,j,k} \right\rangle [\bar{S}'_x]_{i,j,k} \qquad \text{A2.1}$$

$$[\bar{\psi}]_{i-1,j,k} \approx \left\langle [I]+\frac{h_x^{i-1}}{2}[N]_{i-1,j,k} \right\rangle [\psi(x_i)]_{i-1,j,k} + \left\langle -\frac{h_x^{i-1}}{2}[I]-\frac{h_x^{i-1\,2}}{6}[N]_{i-1,j,k} \right\rangle [\bar{S}'_x]_{i-1,j,k} \qquad \text{A2.2}$$

The flux parts of 1.41 and of 1.42 are

$$[\bar{\phi}]_{i,j,k} = [\phi(x_i)]_{i,j,k} - \frac{h_x^i}{2}[D_x]^{-1}_{i,j,k}[J_x(x_i)]_{i,j,k} + \frac{h_x^{i\,2}}{6}[D_x]^{-1}_{i,j,k}[\bar{S}_x]_{i,j,k} \qquad \text{A2.3}$$

$$[\bar{\phi}]_{i-1,j,k} = [\phi(x_i)]_{i-1,j,k} + \frac{h_x^{i-1}}{2}[D_x]^{-1}_{i-1,j,k}[J_x(x_i)]_{i-1,j,k} + \frac{h_x^{i-1\,2}}{6}[D_x]^{-1}_{i,j,k}[\bar{S}_x]_{i-1,j,k} \qquad \text{A2.4}$$

We take the difference between A2.3 and A2.4, and use flux and current continuity to find

$$[J_x(x_i)]_{i,j,k} = -(\frac{h_x^i}{2}[D_x]_{i,j,k}^{-1} + \frac{h_x^{i-1}}{2}[D_x]_{i-1,j,k}^{-1})^{-1}([\bar{\phi}]_{i,j,k} - [\bar{\phi}]_{i-1,j,k} - \frac{h_x^{i\,2}}{6}[D_x]_{i,j,k}^{-1}[\bar{S}_x]_{i,j,k} + \frac{h_x^{i-1\,2}}{6}[D_x]_{i-1,j,k}^{-1}[\bar{S}_x]_{i-1,j,k}) \quad \text{A2.5}$$

Which gives the relationship between a surface average current and the average fluxes of the two nodes delimited by the surface. An identical calculation for the node $(i+1, j, k)$ gives the result

$$[J_x(x_{i+1})]_{i,j,k} = -(\frac{h_x^{i+1}}{2}[D_x]_{i+1,j,k}^{-1} + \frac{h_x^i}{2}[D_x]_{i,j,k}^{-1})^{-1}([\bar{\phi}]_{i+1,j,k} - [\bar{\phi}]_{i,j,k} - \frac{h_x^{i+1\,2}}{6}[D_x]_{i+1,j,k}^{-1}[\bar{S}_x]_{i+1,j,k} + \frac{h_x^{i\,2}}{6}[D_x]_{i,j,k}^{-1}[\bar{S}_x]_{i,j,k}) \quad \text{A2.6}$$

using the definition of the face-averaged net leakages for x direction, the final equation can be expressed in the form 1.39, except the elements inside the matrix are different. A similar approach can be down for the other two directions. Finally we obtain three equations of net leakages. With the neutron balance equation, the resulting super-matrix equations can be written as 1.40, same as the equations of the Analytic Nodal Method, but with the different content of each sub-matrix. Each element inside these sub-matrixes can be easily obtained by expressions A2.5, A2.6 and the similar expressions for the other directions. The global reactor equation is one of the form of classical eigenvalue problem, and the elements of matrix independent on the eigenvalue γ.

A2.2 Results of the Typical CANDU-6 Problem and Conclusion

We developed the modules used for Coarse Mesh Finite Difference Method with flat transverse leakage approximation and implemented them into the NDF code. The typical CANDU-6 problem of static status has been calculated by these modules. The description of typical CANDU-6 problem is shown in Section A1.3 of Appendix 1.

The solution of typical CANDU-6 problem with 26 x 26 x 12 spatial meshes is summarized in Table A2.1. A comparison of Coarse Mesh Finite Difference Method with flat transverse leakage approximation (CMFD+F) to Coarse Mesh Finite Difference Method (CMFD) is given in Figure A2.1. The reference is the result of CMFD with split 104 x 104 x 48, obtained by the NDF code.

These results indicate that introducing the flat transverse leakage approximation into the Coarse Mesh Finite Difference Method causes a loss of accuracy. This is attributed to an inconsistency between the exponential function expansions for flux shape and leakage shape. This inconsistency is the most probable cause of the obvious accuracy loss.

Table A2.1: Summary of results for the 3-D typical CANDU-6 problem

	Coarse Finite Difference Method (CMFD)	Coarse Finite Difference Method with flat transverse leakage approximation
Eigenvalue	1.03067	1.03103
$\varepsilon_{max}(I,J)(channel,\%)$	2.176 (G21)	3.157 (G21)
$\bar{\varepsilon}$ $(channel,\%)$	0.735	1.018
$P_{max}(I,J)$ $(channel)$	1.249 (E14)	1.253 (E14)

Reference eigenvalue: 1.03057

Reference maximum channel power density: 1.250

Outer iteration convergence criterion: 10^{-6}

Flux iteration convergence criterion: 10^{-5}

	1	2	3	4	5	6	7	8	9	10	11	12	13	14	15	16	17	18	19	20	21	22
A									-1.05	-0.77	-1.24	-1.28	-0.88	-1.22								
									-2.20	-0.50	-0.55	-0.58	-0.59	-2.35								
B						-1.12	-0.55	-0.13	0.90	0.87	0.56	0.52	0.75	0.70	-0.39	-0.87	-1.51					
						-2.02	-0.65	-0.63	0.84	1.14	1.15	1.12	1.04	0.68	-0.84	-0.93	-2.34					
C					-0.45	1.13	1.08	1.00	0.97	0.87	0.69	0.65	0.74	0.77	0.72	0.73	0.72	-0.91				
					-1.92	0.93	1.22	1.20	1.16	1.13	1.10	1.07	1.03	0.99	0.96	0.93	0.58	-2.30				
D				-0.38	1.27	1.18	1.02	0.93	0.84	0.76	0.46	0.42	0.62	0.62	0.63	0.65	0.75	0.78	-0.91			
				-1.94	0.92	[illegible]	[illegible]	1.21	1.18	1.06	0.58	0.54	0.94	1.00	0.96	0.91	0.76	0.51	-2.39			
E			-1.03	1.22	1.19	0.97	0.91	0.87	0.82	0.75	0.40	0.35	0.61	0.58	0.56	0.52	0.51	0.67	0.65	-1.63		
			-2.30	0.86	1.10	1.05	1.16	1.07	1.10	0.91	0.30	0.26	0.79	0.90	0.81	0.83	0.66	0.67	0.38	-2.79		
F			-0.12	1.11	0.88	0.66	0.37	0.16	-0.62	-0.79	-1.08	-1.13	-0.95	-0.86	-0.17	-0.04	0.18	0.34	0.52	-0.75		
			-0.86	1.02	1.06	0.92	0.59	0.36	-0.78	-0.96	-1.29	-1.33	-1.09	-0.98	0.08	0.25	0.52	0.61	0.53	-1.38		
G		-1.51	0.83	0.98	0.74	0.48	-0.14	-0.29	-0.63	-0.68	-0.67	-0.72	-0.84	-0.89	-0.63	-0.56	-0.02	0.19	0.36	0.18	**-2.18**	
		-2.60	0.65	0.98	0.98	0.77	-0.14	-0.44	-0.93	-1.06	-0.85	-0.89	-1.19	-1.14	-0.73	-0.50	0.35	0.51	0.46	0.10	**-3.16**	
H		-0.19	0.90	0.78	0.46	0.17	-0.20	-0.29	-0.65	-0.75	-0.81	-0.87	-0.92	-0.92	-0.66	-0.64	-0.35	-0.12	0.15	0.23	-0.88	
		-0.82	0.92	0.91	0.54	0.22	-0.30	-0.57	-1.08	-1.18	-1.09	-1.13	-1.32	-1.31	-0.87	-0.67	-0.21	0.05	0.38	0.36	-1.40	
J	-1.17	0.76	0.82	0.69	0.39	-0.33	-0.63	-0.70	-0.82	-0.88	-1.01	-1.07	-1.05	-1.10	-1.07	-1.08	-0.86	-0.21	0.04	0.14	0.05	-1.90
	-2.22	0.75	0.95	0.83	0.46	-0.50	-0.94	-1.10	-1.22	-1.32	-1.38	-1.43	-1.46	-1.45	-1.41	-1.32	-0.94	-0.04	0.29	0.38	0.15	-2.83
K	-0.87	0.74	0.69	0.52	-0.07	-0.76	-0.68	-0.69	-0.86	-0.95	-1.15	-1.21	-1.12	-1.15	-1.07	-1.14	-1.29	-0.68	-0.14	-0.01	0.01	-1.61
	-0.55	1.08	1.00	0.77	-0.23	-1.14	-0.97	-1.08	-1.29	-1.41	-1.67	-1.72	-1.56	-1.52	-1.39	-1.36	-1.58	-0.73	0.22	0.42	0.47	-1.17
L	-1.18	0.63	0.70	0.68	0.47	-0.18	-0.49	-0.61	-0.84	-0.94	-1.21	-1.27	-1.12	-1.12	-0.99	-0.95	-0.72	-0.14	0.02	0.00	-0.09	-1.92
	-0.55	1.14	1.04	0.83	0.49	-0.38	-0.89	-1.05	-1.28	-1.44	-1.86	-1.91	-1.58	-1.52	-1.37	-1.28	-0.83	-0.02	0.28	0.45	0.52	-1.17
M	-1.13	0.69	0.76	0.72	0.45	-0.20	-0.44	-0.54	-0.78	-0.90	-1.20	-1.27	-1.07	-1.07	-0.92	-0.91	-0.74	-0.16	0.06	0.07	-0.03	-1.86
	-0.53	1.16	1.09	0.92	0.49	-0.37	-0.79	-0.98	-1.23	-1.40	-1.86	-1.91	-1.55	-1.47	-1.29	-1.18	-0.82	-0.02	0.37	0.51	0.56	-1.15
N	-0.74	0.90	0.90	0.80	0.45	-0.20	-0.40	-0.48	-0.71	-0.84	-1.21	-1.27	-1.01	-0.99	-0.85	-0.86	-0.73	-0.14	0.15	0.22	0.19	-1.47
	-0.49	1.17	1.14	1.03	0.55	-0.32	-0.69	-0.89	-1.12	-1.27	-1.82	-1.87	-1.41	-1.35	-1.20	-1.07	-0.77	0.06	0.49	0.56	0.57	-1.10
O	-1.01	0.98	1.09	1.03	0.94	0.26	-0.29	-0.42	-0.58	-0.61	-0.63	-0.69	-0.78	-0.85	-0.78	-0.74	-0.26	0.36	0.40	0.42	0.28	-1.71
	-2.10	0.90	1.16	1.17	1.29	0.38	-0.58	-0.83	-0.96	-1.03	-0.95	-1.00	-1.17	-1.18	-1.13	-0.95	-0.05	0.80	0.64	0.60	0.32	-2.69
P		0.00	1.11	0.97	0.59	0.27	-0.01	-0.06	-0.40	-0.49	-0.54	-0.59	-0.65	-0.66	-0.40	-0.43	-0.22	0.03	0.36	0.46	-0.67	
		-0.60	1.20	1.22	0.77	0.46	0.03	-0.22	-0.72	-0.81	-0.71	-0.75	-0.94	-0.94	-0.50	-0.32	0.05	0.31	0.71	0.65	-1.16	
Q		-1.39	0.96	1.09	0.77	0.38	-0.01	-0.08	-0.37	-0.43	-0.52	-0.57	-0.58	-0.61	-0.41	-0.41	-0.09	0.24	0.51	0.34	-2.02	
		-2.29	0.98	1.28	1.02	0.71	0.19	-0.03	-0.48	-0.61	-0.52	-0.56	-0.73	-0.68	-0.30	-0.15	0.31	0.58	0.79	0.46	-2.82	
R			-0.02	1.24	0.99	0.56	0.53	0.39	-0.31	-0.41	-0.51	-0.56	-0.55	-0.54	0.09	0.15	0.12	0.49	0.69	-0.60		
			-0.50	1.36	1.19	0.85	0.97	0.84	-0.25	-0.39	-0.40	-0.44	-0.51	-0.44	0.59	0.66	0.48	0.77	0.90	-0.99		
S			-0.89	1.37	1.23	0.81	1.12	1.17	1.16	1.14	0.85	0.81	1.01	0.95	0.88	0.77	0.40	0.76	0.85	-1.44		
			-1.91	1.25	1.22	0.96	1.63	1.63	1.70	1.57	1.01	0.98	1.46	1.53	1.39	1.33	0.61	0.82	0.82	-2.36		
T				0.07	1.87	1.72	1.45	1.32	1.23	1.16	0.88	0.84	1.04	1.03	1.05	1.12	1.33	1.42	-0.41			
				-1.44	1.87	2.05	1.83	1.82	1.84	1.72	1.26	1.22	1.62	1.67	1.60	1.56	1.73	1.50	-1.84			
U					-0.02	1.61	1.53	1.43	1.38	1.22	0.79	0.75	1.10	1.20	1.19	1.23	1.24	-0.42				
					-1.09	1.83	1.92	1.87	1.87	1.83	1.34	1.31	1.74	1.71	1.67	1.67	1.53	-1.42				
V						-0.72	-0.12	0.32	1.39	1.43	1.32	1.29	1.33	1.22	0.10	-0.40	-1.05					
						-1.26	0.06	0.07	1.57	1.93	2.28	2.25	1.85	1.43	-0.12	-0.17	-1.54					
W									-0.55	-0.22	-0.62	-0.66	-0.31	-0.70	———————							*Percent errors for CMFD*
									-1.49	0.30	0.47	0.44	0.23	-1.61	———————							*Percent errors for CMFD+F*

Reference is the result of CMFD (104 x 104 x 48)
The maximum errors are shown in bold character

Figure A2.1: Comparison of percent errors of channel power densities from CMFD (26 x 26 x 12) and CMFD with flat transverse leakage approximation (26 x 26 x 12) for the typical CANDU-6 without Xenon effect problem